Climate Variability and Irrigation Impacts on Stream-Aquifer Dynamics in the Apalachicola-Chattahoochee-Flint River Basin

by

Sarmistha Singh

A dissertation submitted to the Graduate Faculty of
Auburn University
in partial fulfillment of the
requirements for the Degree of
Doctor of Philosophy

Auburn, Alabama
December 12, 2015

Keywords: Baseflow, Streamflow, Climate Variability, Drought, Irrigation, JRFit, MODFE

Approved by

Puneet Srivastava, Chair, Professor of Biosystems Engineering
Asheber Abebe, Professor of Mathematics and Statistics
Ming-Kuo Lee, Professor of Geosciences
Mark Dougherty, Associate Professor of Biosystems Engineering

Dedication

This dissertation is dedicated to my beloved parents…

Mrs. Pravata Nalini Singh

&

Mr. Atulya Kumar Singh

Abstract

Climate variability cycles are responsible for short term fluctuations in climatic conditions thereby, affecting the water cycle and the availability of freshwater resources around the world. In Southeast United States, climate variability induced droughts have been a major factor affecting the availability of freshwater resources that threaten endangered mussel species in the Flint River and shellfish industry in the Apalachicola Bay. Recurring droughts have also led to the Tri-State Water Wars in this region. One of the primary issues related to the conflict is the reduction in baseflow levels in the Flint River during droughts due to irrigation withdrawal from the Upper Floridan Aquifer (UFA). Therefore, this research was conducted to study the compounding effect of climate variability induced drought and anthropogenic activities, such as, irrigation water withdrawal on baseflow levels in Apalachicola-Chattahoochee-Flint (ACF) River basin. The non-parametric Joint Rank Fit (JRFit) procedure and MODular Finite-Element Model (MODFE) were used to study and understand the relationships among droughts, irrigation, and stream-aquifer interactions in the study area with the final goal of identifying critical reaches and tributaries of the lower Flint River that are largely responsible for lowering of flow levels in the river. Results indicate that baseflows exhibits El Niño–Southern Oscillation (ENSO), Pacific Decadal Oscillation (PDO), Atlantic Multidecadal Oscillation (AMO), and North Atlantic Oscillation (NAO) tele-connection in this region. Interaction tests showed that La Niña is modulated by the phases of PDO and AMO. The results of this study also suggest that streamflow levels have decreased significantly after the introduction of irrigation in the study area. Results suggest that

lowering of flow levels mainly occurs during La Niña phases and gets exacerbated during growing periods. Analysis of presumptive standard flow showed that flow levels repeatedly violated the standards in recent drought events and can result in impairment of aquatic ecosystems. The results from the MODFE model indicated that increased ground-water withdrawal resulted in decrease in the stream-aquifer flux in the study area. The results from sensitivity analysis and simulated water restrictions suggested that acreage buyout in the sensitive areas help in greater recovery of stream-aquifer flux than, that achieved by reducing irrigation intensity (15% or 30%) throughout the study area. Moreover, analysis of acreage buyout suggested that water restrictions on irrigation withdrawal can have significant impacts on stream-aquifer flux in the study area, especially in the critical watersheds such as Spring Creek and Ichawaynochaway Creek.

The results of study are helpful in better understanding of the combined impact of climate induced droughts and anthropogenic stresses on stream-aquifer dynamics of Flint River and might help the state of Georgia to formulate an alternative drought-water use policy that can address the current water scarcity condition. Additionally, the results from this study can help better manage groundwater resources, protect surface water flows, and help avoid irrigation induced streamflow depletion in some of the most vulnerable tributaries of the Flint River.

Acknowledgement

Though the following dissertation is an individual work, it would have been hard to reach the heights or explore the depths without the guidance, help, support, and effort of many people. I would like to express my sincere gratitude to my advisor Dr. Puneet Srivastava for providing me this opportunity, support, encouragement, and helping me to be an independent thinker. I would like to express my deepest appreciation to my dissertation committee members Dr. Ash Abebe, Dr. Ming-Kuo Lee, and Dr. Mark Dougherty for their valuable suggestions, support and feedback during this research. Especially, I am highly indebted and extremely grateful to Dr. Ash Abebe for devoting time towards me from his busy schedule, and for his persistent help, support, kind suggestions, encouragement, and making me better along the way. I would like to express my heartfelt gratitude to Dr. Alan Wilson, Mr. Lynn Torak, Mr. Mark Masters, and Dr. Kathleen Miller for their valuable help, suggestions and feedback during the course of my research. I am also thankful to the colleagues in my research group Nafiul Islam, Ryan McGehee, Sarah Richard, Nischal Mishra, Golbahar Mirhosseini and Brittney Lindley for their help, encouragement and companionship.

Most importantly, I would like to express my heartfelt gratitude to my best friend Mitu Mohanty for his constant support, encouragement, help, and timeless friendship. I am forever indebted to my parents for their unconditional love, support, encouragement, blessings and allowing me to fulfill my dreams. I thank my father for instilling in me an optimistic attitude through believing in me and showing the true value of hard work through his example. I also thank

my mother for instilling in me the determination and discipline, and for enduring all the ups and downs during this long journey.

I would like to express my deepest gratitude and love to my friend, guide and fiancé Subhasis Mitra for his unconditional love, support, constant guidance, help and inspiring me to fulfil my dreams. I can't even thank him enough for the countless things he has done for me during this journey. I express my heartfelt appreciation to him for believing in me and encouraging me during the endless periods of self-doubts.

Last but not the least, I would like to thank all my friends and each member of my big extended family. It is only through their love, support and encouragement that I have had the courage and strength to make this dream come true.

Table of Contents

Abstract iii

Acknowledgments v

List of Tables. xiii

List of Figures. xvii

List of Abbreviations xxi

Chapter 1 Introduction. 1

1.1 Background. 1

1.2. Overview of Climatic Oscillations. . . . . … 3

1.2.1 El Niño Southern Oscillation (ENSO) 3

1.2.2 El Niño Phase. . . . . …5

1.2.3 La Niña Phase 6

1.2.4. Neutral Phase. 7

1.2.5 ENSO Indices . . . . . …8

1.2.6 ENSO Impacts. 9

1.2.7. Pacific Decadal Oscillation (PDO) and its impact on the Southeast . . . …….. .13

1.2.8. Atlantic Multidecadal Oscillation (AMO) and its impact on the Southeast……15

1.2.9. North Atlantic Oscillation (NAO) and its impact on the Southeast……... 16

1.3 Droughts impacts on the Southeast USA . . . . . …18

1.4 Tri-State Water War 19

1.5 Problem Statement 23

1.6 Dissertation Objectives 24

1.7 Dissertation Organization. 25

Chapter 2 Baseflow Response to Climate Variability Induced Droughts in the Apalachicola-Chattahoochee-Flint River Basin 26

2.1 Abstract 26

2.2 Introduction 27

2.3 Methodology 30

2.3.1 Data 31

2.3.2 Streamflow Data. 33

2.3.3 Oceanic-Atmospheric Cimate Variability Indicators. 34

2.3.3.1 Interannual Climate Variability (ENSO) 34

2.3.3.2 Decadal and Interdecadal Climate Variability (PDO, AMO and NAO)……35

2.3.4 Statistical Method 36

2.4 Results and Discussion. 39

2.4.1 Individual Analysis. 39

2.4.1.1. ENSO. 39

2.4.1.2. PDO 40

2.4.1.3. AMO 41

2.4.1.4. NAO 42

2.4.1.5. Graphical Summary of Individual Analyses……43

2.4.2. Coupled Analyses. 45

2.4.2.1. PDO – ENSO Interaction. 45

2.4.2.2. AMO – ENSO Interaction. 47

2.4.2.3. NAO – ENSO Interaction. 49

2.4.2.4. Graphical Summary of Coupled Analyses……51

2.5 Conclusions……. 53

Chapter 3 Powerful Nonparametric Analysis for Cluster-Correlated Climate and Hydrologic Data 56

3.1 Abstract 56

3.2 Introduction. 56

3.3 Statistical Methods 59

3.3.1 The Two-Sample Problem 59

3.3.2 Linear Models……. 62

3.3.2.1 The Two-Sample Problem as Simple Linear Regression…….……...62

3.3.2.2 General Linear Model – R Fit. 64

3.3.2.3 Linear Models with Cluster Correlation – JR Fit. 67

3.3.3. Monte Carlo Evaluation of JR Fit. 69

3.4. Results 71

3.5. Conclusion and Recommendations 73

Chapter 4 Combined Effect of Irrigation and Droughts on Surface and Baseflow Levels in the Lower Flint River Basin 74

4.1 Abstract 74

4.2 Introduction. 75

4.3 Methodology... 78

4.3.1 Study Area. 79

4.3.2 Data 80

4.3.3 Climate Variability (ENSO) Data……. 80

4.3.4 Streamflow Data…….. 81

4.3.5 Baseflow Data……. 82

4.3.6 Statistical Method…….. 82

4.3.7. Non-Irrigation and Irrigation Flow Comparison. 83

4.3.8. One-Day and Seven-Day Low Flows. 84

4.3.9. Flow duration curve analysis. 85

4.3.10. Presumptive standard flow level analysis……. 85

4.4 Results and Discussion 88

4.4.1 Streamflow Analysis. 88

4.4.2 Baseflow Analysis……. 90

4.4.3 1-Day and 7-Day Low Flow Analysis 91

4.4.4 Growing and Non-Growing Period Analysis……..….....94

4.4.4.1 Streamflow Analysis…… 94

4.4.4.2 Baseflow Analysis…… …… 96

4.4.5 Flow Duration Analysis…….97

4.4.6 Presumptive Standard Flow (PSF) Level Analysis 99

4.7 Conclusions 100

Chapter 5 Effects of Groundwater Pumpage on Stream-Aquifer Interaction during Droughts in the Lower ACF River Basin ……. 102

5.1 Abstract 102

5.2 Introduction 103

5.3 Methodology ……... 107

5.3.1 Study Area . ……. 107

5.3.2 Upper Floridan Aquifer and Stream-Aquifer Flow . . . . . .……... 109

5.3.3 MODular Finite-Element (MODFE) Model . . . . . .……. 111

5.3.3.1 Finite Element Mesh . . . .……... 112

5.3.3.2 Governing Equation . . . .……... 113

5.3.3.3 MODFE Input Parameters 114

5.3.3.4 Infiltration 115

5.3.3.5 Specified Head Boundary at UFA Updip Limit 116

5.3.3.6 Specified-Flux Boundaries . . . . ….. 116

5.3.3.7 Irrigation/Municipal Pumpage and Springs 117

5.3.3.8 Head-Dependent Flux Boundaries (HDFB) . . . .…. 118

5.3.3.9 Regional Groundwater Flow .. . . ……. 118

5.3.3.10 Flow Across Streambeds 119

5.3.3.11 Vertical Leakage across USCU and Lake-Beds . . . . …. . ... .120

5.3.4 Transient Simulation (May 2010 - September 2012) and Model Validation ..122

5.3.5 Model Scenarios . . . . . .……... 124

5.3.5.1 Capacity Use Areas (CUA) . .. .……... 126

5.3.5.2 Restricted Use Areas (RUA) 126
5.3.6 Sensitivity Analysis 126
5.3.7 Cost Analysis 128
5.4 Results and Discussion 128
5.4.1 Model Validation 128
5.4.2 Sensitivity Analysis 130
5.4.3 Simulation analysis for WY 2011 and WY 2012 133
5.4.3.1 Spring Creek 133
5.4.3.2 Ichawaynochaway Creek 137
5.4.3.3 Muckalee Creek 139
5.4.3.4 Lower Flint River Basin (LFRB) 141
5.4.4 Cost Analysis 144
5.5 Conclusions 144
Chapter 6 Conclusions 147
6.1 Summary and Conclusions 147
6.1.1 Objective 1 148
6.1.2 Objective 2 149
6.1.3 Objective 3 150
6.1.3 Objective 4 151
6.2 Implication of the Study 152
Chapter 7 Future Research. 153
References 155
Appendix A Streamflow Gauging Stations from USGS 169
A.1. USGS long term streamflow gauging stations 169
A.2. USGS long term streamflow gauging stations used in Chapter 4 169
Appendix B Irrigated Acreage in the lower Flint River Basin 170
B.1. Irrigated acreage in the lower Flint River Basin 170

Appendix C Precipitation Analysis . . . . ……... 171

C.1. Precipitation Analysis for Irrigated and Non-Irrigated period for Albany station in chapter 4 . . . . ……... . . .171

Appendix D MODFE Simulated Stream-Aquifer Flux for WY 2012 172

D.1. MODFE simulated irrigation and stream-aquifer flux for WY 2012 in Chapter 4..172

List of Tables

Table 2.1 Streamflow gauging stations showing the USGS station ID, their assigned names used in the manuscript, and their respective date ranges used for the study 33

Table 2.1 The years identified as positive and negative phases of Pacific Decadal Oscillation (PDO), Atlantic Multidecadal Oscillation (AMO), and North Atlantic Oscillation (NAO) 36

Table 2.2 JRFit estimated median monthly baseflows and p-values of differences in baseflow during El Niño and La Niña phases 40

Table 2.3 JRFit estimated median monthly baseflows and p-values of differences in baseflow during PDO positive and negative phases …..... 40

Table 2.4 JRFit estimated median monthly baseflows and p-values of differences in baseflow during AMO positive and negative phases 41

Table 2.6 JRFit estimated median monthly baseflows and p-values of differences in baseflow during NAO positive and negative phases 42

Table 2.7 Simple-main effect comparisons of baseflow medians for El Niño and La Niña phases combined with positive and negative phases of PDO 46

Table 2.8 Simple-main effect comparisons of baseflow medians for El Niño and La Niña phases combined with positive and negative phases of AMO …..... 47

Table 2.9 Simple-main effect comparisons of baseflow medians for El Niño and La Niña phases combined with positive and negative phases of NAO 50

Table 4.1 The selected streamflow gauging stations used in this study showing the USGS station ID, location, their assigned names used in the manuscript, and their respective date ranges 81

Table 4.2 JRFit estimated median monthly streamflows in cms, p-values and percentage differences in streamflows during NI and IR periods 88

Table 4.3 JRFit estimated median monthly streamflows in cms, p-values, and percentage differences in streamflows from NI to IR periods associated with phases of ENSO .. 90

Table 4.4 JRFit estimated median monthly baseflow in cms, p-values and percentage differences in baseflows from NI to IR periods 90

Table 4.5 JRFit estimated median monthly baseflows in cms, p-values and percentage differences in baseflows from NI to IR periods associated with phases of ENSO …..... 91

Table 4.6 JRFit estimated median monthly one-day low flows in cms, p-values and percentage differences in one-day low flows from NI to IR periods 91

Table 4.7. JRFit estimated median monthly seven-day low flows in cms, p-values and percentage differences in seven-day low flows during non-irrigated and irrigated periods ……92

Table 4.8 JRFit estimated median monthly one-day low flows in cms, p-values and percentage differences in one-day low flows from NI to IR periods associated with phases of ENSO 92

Table 4.9 JRFit estimated median monthly seven-day low flows in cms, p-values and percentage differences in seven-day low flows from NI to IR periods associated with phases of ENSO 94

Table 4.10 JRFit estimated median monthly streamflows in cms, p-values and percentage differences in streamflows from NI to IR periods associated with non-growing and growing seasons ……...94

Table 4.11 JRFit estimated median monthly streamflows in cms, p-values and percentage differences in streamflows from NI to IR periods associated with non-growing season for the phases of ENSO 95

Table 4.12 JRFit estimated median monthly streamflows in cms, p-values and percentage differences in streamflows from NI to IR periods associated with growing season for the phases of ENSO 96

Table 4.13 JRFit estimated median monthly baseflows in cms, p-values and percentage differences in baseflows from NI to IR periods associated with non-growing and growing seasons ……...…96

Table 4.14 JRFit estimated median monthly baseflows in cms, p-values and percentage differences in baseflows from NI to IR periods associated with non-growing season for the phases of ENSO 97

Table 4.15. JRFit estimated median monthly baseflows in cms, p-values and percentage differences in baseflows from NI to IR periods associated with growing season for the phases of ENSO 97

Table 5.1 Simulated stream-aquifer flow, Measured flow and associated target ranges for stream reaches for the month of July 2011 that are used for model stream-aquifer flux validation. All the flow values are in cubic feet per second (Mitra, 2014) 129

Table 5.2 Validation statistics of the groundwater residuals for the simulated model for the month of July 2011 (Mitra, 2014) …..... 129

Table 5.3 Irrigation withdrawal in cfd and simulated stream-aquifer flux for current and different scenarios in TCMD for Spring Creek …..... 134

Table 5.4 Percentage recovery of stream-aquifer flux under different scenarios as compared to current stream-aquifer flux …..... 134

Table 5.5 Irrigation withdrawal in cfd and simulated stream-aquifer flux for current and different scenarios in TCMD for Ichawaynochaway Creek 138

Table 5.6 Percentage recovery of stream-aquifer flux under different scenarios as compared to current stream-aquifer flux 138

Table 5.7 Irrigation withdrawal in cfd and simulated stream-aquifer flux for current and different scenarios in TCMD for Muckalee Creek 140

Table 5.8 Percentage recovery of stream-aquifer flux under different scenarios as compared to current stream-aquifer flux 141

Table 5.9 Irrigation withdrawal in cfd and simulated stream-aquifer flux for current and different scenarios in TCMD for lower Flint River basin 142

Table 5.10 Percentage recovery of stream-aquifer flux under different scenarios as compared to current stream-aquifer flux 142

Table 5.11 Acreage buyout analysis for different water restriction scenarios 144

Table A.1. List of long-term streamflow gauging stations with their coordinates in degree decimals used for JRFit analysis used in Chapter 2 169

Table A. 2. USGS long term streamflow gauging stations used in Chapter 4 169

Table C.1. Precipitation Analysis for Irrigated and Non-Irrigated period for Albany station 171

Table D.1. Irrigation withdrawal in cfd and simulated stream-aquifer flux for current and different scenarios in TCMD for Spring Creek 172

Table D.2. Percentage recovery of stream-aquifer flux under different scenarios as compared to current stream-aquifer flux for Spring Creek 173

Table D.3. Irrigation withdrawal in cfd and simulated stream-aquifer flux for current and different scenarios in TCMD for Ichawaynochaway Creek 173

Table D.4. Percentage recovery of stream-aquifer flux under different scenarios as compared to current stream-aquifer flux for Ichawaynochaway Creek 174

Table D.5. Irrigation withdrawal in cfd and simulated stream-aquifer flux for current and different scenarios in TCMD for Muckalee Creek 174

Table D.6. Percentage recovery of stream-aquifer flux under different scenarios as compared to current stream-aquifer flux for Muckalee Creek 175

Table D.7. Irrigation withdrawal in cfd and simulated stream-aquifer flux for current and different scenarios in TCMD for lower Flint River basin 175

Table D.8. Percentage recovery of stream-aquifer flux under different scenarios as compared to current stream-aquifer flux for lower Flint River basin 176

List of Figures

Figure 1.1 Southern Oscillation SST indices from 1950 to 2010 5

Figure 1.2 El Niño phase of ENSO ……..... 6

Figure 1.3 La Niña phase of ENSO ……..... 7

Figure 1.4 Neutral phase of ENSO ……..... 7

Figure 1.5 Negative (left side) and Positive (right side) phases of PDO showing anomaly patterns of wintertime SST (colors), SLP (contours) and surface windstress (arrows) 14

Figure 1.6 PDO indices showing negative and positive phases from 1900 to 2010…..... 14

Figure 1.7 AMO indices showing negative and positive phases from 1880 to 2010 16

Figure 1.8 Positive and Negative phases of NAO showing pressure gradients across the North Atlantic Ocean 17

Figure 1.9 NAO indices showing negative and positive phases from 1860 to 2010 19

Figure 1.10 The Apalachicola-Chattahoochee-Flint River Basin 22

Figure 2.1 Apalachicola-Chattahoochee-Flint (ACF) River basin in Alabama, Georgia, and Florida. The stream flow gauging stations selected for this study are shown as green dots. Note that the flows in the Flint River are mostly unregulated 32

Figure 2.2 Significance of individual analyses for phases of ENSO, PDO, AMO and NAO at the level of 1%, 5% and 10% for each station. Taller bars represent smaller p-values 43

Figure 2.3 Box and whisker plots of percent increase/decrease in baseflows across all six stations due to individual effects of the phases of ENSO, PDO, AMO and NAO. The boundaries of the box represent the first (Q1) and third (Q3) quartiles and the whiskers extend from the boundaries of the box to the extreme data points which are no more than 1.5 times the interquartile range (Q3 - Q1) 44

Figure 2.4 Percent change in median baseflows for El Niño and La Niña phases when they are associated with positive and negative phases of PDO. Also shown (green bars) are the median baseflows associated with PDO phase alone ……..... 46

Figure 2.5 Percent change in median baseflows for El Niño and La Niña phases when they are associated with positive and negative phases of AMO. Also shown (green bars) are the median baseflows associated with AMO phase alone 48

Figure 2.6 Percent change in median baseflows for El Niño and La Niña phases when they are associated with positive and negative phases of NAO. Also shown (green bars) are the median baseflows associated with NAO phase alone 50

Figure 2.7 Box and whisker plots of the percent increase/decrease in baseflows for all six stations. The boundaries of the box represent the first (Q1) and third (Q3) quartiles and the whiskers extend from the boundaries of the box to the extreme data points which are no more than 1.5 times the interquartile range (Q3 - Q1) 51

Figure 2.8(a) Significance of differences in El Niño baseflows during the positive and negative phases of PDO, AMO and NAO at the level of 1%, 5% and 10% for each station. Taller bars represent smaller p-values …..... 52

Figure 2.8(b) Significance of differences in La Niña baseflows during the positive and negative phases of PDO, AMO and NAO at the level of 1%, 5% and 10% for each station. Taller bars represent smaller p-values 53

Figure 3.1 Estimated relative efficiencies versus REML. Solid line represents the theoretical ARE $3/\pi$ of JR vs LS for Gaussian ($d = \infty$) case when $\rho = 0$ 72

Figure 4.1 The lower Flint River Basin (FRB) showing the critical sub-watersheds. The stream flow gauging stations selected for this study are shown as green circles ….....79

Figure 4.2 Representation of the sustainability boundary approach. The sustainability boundaries are defined as the limits to which natural flows can be altered and are expressed as a percentage of natural flows 87

Figure 4.3 JRFit estimation of median streamflows, baseflows, 1-day and 7-day low flows for (a) station A, (b) station B, (c) station C, and (d) station D 93

Figure 4.4 Flow duration curve for non-irrigated and irrigated periods for (a) station A, (b) station B, (c) station C, and (d) station D 98

Figure 4.5 Monthly presumptive standard streamflow levels, associated upper and lower bounds, and streamflow levels for the year 1954, 2000 and 2007 for station A …..... 99

Figure 5.1 Location of the study area showing location of irrigation wells in Spring Creek, Ichawaynochaway Creek, Muckalee creek and lower Flint River Basins (LFRB) ... 108

Figure 5.2 Stream and Groundwater flow system of the Upper Floridan aquifer in the lower Apalachicola-Chattahoochee-Flint River Basin showing components of the ground-water budget simulated by the model (Jones and Torak, 2006) …..... 110

Figure 5.3 MODFE model set up in the study area showing the types of boundary, stream and finite element mesh nodes 111

Figure 5.4 Location of capacity and restricted use watersheds in the study area …..... 125

Figure 5.5 Principal component analysis results showing first three principal components and K-cluster analysis showing black, red and green dots indicating high, moderate and low sensitive stream zones 131

Figure 5.6 High, moderate, and low sensitive zones for linear (number are in red) and non-linear (number are in black) streams 132

Figure 5.7 Simulated stream-aquifer flux for current and different scenarios in TCMD for Spring Creek 136

Figure 5.8 Simulated stream-aquifer flux for current and different scenarios in TCMD for Ichawaynochaway Creek 139

Figure 5.9 Simulated stream-aquifer flux for current and different scenarios in TCMD for Muckalee Creek 140

Figure 5.10 Simulated stream-aquifer flux for current and different scenarios in TCMD for Lower Flint River Basin 143

Figure B. 1. Increase in irrigated acreage in the lower Flint River Basin since 1970s 170

List of Abbreviations

ACF	Apalachicola-Chattahoochee-Flint River basin
AMO	Atlantic Multi-Decadal Oscillation
CPC	Climate Prediction Center
ENSO	El Niño Southern Oscillation
FDC	Flow Duration Curve
FRB	Flint River Basin
FRDPA	Flint River Drought Protection Act
GAEPD	Georgia Environmental Protection Division
GW	Groundwater Levels
HDFB	Head-Dependent Flux Boundaries
JRFit	Joint Rank Fit
MAF	Mean Annual Flow
MEI	Multivariate ENSO Index
MODFE	MODular Finite Element Model
NAO	North Atlantic Oscillation
NCAR	National Center for Atmospheric Research
NOAA	National Oceanic and Atmospheric Administration
PCA	Principal Component Analysis

PDO	Pacific Decadal Oscillation
SFB	Specified-Flux Boundaries
SOI	Southern Oscillation Index
SST	Sea-Surface Temperatures
UFA	Upper Floridan Aquifer
USCU	Upper Semi-Confining Unit
USGS	United States Geological Survey
WHAT	Web-based Hydrograph Analysis Tool
WY 2011	Water Year 2011
WY 2012	Water Year 2012

Chapter 1

Introduction

"A change in consciousness must occur in order for us to share water and use it wisely."

....Barbara Helen Harmony

1.1. Background

Water is the most precious resource in the world. It sustains life and allows our socio economy to thrive. Therefore, it is a fundamental cornerstone of maintaining peace, prosperity, and security across the world. Water is becoming an increasingly scarce commodity in the United States as well. An ever growing global population and increasing need for irrigated agriculture is putting tremendous stress on freshwater bodies such as lakes, streams, and aquifers. In the past 50 years, the demand for water consumption for human use has increased by almost three-fold, and five out of eight people will be living under water scarcity conditions by 2025 if the trend continues (Postel et al. 1996). Beside these anthropogenic factors, water scarcity can be exacerbated by interannual, decadal and multi-decadal climate variability cycles. Therefore, identification, interaction and quantification of these natural climate variablities is essential to minimize the potential adverse effect of natural climate variability on society-- particularly on water resources and agriculture (Climate Research Committee and National Research Council 1995).

Climate variability is the result of natural and large-scale features of climate-ocean atmospheric phenomena that describes short term changes in climate and lasts for months, seasons

or years. Time has been a constant witness to this variability in the earth's climate system. Besides time, various other information sources such as visual observations, paleoclimatic data, and instrumental records have also been witness of these climatic oscillations on a time scale ranging from yearly to decadal to centuries. Understanding and determining the temporal and spatial effect of these climate variations, and their impact on the components of the hydrologic cycle is one of the major concerns and priorities for researchers and decision makers. The behavior of extreme events such as hurricanes, floods, heat waves and droughts around the world can be significantly altered by these climate variability cycles, such as El Niño Southern Oscillation (ENSO), Pacific Decadal Oscillation (PDO), North Atlantic Oscillation (NAO), and Atlantic Multi-Decadal Oscillation (AMO) (Intergovernmental Panel on Climate Change, IPCC 2001). The limited understanding of the physical mechanisms of the cause and occurrence of the above mentioned climate variations and their interaction with each other makes it difficult to quantify the effect of these oscillations on hydrology and their consequent effects on society at large.

In the last few decades, water resources researchers have shown growing interest in quantifying the effect of climate variability on the components of the hydrologic cycle such as precipitation, streamflow, baseflow, groundwater, etc. This increasing interest has advanced the science to better understand the ocean-atmospheric phenomena and has helped issue short term climate forecasts that can be utilized for water management and also reduce climate induced risk and vulnerabilities. Recently, researches have also shown interest in studying the interaction of inter-annual cycles with decadal and multi-decadal cycles and their impacts on hydrology around the world.

Among all the above mentioned extreme events, in the Southeast USA, drought is a common phenomenon caused by climate variability. The Southeast often suffers from low surface

water availability during summer months due to very high evaporation rate, increased water demand by ever growing urban centers and irrigated agriculture, and more so due to climate variability induced droughts. During the past few decades, the Southeast has experienced several droughts that have caused losses in agricultural productivity, increased wildfires, prompted water use restrictions on municipal and irrigated waters uses, and induced water conflicts in neighboring states. Identification of the onset and persistence of drought can be elusive since the climatic signals are chaotic, noisy, and encompass annual, inter annual, decadal or multidecadal periods of variability. To determine the impact of climatic oscillations induced droughts on water resources, it is important to study the climate variability effects on hydrology to be able to cope with and better manage future water shortages due to these climate variability induced droughts. Therefore, this dissertation focuses on studying the effect of climate variability induced drought on hydrologic components in the Southeast USA. In this study, climatic cycles have been defined as fluctuations of ocean-atmospheric anomalies that extend from monthly to multidecadal time scale.

1.2. Overview of Climatic Oscillations

1.2.1. El Niño Southern Oscillation (ENSO)

El Niño Southern Oscillation (ENSO) phenomenon is the fluctuation of sea surface temperature caused by the interaction between large-scale ocean and atmospheric circulation in equatorial Pacific Ocean. El Niño is the periodic warming of the Pacific Ocean off the coast of Equatorial South America towards end of December which was detected by fishermen, and it is referred to the celebration of the birth of the Christ Child. The term “Southern Oscillation” is referred to the variability of the strength of the Walker Circulation that results from the pressure gradient between the North Australian-Indonesian low-pressure trough and the Southeast Pacific

subtropical high-pressure cell (Philander and Rasmusson, 1985). It is an irregular and interannual cycle of fluctuations in mean sea level pressure between the eastern and western Pacific Ocean which occurs due to changes in the direction and intensity of trade winds that are also responsible for the fluctuations of sea surface temperature (SST) in this region.

The Southern Oscillation is quantified through the Southern Oscillation Index (SOI) which is referred as the pressure difference between Easter Island in the Southeast Pacific and Djakarta, Indonesia. The SOI is calculated from the normalized difference in monthly mean pressure anomalies between Tahiti (18°S, 150°W) and Darwin (12°S, 131°E) (Chen, 1982). The positive phase of SOI is associated with La Niña (cold) events where pressure anomaly is higher than normal in the Southeast Pacific and lower than normal at the north of Australia. On the contrary, the negative phase indicates El Niño (warm) events with below-normal pressure in the Southeast Pacific and above-normal pressure at the north of Australia. A plot of SOI is presented in figure 1.1. The ENSO cycle maintains an irregular periodicity of 2-7 years that gives a level of predictability while retaining variability in its occurrence, magnitude and climatic effects around the world (Gershunov and Barnett, 1998a and 1998b; Cane, 2005). Although the exact reason behind the ENSO is not known yet, it is proposed that ENSO involves the relaxing of Easterly trade winds and anomalous warming of surface equatorial Pacific water near Peru.

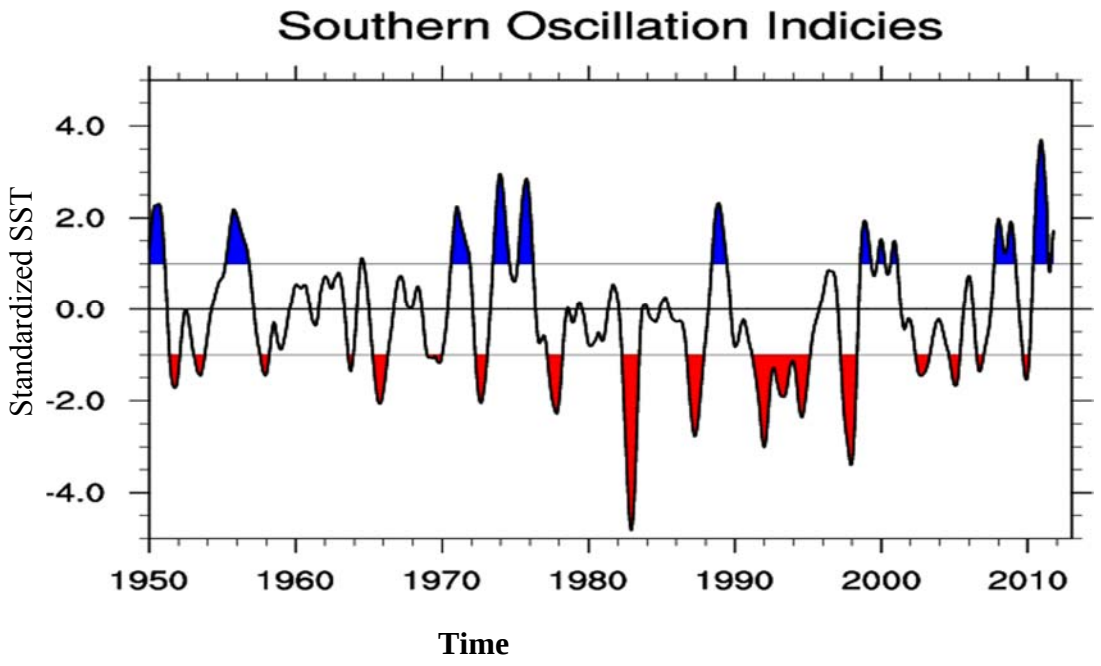

Figure 1.1. Southern Oscillation SST indices from 1950 to 2010.
(Source: https://climatedataguide.ucar.edu/climate-data/overview-climate-indices)

Further, it is associated with a decrease in the coastal upwelling of the cold subsurface water and consequently it changes sea level pressures and surface patterns in variables such as temperature and precipitation (Green et al., 1997). ENSO is one of the steadiest low-frequency climate variability that has impacts on both regional and local scales (Ropelewski and Halpert, 1986). ENSO consists of three phases, namely El Niño, La Niña and Neutral.

1.2.2. El Niño Phase

The phenomena named El Niño means “little boy” or “Christ child” in Spanish, and is referred as "a warm event" or "a warm episode" that starts at the beginning of the year (during the Christmas time). El Niño occurs by weakening trade winds that allows the warm water to flow towards the eastern Pacific from the western Pacific region (Figure 1.2). This warm water in the

eastern Pacific (off the coast of South America) is responsible for changes in the atmospheric weather of the region. The hot and humid air over the ocean results in stronger and bigger Tropical thunderstorms that moves eastward with the Pacific's warm water. Therefore, rain falls over the deserts of Peru which normally would occur over the tropical rain forests of Indonesia. This causes flooding in the eastern Pacific (South America) and forest fires and drought in the western Pacific (Indonesia).

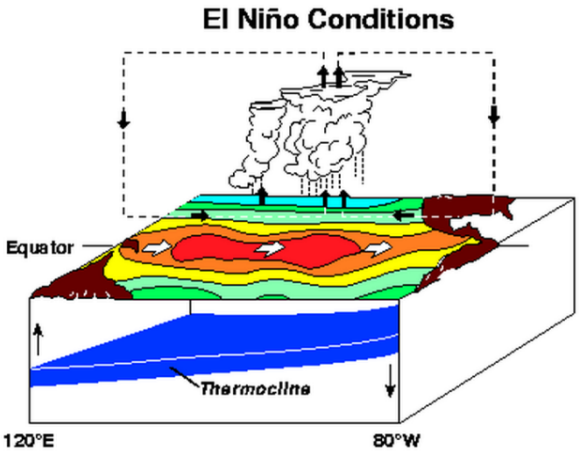

Figure 1.2. El Niño phase of ENSO
(Source: http://www.pmel.noaa.gov/tao/elNiño/Niño_normal.html)

1.2.3. La Niña phase

The phenomena named La Niña means "little girl" in Spanish, and is referred as anti-El Niño, or simply "a cold event" or "a cold episode". The La Niña phase is characterized by strong trade winds blowing from eastern Pacific towards the western Pacific which causes unusual warming of ocean temperatures in the Equatorial Pacific (Figure 1.3). This concentrated heat in the western Tropical/Equatorial Pacific intensifies both convection and westerly winds that move back to the east by introducing a strong Walker circulation (air circulation) in the lower

atmosphere. La Niña condition is also responsible for unusual cooling of ocean temperatures in the eastern equatorial Pacific.

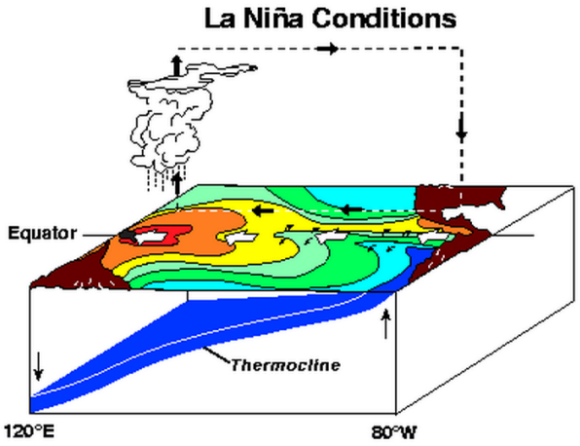

Figure 1.3. La Niña phase of ENSO
(Source: http://www.pmel.noaa.gov/tao/elNiño/Niño_normal.html)

1.2.4. Neutral Phase

In the Neutral phase, trade winds blow from east Pacific towards the west Pacific that causes warm water ponding at the western Equatorial Pacific while upwelling occurs in the eastern Pacific along the coast of South America (Figure 1.4).

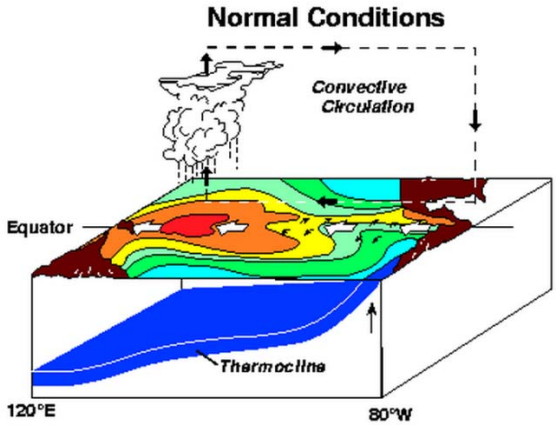

Figure 1.4. Neutral phase of ENSO
(Source:http://www.pmel.noaa.gov/tao/elNiño/Niño_normal.html)

1.2.5. ENSO Indices

Researchers have created the climatic indices as monitoring tools that describe significant pattern or state of climate system. These indices are generally represented as time series where one index value represents a particular point in time. There are several types of indices which describe different atmospheric events including air pressure differences, sea surface temperatures (SSTs), monsoon precipitation, hurricane activity, drought events, solar radiation, etc. Spatially averaged areas of SST in different parts of the world have been used to describe various climatic cycles such as El Niño/Southern Oscillation (ENSO). There are various climate indicators such as Niño-1, Niño 2, Niño 3, Niño-4, Niño-3.4, Japan Meteorological Agency (JMA), and the modified JMA (Rasmusson and Carpenter 1982; Glantz 2001) calculated using 100-year SST anomaly datasets that define the phase and strength of ENSO. The Oceanic Niño Index (ONI) was developed by the National Oceanic and Atmospheric Administration. Each of these indices are slightly different ENSO definitions according to coordinates and regions around the world for index calculation; however, there is no agreement within the scientific community over the best index to define ENSO years or the strength, timing, and duration of events. Niño 1 and Niño 2 regions have been found to be highly responsive to seasonal and El Niño induced changes than Niño 3 region. In Niño 4 region, changes in SSTs are influenced by longitudinal shifts of the east-west temperature gradients along the equator. The variation of SST for the Niño 3.4 region is calculated in the region of 170°W - 120°W and 5°N -5°S of the Pacific ocean (Trenberth and Hoar, 1996). The region of JMA index is JMA is located within the Niño-3 region (4°N-4°S and 150°-90°W) and is defined by spatial average of 5-month running mean of SST anomalies.

Similar to SST ENSO indicators, mean sea-level pressure (MSLP) also serve as ENSO indicators such as Southern Oscillation Index (SOI) defined by the Australian Bureau of

Meteorology or the US Climate Prediction Center. SOI is defined based on the differences of mean sea level atmospheric pressure between two locations in the Eastern Pacific and Western Pacific (Troup 1965; Chen 1982; Ropelewski and Jones 1987). Prolonged periods of negative SOI values have been found to be associated with abnormally warm ocean waters across the eastern tropical Pacific, which represents El Niño episodes, and prolonged positive periods of SOI have been found to coincide with La Niña episodes.

Other complex indicators are the combination of different temperature and pressure indices such as the trans-Niño index (TNI) (Trenberth and Stepaniak 2001) and the multivariate ENSO index (MEI) (Wolter and Timlin 1993). The TNI index is defined as the scaled difference between sea surface temperature anomalies averaged in the Niño 1+2 and Niño 4 regions. It has been found to be able to show the formation of ENSO phases but unable to capture their occurrence very well. The MEI is a composite index that uses SST, sea-level pressure, zonal and meridional surface wind, cloudiness, and surface air temperature (Wolter and Timlin, 1993) and has strong correlation with SOI indices in identifying ENSO phases.

The Niño-3.4 index region sea level temperature and pressure anomalies have been found to exhibit strong correlation with the Southeast United States climatic variations. Therefore, the Niño-3.4 index has been used in this study.

1.2.6. ENSO Impacts

ENSO is one of the primary influencing factors of climatic variations that are responsible for extreme weather conditions across the world (Molnar and Cane, 2007). Several studies have found that ENSO affects temperature, precipitation and different components of hydrologic cycle around the world (Chiew et al., 1998; Roy, 2006; Keener et al., 2007; Barsugli et al. 1999; McCabe

and Dettinger, 1999). Particularly, equatorial South America experiences the most prominent signals of ENSO where El Niño phases and La Niña phases are associated with below and above normal precipitation, respectively (Aceituno, 1988). However, El Niño phase results in greater than normal precipitation and cooler temperatures in eastern equatorial and Southeast Africa (Ropelewski and Halpert, 1987; Halpert and Ropelewski, 1992). Northern Europe receives lower precipitation during El Niño phases, whereas, Central and Western Europe experiences higher temperature and lower precipitation. These effects are reversed during the La Niña phase in Northern Europe (Fraedrich and Muller, 1992). In eastern Australia, the La Niña phase brings more winter precipitation, whereas, the El Niño year coincides with dryer periods (Nicholls et al., 1996). Investigations have also reported relationships between ENSO events with precipitation from the Indian Monsoon (Ropelewski and Halpert, 1987; Charles et al., 1997). Historically, El Niño events have also been found to be often linked with failed Indian monsoon (Ropelewski and Halpert, 1987; Kiladis and Diaz, 1989; Charles et al., 1997). Several studies have observed significant ENSO correlations with temperature and precipitation in the North American continent as well (Rasmusson and Wallace, 1983; Ropelewski and Halpert, 1986; Halpert and Ropelewski, 1992). They have found that Northern United States experiences warmer winters and less precipitation during El Niño events whereas the southwestern United States has higher than normal precipitation during El Niño summers. However, these patterns are reversed during La Niña events.

The effects of ENSO induced variability in the United States (including the Southeast) temperature and precipitation have been widely studied. It is found that associations of surface climate patterns are strongest during winter in the Southeast. One of the founding studies performed by Ropelewski and Halpert (1986) on North American precipitation and temperature patterns associated with ENSO observed increased precipitation during the El Niño (warm) phase

of ENSO from October of the onset year to March of the following year in the Southeast. The median precipitation was greater than normal occurring in 18 of the 22 warm ENSO events studied. They also determined that temperatures were generally cooler than normal during El Niño events during the winter. Similar types of study have also been conducted by Gershunov and Barnett (1998a) on temperature and precipitation; however, they focused more on the extreme events occurring in the tails of probability density functions. Their study of wintertime (December, January and February) ENSO phases showed that El Niño phases are strongly associated with the frequency of heavy rainfall events by 15%-30% along the Southeastern seaboard; while La Niña events are negatively correlated with heavy rainfall frequencies in much of the southern United States, as strong as 30%-50% near Northern Florida. However, in association with temperature, it is found that the frequency of cold outbreaks in winter El Niño events are higher than during La Niña. The central tendency of temperature shifts towards the negative direction during El Niño events, reflecting colder temperatures in the Southeast for the El Niño phase.

A conclusive study by the Center for Ocean-Atmospheric Prediction Studies (COAPS) also confirmed the association of ENSO with changes in temperature and precipitation patterns in the Southeast. They have also found that an El Niño event involves wetter than normal fall, winter, and spring seasons, with decreased temperatures during winter, while a La Niña event associated with warmer and dryer winter and spring (Green et al. 1997). Moreover, another study by COAPS also supports the evidence of an increase in precipitation along the Gulf, from 2-3 cm in the DJF months of El Niño phase and 1-2 cm dry departure in the Southeast during La Niña events from the root mean square differences (Smith et al. 1998).

The possible physical explanations have also been explored for the winter precipitation changes in the Southeast related to ENSO. Smith et al. (1998) analyzed anomalies and their

robustness in low level winds, convergence, jet stream locations, sea level pressure, and vorticity advection as potential conduits for variation in precipitation. Their study showed the possible physical explanations for both El Niño and La Niña phases of ENSO. The El Niño phase exemplifies a stronger than normal Aleutian low, a weak Pacific High, and an eastward expanding Bermuda High. It provides low level moisture for increased precipitation by allowing southwesterly flow into the entire Gulf. This southwesterly flow is 90% statistically robust and also associated with a southwest to northeast jet at 300 hPa over the Southeastern United States during El Niño events.

In contrast, the La Niña phase has mostly opposite features of the El Niño event, which sets up a weaker Aleutian Low, a stronger than normal Pacific High, and a more westerly location of the Bermuda high from neutral time. The westerly Bermuda high illustrates an anticyclone off the coast of Cape Hatteras by influencing stronger than normal easterly winds over the south and Gulf. This Southeasterly flow provides low level moisture in the western Gulf and drier air in the eastern Gulf. The Southeasterly flow is associated with the zonally oriented 300 hPa eastern jet which allows a conducive area for lift relocated northwest over the lower and middle Mississippi Valley. Therefore, the Southeast experiences less precipitation during La Niña phases.

In addition to the influence of ENSO on temperature and precipitation around the world (Chiew et al., 1998; Roy, 2006; Keener et al., 2007), ENSO have also been found to affect streamflow, groundwater, flood frequency, droughts, monsoon, and crop yield across the world including the Southeast US (Rajagopalan and Lall, 1998; Kahya and Drakup, 1993; McCabe and Dettinger 1999; Piechota and Dracup, 1999; Hansen et al. 2001; Tootle et al., 2005; and Gurdak et al., 2007). Several studies have found strong correlation between ENSO with precipitation and streamflow (Redmond and Koch, 1991; Eltahir, 1996; Berri and Flamenco, 1999; Simpson and

Colodner, 1999). The above studies showing the effect of past ENSO events on the hydrologic cycle provides a possibility for better forecasting and management of water resources during droughts induced by climate variability cycles.

1.2.7. Pacific Decadal Oscillation (PDO) and its impact on the Southeast

The PDO is a long lived ENSO like cycle with similar patterns of temperature, pressure, wind, and precipitation characteristics. However, PDO varies on spatial and temporal basis from ENSO. On spatial basis, the primary climatic fingerprints of the PDO are visible in the Northern Pacific region. However, the climate signatures of the ENSO exist in the tropical Pacific. On a temporal basis, the PDO phases persist for 20 to 30 years while the ENSO persist for 6 to 18 months. The PDO index used in the study is defined as the major principal component of monthly SST variability in the North Pacific Ocean. The phases of the PDO are classified by the fluctuations in SST and sea level pressure (SLP) in the North Pacific region. Positive (negative) phase of the PDO has been associated with anonymously warmer (cooler) SST and a wave-like pattern with a stronger (weaker) than average Aleutian low in the North Pacific region (Manuta, 2002) (Figure 1.5). The PDO index used in this study has an annual cycle since it is based on mean SLP changes in the Northern Pacific which changes with the seasonal insolation variations (Figure 1.6).

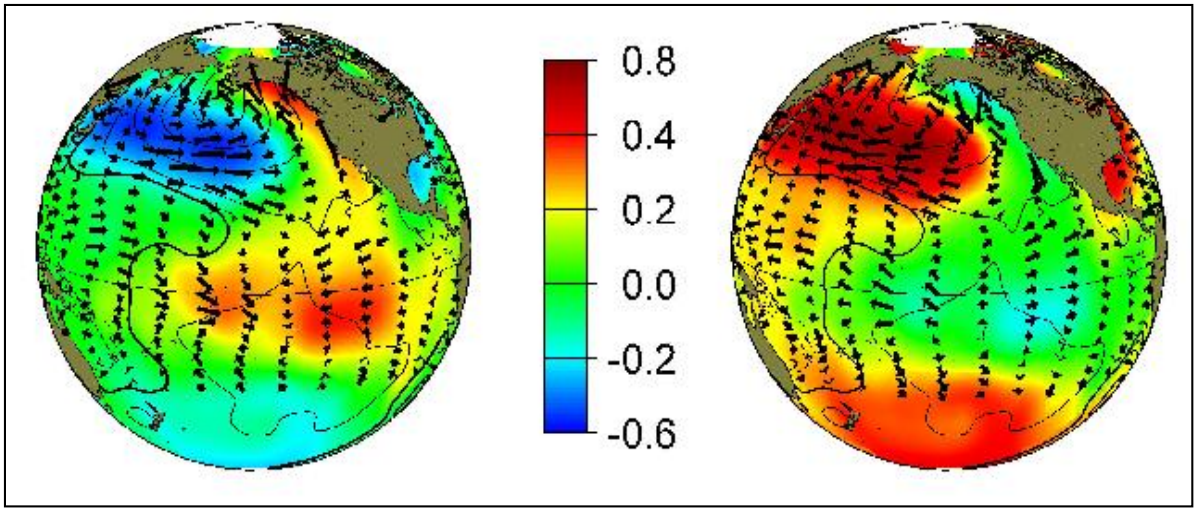

Figure 1.5. Negative (left side) and Positive (right side) phases of PDO showing anomaly patterns of wintertime SST (colors), SLP (contours) and surface windstress (arrows). (Source: http://jisao.washington.edu/pdo/).

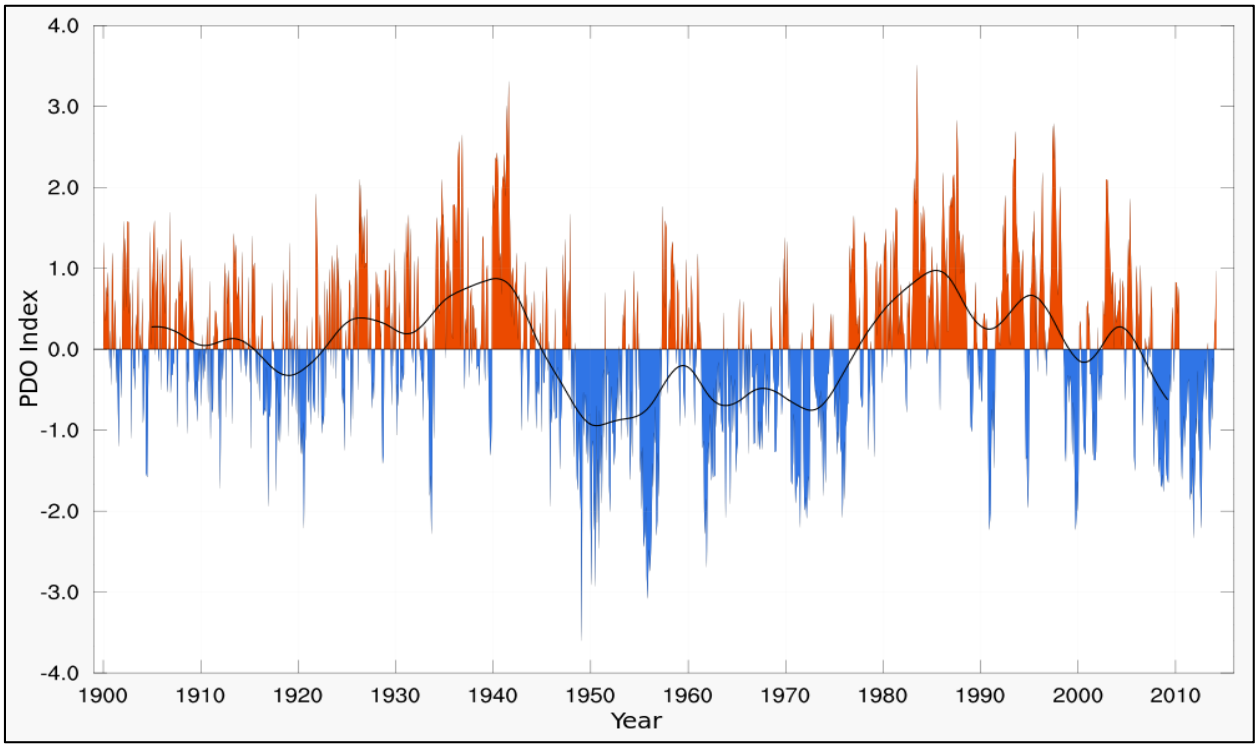

Figure 1.6. PDO indices showing negative and positive phases from 1900 to 2010. (Source: http://en.wikipedia.org/wiki/Pacific_decadal_oscillation#/media/File:PDO.svg)

Studies have shown that PDO oscillation has strong association with the climate and weather patterns in the Southeastern United States (Mantua, 2002). Barlow and Berbery (2000) have studied the effect of PDO phases on drought and precipitation patterns in the United States. They found that the PDO positive phase has negative correlation with summertime *Palmer Drought Severity Index* (PDSI) precipitation in the Southeast United States, meaning decreased summer precipitation during positive phase of PDO.

1.2.8. Atlantic Multidecadal Oscillation (AMO) and its impact on the Southeast

The AMO cycle is the warming and cooling of SST in the North Atlantic Ocean with a periodicity of 60 to 85 years. This fluctuation of SST is the result of the changes in the intensity of the Atlantic Thermohaline circulation (Enfield et al., 2001). The cooling and warming of SST are associated with negative and positive phases of AMO cycles (Figure 1.7). Numerous studies have found strong correlation between AMO signal and precipitation patterns across the contiguous US. Likewise PDO, AMO consists of a positive and negative phase. The AMO positive phases are associated with decreased precipitation pattern across the Southeast US and increased precipitation patterns during the AMO negative phase. Enfield et al. (2001) have also found strong correlations with summer precipitation and AMO signals across the US. They have also found negative correlations between summer precipitation and the AMO positive phase in the ACF basin, meaning drier summer across Georgia stations. McCabe et al. (2004) found positive correlations between the AMO cycle and drought frequency across much of the US. According to a report from the Southwest Florida Water Management District (Kelly et al. 2004), seasonal peak flows decreased consistently in northern Florida rivers, including the Apalachicola River during the AMO positive phase (1940-1969).

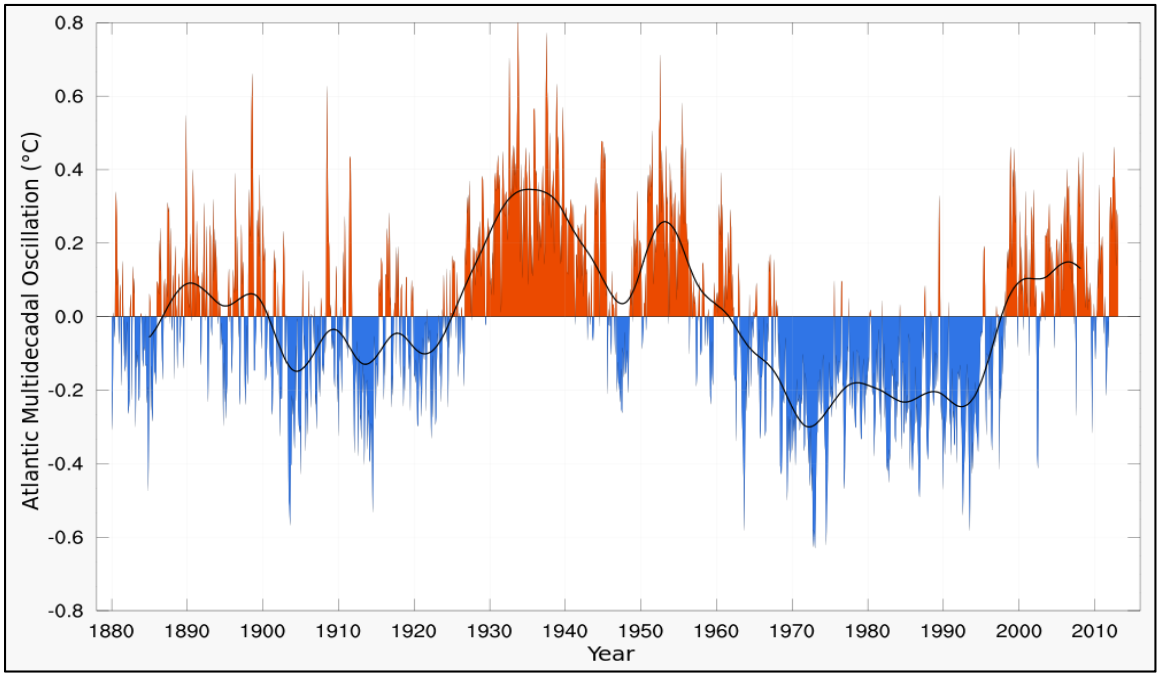

Figure 1.7. AMO indices showing negative and positive phases from 1880 to 2010. (Source:http://en.wikipedia.org/wiki/Atlantic_multidecadal_oscillation#/media/File:Amo_timeseries_1856-present.svg)

Conversely, a sharp increase in seasonal peak flow was reported in northern Florida rivers during the AMO negative phase (1970-1999). Tootle et al. (2005) have also found similar results on streamflow in connections to AMO cycles in the lower Appalachians/Gulf of Mexico region. Their results showed that streamflow has negative (positive) correlation with AMO positive (negative) phase, meaning streamflow decreased (increased) during the AMO positive (negative) phase. They have also found significant number of anomalies in streamflow during AMO phases.

1.2.9. North Atlantic Oscillation (NAO) and its impact on the Southeast

The NAO cycle has significant influence on surface temperature and precipitation patterns across Northern Hemesphere, including the coast of US (Barnston and Livezey, 1986) and is considered the most prominent teleconnection pattern across all the seasons. The NAO index is

the measure of surface sea-level pressure difference between an area of high pressure over the Azores (Subtropical High) and an area of low pressure near Iceland (Subpolar Low). The NAO has two phases namely, positive and negative (Figure 1.8 and 1.9). The positive phase of the NAO has below normal pressure across Arctic and above normal pressure over the central North Atlantic (Hurrell, 1995). The negative phase has the opposite pattern of pressure over these regions. This fluctuation in pressure level significantly alters the alignment of the jet stream and also increases the southerly flow over the eastern US (Hurrell et al., 2003) and consequently affecting the precipitation and temperature patterns across this region. The mean SLP patterns of NAO have also been associated with precipitation and temperature pattern of the Southeast US. During winter months, positive phase of NAO showed negative correlation with the Southeastern precipitation, meaning decreased precipitation during positive phase of NAO (Hurrell et al., 2003).

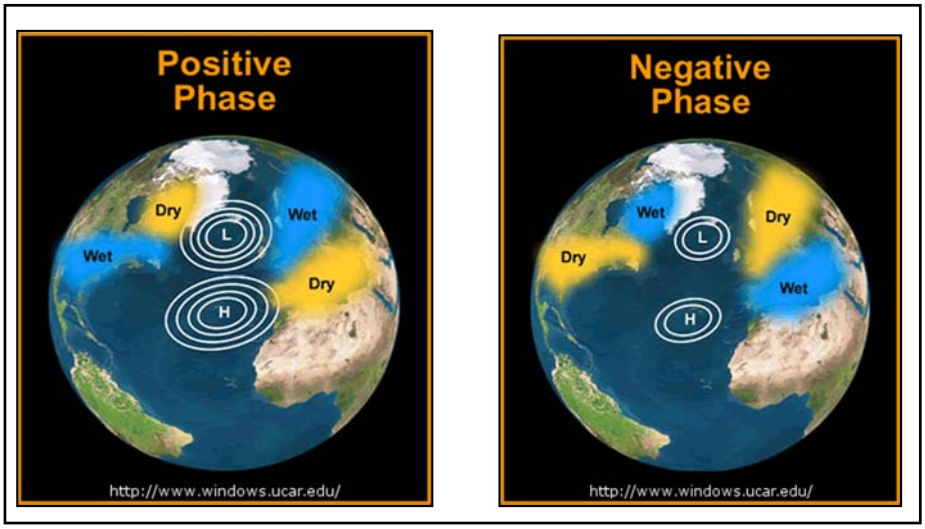

Figure 1.8. Positive and Negative phases of NAO showing pressure gradients across the North Atlantic Ocean. (Source: http://www.windows.ucar.edu/)

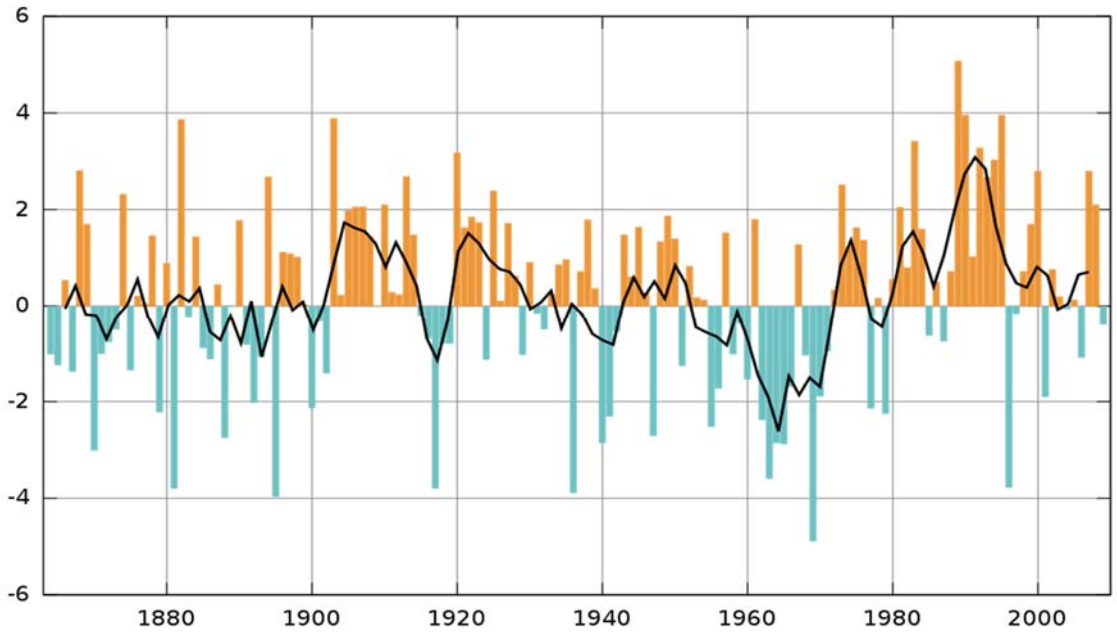

Figure 1.9. NAO indices showing negative and positive phases from 1860 to 2010. (Source: http://en.wikipedia.org/wiki/North_Atlantic_oscillation#/media/File:Winter-NAO-Index.svg)

1.3. Droughts impacts on the Southeast USA

Large seasonal to inter-annual (SI) climate variability in the Southeast US has been found to be significantly influenced by ENSO and also responsible for frequent droughts in the Southeast US (Ropelewski and Helpert, 1986; Dai and Wigley, 2000). La Niña period has enormous impact on the overall water resources of the region since it is responsible for a dryer winter season where winter is considered as a recharge period in this region. Generally in summer months, the Southeast suffers from low surface water availability even during non La Niña periods since it has very high evapotranspiration rates, intra-annual climate variability, increased irrigated agriculture and increased demand by growing urban centers. Since the early 1980s, the Southeast USA has experienced several severe droughts that have caused agricultural productivity losses, prompted

water-use restrictions (municipal and irrigation), and induced water conflicts between neighboring states of Alabama, Florida and Georgia (e.g., the Tri-State Water Wars). For example, La Niña phase of 1998 -1999 was associated with a drought the effects of which persisted until 2000 in Florida and until 2001 in northern Georgia and Alabama. More recently, the drought conditions during the winter of 2007 and during 2010-2012 associated with La Niña phases caused/had an economic losses/impacts in billions of dollars in the Southeast especially losses in agricultural sector in Georgia region. The University of Georgia's Center for Agribusiness and Economic Development estimated that the 2007 drought was liable for losses in agricultural economic output by as much as $1.3 billion in Georgia (CAED 2007). Since drought is a recurring phenomenon in the Southeast states and typically returns every two to seven years with La Niña, understanding of drought, severity of drought, and its impact on flow levels is important for drought preparedness.

1.4. Tri-State Water War

The Apalachicola-Chattahoochee-Flint (ACF) River Basin is one of the most important and contentious river basins in Southeastern United States. Since 1980's, the water wars in the ACF started when a series of droughts in the Southeast greatly reduced flows in the three named rivers. These reductions in flow levels led to water use restrictions in the region where water restrictions and allocation became a source of debate among the states of Alabama, Georgia, and Florida who share the water resources of the ACF basin. The ACF basin originates in northern Georgia and incorporates the drainage area of the Chattahoochee River (AL and GA), the Flint River (GA) and the downstream Apalachicola River (FL) (Figure 1.10). The Chattahoochee River flows from north to south along the border of Alabama and Georgia with tributaries existing in eastern Alabama and eventually joins with the Flint River at Lake Seminole at the Georgia/Florida

border. Similarly, the Flint River runs through western and central Georgia and finally meets the Chattahoochee River at Lake Seminole. The Apalachicola River drains from Lake Seminole down to the Gulf by Apalachicola Bay, Florida which is the largest forested floodplain and sustains a sensitive habitat for many endangered wildlife species. The flow in Chattahoochee is regulated by a number of dams while the Flint River is considered as unregulated. The area of ACF is approximately 50,800 km^2 with approximately 619 kilometers (385 miles) long and 80 kilometers (50 miles) wide. The major portion of this basin lies in Georgia (74%), with the remainder in the western panhandle of Florida (11%) and eastern Alabama (15%) (USACE 1998).

The ACF basin has a diverse group of water use stakeholders such as agriculture, recreation, industry and hydropower production. The city of Atlanta is a large municipal and industrial water user of the headwaters of the Chattahoochee. This growing metropolitan area of Atlanta demands significant water form several reservoirs in the northern Chattahoochee River. The ACF basin water resources have also been used to provide cooling to multiple Alabama power plants including the Farley Nuclear plant. The Flint River flows through a highly irrigated agricultural region where most of the irrigation water is pulled from the southern part of the basin. The lower ACF basin in Florida supports a significant seafood industry including large Oyster industry present in the Apalachicola Bay. This floodplain system are regarded as one of the planet's "biodiversity hotspots," providing a home to the fat threeridge mussel (*Amblema neislerii*), gulf sturgeon (*Acipenser oxyrinchus desotoi*), and the purple bankclimber mussel (*Elliptoideus sloatianus*) protected under the Endangered Species Act (Ruhl, 2005). A crucial part of the region's economic growth depends on human access to water where basin stakeholders have significant and differed demands on the water supplied by the ACF basin (Meruelo, 2006; Jordan et al., 2006).

A series of droughts in the 1980's lead to reduced hydropower production, implemented water restriction on municipalities and industries water use, and even navigation was suspended on the Apalachicola River for several months in 1988 (USACE 1998). Therefore, in 1990 the United States Army Corps of Engineers (Corps) started studying and approving water allocation requests to Georgia municipalities. Then, based on several environmental laws Alabama filed suit in a federal court against the Corps to stop granting any reallocations of water. Eventually, Florida became involved in this conflict to protect natural flow hydrograph of Apalachicola River. This litigation was left on hold until three states studied the physical and socioeconomic conditions of the Apalachicola Bay and the ACF basin which is known as the Comprehensive Study. Finally, in the year 1997, the states and federal government entered to protect "water quality, ecology, and biodiversity" by aiming to develop a fair water allocation formula for the ACF basin (Ruhl, 2005). Georgia entered into the "water wars" by filing suit in a federal court in the year 2000. According to Georgia, Corps unfairly interfered with the state's water use and denied any further water reallocations. A group of power distributors also filed a suit stating that the Corps managed waters to inflate the price of electricity paid by hydropower producers. The 1997 compact expired in August 2003 leaving the fate of the states and ACF basin undetermined (Ruhl, 2005). Then, all the litigations were consolidated into one forum and awaited for debate in U.S. District court in Florida (Gilbert, 2007). During an ongoing drought in Georgia in 2007, the Georgia governor filed a lawsuit against the Corps over concerns about the water releases from Atlanta's primary water reservoir i.e., Lake Lanier during droughts. According to Corps, despite the alarming low levels of the lake, Georgia must maintain minimum flows of 5,000 cubic feet per second in order to preserve the habitat for several endangered species in the downstream Apalachicola River (Cusick, 2007).

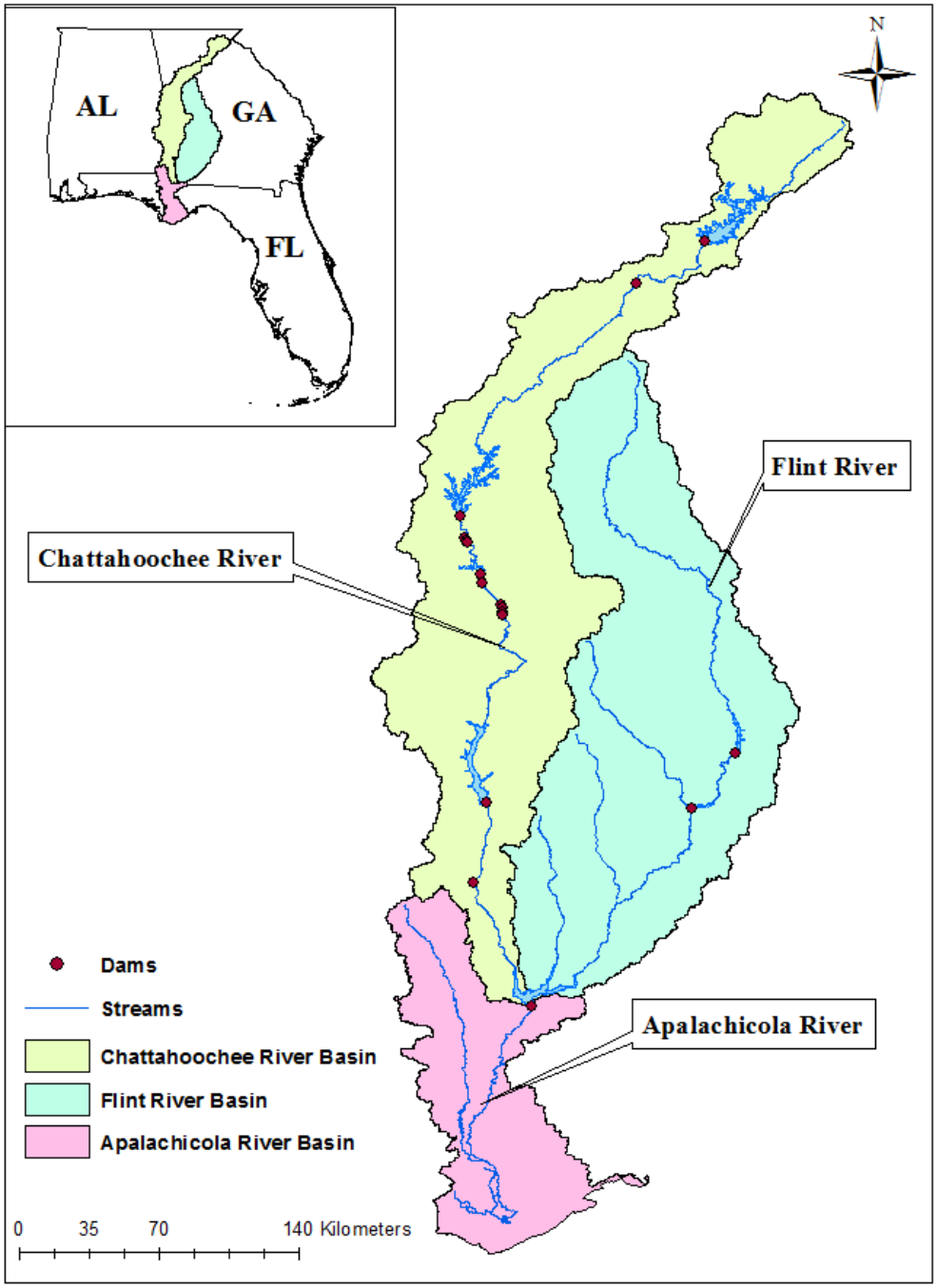

Figure 1.10. The Apalachicola-Chattahoochee-Flint River Basin.

The ACF basin is highly sensitive to the uses, management and allocation of the water resources. Therefore, it is essential to study the related water resources issues. This high interest issue has caused several researchers to conduct studies on the water resources of the ACF basin

especially related to drought indicators and streamflow levels. One such study by Light et al. (2006) studied the impact of the decline in water level of Apalachicola River on floodplain in past 50 years. Another study by Steinemann (2003) focused on developing a drought plan by providing a probabilistic framework to evaluate different drought indicators for the ACF basin. However, an elaborate study has yet to be conducted in order to investigate the climatological factors possibly involved in the yet to be discovered drought patterns of the ACF and its impact on flow levels. This climatic and anthropogenic tied issue motivated this study to be focused on the relationships between global scale climate oscillations and irrigation on flow levels in the study area.

1.5. Problem Statement

To address the issues related to climate variability and irrigation induced flow depletion in the study area, it is important to understand and quantify the effects of climate variability induced droughts on hydrologic cycle components and its interaction with anthropogenic activities such as irrigation in southwest Georgia. This study can provide an insight on how irrigation pumpage primarily for agricultural purposes lead to lowering of flow levels in the Flint River during droughts. Initially, the study focused on analysis of large-scale climate phenomena as well as the interactions of interannual with decadal and multidecadal oceanic-atmospheric phenomena that can provide valuable information regarding droughts and their impact on water resources. This study also offers an application of powerful non-parametric technique called Joint Rank Fit (JRFit) procedure that provides a robust test of the significance of interactions between the phases of ENSO-PDO, ENSO-AMO and ENSO-NAO baseflows to understand the onset, persistence and severity of droughts.

Equally important is to study the combined stress of climate variability induced droughts and irrigation withdrawal on water resources to understand the lowering of flow levels (including low flows) which is of prime concern in the study area and causes water conflicts among the neighboring states in the Southeast United States. Further, identification of critical areas and associated tributaries of the Flint River that are sustained by baseflow and responsible for lowering of flow levels in the river due to drought and pumpage might help reduce the fingerprint of irrigation induced streamflow depletion. Furthermore, analysis of the effectiveness of suggested possible water restrictions on irrigation would add great value to the knowledge related to sustainability of steam-aquifer flux (surface and groundwater resources) in the study area.

1.6. Dissertation Objectives

The objectives of this dissertation are to:

1. Quantify the impact of interannual and multidecadal climate variability cycles on baseflow levels.
2. Compare non-parametric and parametric statistical procedures for the testing of climatic and hydrologic datasets.
3. To study and quantify the combined effect of droughts and irrigation water withdrawal on surface and baselow levels in the study area, and
4. Quantify the effect of irrigation water withdrawal and effectiveness of water restriction scenarios on stream-aquifer interactions in the lower Flint River and its tributaries.

1.7. Dissertation Organization

This dissertation focuses on the above mentioned four objectives and includes 7 chapters. Chapter 1 provides an introductory overview, review of literature, study area, problem statement and objectives for the study. Chapter 1 also includes a brief description of ENSO, PDO, AMO, and NAO, their impacts around the world (especially in the southeast), and the Tri-state water war. Chapter 2 to 5 presents the methodology and results for the above mentioned objectives. Chapter 2 presents the detailed study of the modulation of ENSO phases by the phases of PDO, AMO and NAO and its impact on baseflow levels using a novel procedure called JRFit. Chapter 3 discusses the robustness and efficiency of the JRFit procedure for the test and estimation of climatic interactions especially, the datasets that are clustered, correlated and heavy tailed or do not follow Gaussian distribution. Chapter 4 documents the development of irrigation in the Southwestern Georgia and compares the flow levels during pre and post irrigation periods along with ENSO to understand the effect of irrigation water withdrawal during droughts on flow levels in the lower Flint River and its tributaries. Chapter 5 deals with the effects of irrigation in the event of droughts on stream-aquifer flux. This chapter also looks at the effectiveness of various water restriction scenarios in an effort to recover stream-aquifer flux in the lower Flint River Basin. Chapter 6 presents the major conclusions and practical implications of the research findings. Finally, Chapter 7 presents suggestions for future work.

Chapter 2

Baseflow Response to Climate Variability Induced Droughts in the Apalachicola-Chattahoochee-Flint River Basin

2.1. Abstract

Droughts have been a major factor leading to the Tri-State Water Wars in the southeastern United States. One of the primary issues related to the conflict is the reduction in baseflow levels in the Flint River during droughts. This affects the availability of freshwater resources to support the endangered mussel species in the Flint and Apalachicola Rivers and threatens the shellfish industry in the Apalachicola Bay. Study of large-scale climate phenomena as well as the interactions of interannual with decadal and multidecadal oceanic-atmospheric phenomena can provide valuable information regarding regional climatic conditions such as droughts and their impact on water resources. This study was conducted to quantify the impacts of climate variability cycles on baseflow levels in the Flint River. The individual and coupled impacts of the El Niño–Southern Oscillation (ENSO), Pacific Decadal Oscillation (PDO), Atlantic Multidecadal Oscillation (AMO), and North Atlantic Oscillation (NAO) on baseflow were quantified. The non-parametric Joint Rank Fit (JRFit) procedure was used to provide a robust test of the significance of interactions between the phases of ENSO-PDO, ENSO-AMO and ENSO-NAO baseflows. Simple-main effect comparisons were also performed using the JRFit model to estimate significant difference between the positive and negative phase baseflows of PDO, AMO and NAO associated with El Niño or La Niña phases. The results indicate that the phases of ENSO, AMO and NAO

significantly affect baseflows in the Flint River. Interaction tests showed that the PDO and AMO phases modulate ENSO phase baseflows. La Niña associated with positive phases of PDO and AMO resulted in greater decrease in baseflow levels of approximately 28% and 33%, respectively. However, La Niña associated with negative phase of AMO showed above normal baseflows. The results illustrate the importance of coupled analyses of climate variability by providing a better understanding of the severity of droughts and their impact on baseflows. The results obtained from this study can be used by water managers in the region as a guide for the issuance of drought severity-based water restrictions.

2.2. Introduction

Interannual, decadal, and multi-decadal variability of oceanic-atmospheric phenomena affect temperature and precipitation, and can provide information about extreme events such as hurricanes, floods, droughts, and cold waves (IPCC, 2001). Studies have found strong influence of climate variability phenomena, such as El Niño–Southern Oscillation (ENSO), Pacific Decadal Oscillation (PDO), Atlantic Multidecadal Oscillation (AMO), and North Atlantic Oscillation (NAO), on components of hydrologic cycle in many parts of the world. Therefore, comprehensive studies of various climate variability phenomena and their interactions with hydrologic processes can provide useful information towards strategies for mitigating their adverse effects on water resources (Climate Research Committee and National Research Council, 1995).

ENSO, a major mode of climate variability affecting the global climate system (Diaz and Markgraf, 1992), is the fluctuation in sea-surface temperatures (SST) in the equatorial Pacific Ocean with a periodicity of two to seven years. ENSO has three phases, namely Neutral, El Niño and La Niña (Philander, 1990). The terms “El Niño” and “La Niña” refer to respective warming

and cooling of SST at Eastern Tropical Pacific. PDO, AMO and NAO are climatic cycles similar to ENSO that are caused due to fluctuations in ocean-atmospheric temperature and pressure. PDO and AMO are the fluctuations in SST in the North Pacific Ocean and the North Atlantic Ocean, respectively. These fluctuations are characterized by warm/positive (above average SST) and cold/negative (below average SST) phases, forming PDO and AMO cycles in their respective regions that oscillate with a periodicity of 25-30 years and 60-85 years, respectively (Tootle et al., 2005; Johnson et al., 2013). NAO is the fluctuation of mean sea level pressure between Portugal and Iceland. It is an important mode of ocean-atmospheric variability over the North Atlantic Ocean exhibiting strong influence on surface temperature and precipitation patterns during the northern hemispheric winter. The NAO cycle is decadal and like other climatic cycles NAO cycle has negative and positive phases.

Much of the early research focused on studying the relationships between ENSO and hydrologic processes such as precipitation and streamflow in different parts of the US (Piechota and Dracup, 1996; Mitra et al., 2014). Recent studies, however, have started to consider the coupling of PDO, AMO and NAO with ENSO to evaluate the interactive effect of climatic conditions on various components of the hydrologic cycle (Enfield et al., 2001; Tootle et al., 2005; Johnson et al., 2013). While studies have found that the majority of the United States exhibits below normal rainfall and streamflow during the AMO positive phases (Enfield et al., 2001), the effect was magnified during some of the phases of coupled ENSO-AMO and PDO-AMO cycles (Hidalgo and Dracup, 2001, 2003; McCabe et al., 2004; Hidalgo, 2004; Enfield et al., 2001; Rogers and Coleman, 2003).

In the Southeast US, large seasonal to interannual climate variability results in frequent droughts and is majorly influenced by ENSO. The La Niña phase of ENSO brings warm and dry

conditions to the Southeast between the months of October and April (Mearns et al., 2003; Kiladis and Diaz, 1989; Hansen and Maul, 1991; Schmidt and Luther, 2002) and typically returns every two to seven years, making the region vulnerable to ENSO-induced droughts. These ENSO-induced droughts cause severe water shortages that get exacerbated due to increased urbanization and irrigation. Water managers in this region are faced with the increasing challenge of supplying water under the combined stresses of climate variability and population growth. The Apalachicola-Chattahoochee-Flint (ACF) River Basin (Figure 2.1) located in Alabama, Georgia, and Florida provides a great example of this conundrum.

The ACF River Basin is one of the most important (and contentious) river basins in the US. Although the ACF is predominantly affected by ENSO-induced droughts, studies have shown that other climate variability cycles also have considerable influence in the region (Enfield et al. 2001; Kiladis and Diaz, 1989; Hansen and Maul, 1991; Schmidt and Luther, 2002; Johnson et al., 2013). Since 1980, ENSO-induced droughts have been aggravated by demands from the growing population of the Atlanta metropolitan region and increased irrigated agriculture in southwest Georgia. The combined pressure has led to water conflicts among the neighboring states of Georgia, Alabama and Florida (Tri-State Water Conflict) and prompted water use restrictions. Over the last two decades, the conflict has persisted with ongoing negotiations, mandated compromises, and litigations among AL, GA and FL (Jordan et al., 2006).

A major concern related to the dispute is the baseflow reduction during droughts in the Apalachicola River, which is regarded as one of the planet's "biodiversity hotspots" providing habitat for many threatened and endangered species (Ruhl, 2005). During droughts, increased municipal withdrawal from the Chattahoochee River in the Atlanta region leads to lowering of flow levels in the downstream section of the river. Moreover, increased irrigation water withdrawal

from the Upper Floridan Aquifer (UFA) during droughts results in lowering of flow levels in the Flint River. Flow levels in the Flint River during summer months are predominantly sustained by baseflow influx from the UFA. Therefore, increase in irrigation withdrawal from the UFA leads to lowering of the groundwater levels in the aquifer, thereby lowering flow (baseflow) levels in the Flint River owing to stream-aquifer connections. Reduction in flow levels in the Chattahoochee and Flint Rivers during drought inevitably leads to lowering of flow levels in the Apalachicola River situated downstream.

The complexity of drought related water management issues, and the importance of surface and ground water resources for agricultural, municipal, and industrial purposes in the ACF River Basin have motivated this study to quantify the effect of ENSO-induced and decadal climate variability-modulated droughts on baseflow in the area. Thus, the overarching goal of this study is to improve the understanding of how baseflow in the ACF is affected by individual and coupled large-scale interannual and interdecadal ocean-atmosphere phenomena.

2.3. Methodology

To attain the research goal, the nonparametric Joint Rank Fit (JRFit) procedure (Kloke et al., 2009) was used to test and estimate the large-scale, individual impacts of the phases of PDO, AMO, NAO, and ENSO on baseflow. Additionally, the coupled responses of PDO, AMO, and NAO with ENSO were evaluated to determine the severity of ENSO-induced drought on baseflow levels in the study area. This study is the first part of a bigger project that aims to understand the relationships among droughts, irrigation, and baseflow levels in the study area with the final goal of identifying critical reaches and tributaries of the Flint River that are responsible for lowering of

flow levels in the river and thereby helping the State of Georgia to better manage drought-induced streamflow reductions in the river.

The nonparametric Joint Rank Fit (JRFit) procedure is an extension of Wilcoxon rank-sum procedure for the analysis of clustered correlated data. Jaeckel (1972) extended the Wilcoxon rank-sum method to the general linear model by redefining the problem as the minimization of a rank-based dispersion function based on the model residuals. JRfit is the minimization of Jaeckel's dispersion for linear models with cluster-correlated errors. Kloke et al. (2009) show that this procedure results in an unbiased and efficient estimator of the slope parameter and that the estimator has an asymptotic Gaussian distribution. This asymptotic distribution is used to construct efficient significance tests of the model parameters. Further details of the JRfit procedure can be found in Kloke et al. (2009) and Hettmansperger and McKean (2011). The statistical model and estimation approach using JRFit is described in Section 2.2.

2.3.1. Data

To establish the relation between ocean-atmospheric climate variability and baseflow, streamflow data from 6 unregulated streamflow gauging stations on the Flint River (Figure 2.1) and climate variability data from NOAA were used (Appendix A.1).

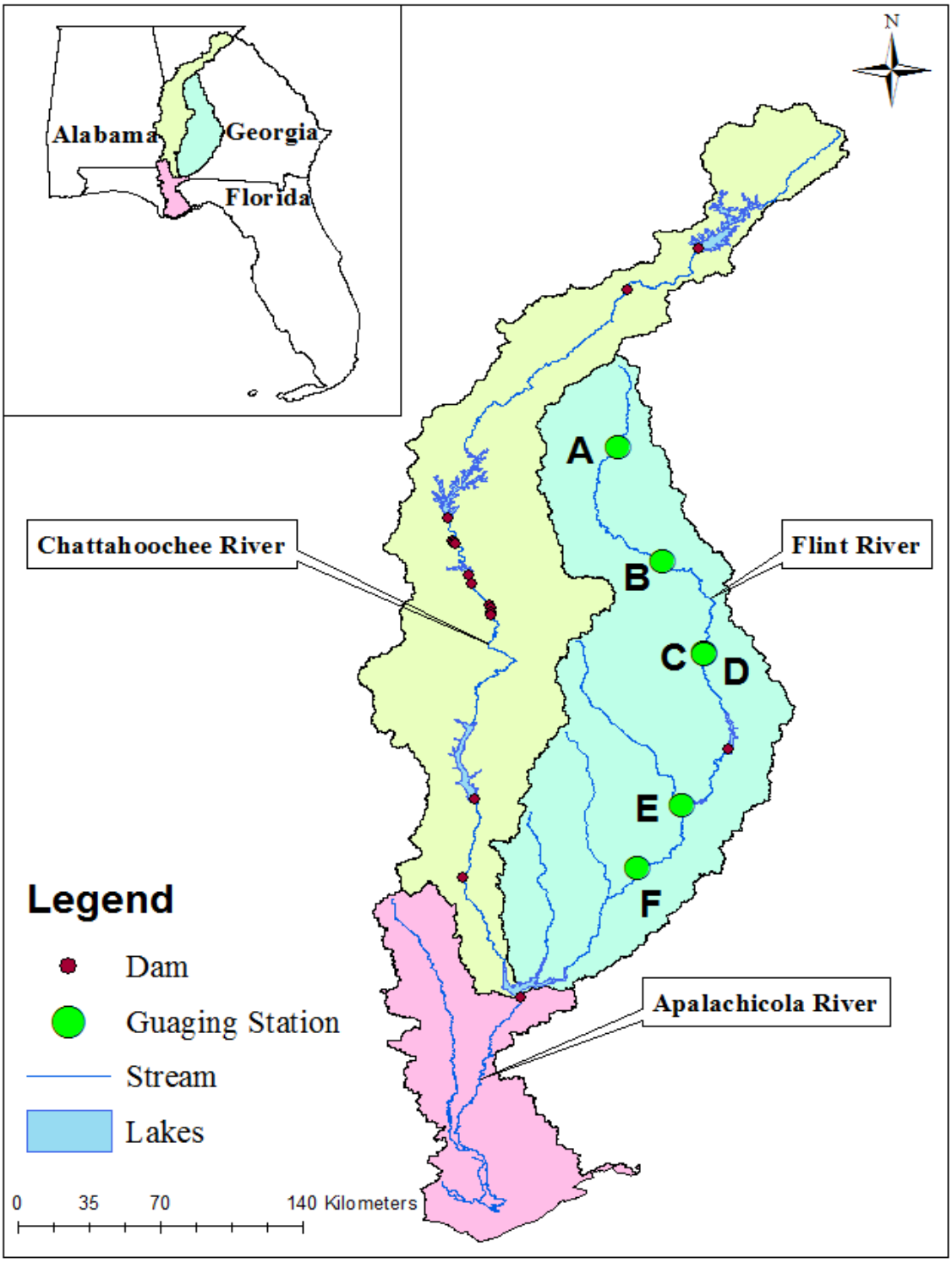

Figure 2.1. Apalachicola-Chattahoochee-Flint (ACF) River basin in Alabama, Georgia, and Florida. The stream flow gauging stations selected for this study are shown as green dots. Note that the flows in the Flint River are mostly unregulated.

2.3.2. Streamflow data

It is important to obtain unregulated (not affected by reservoirs and dams) streamflow datasets in order to study the effect of climate variability on baseflow. However, a major part of the ACF river basin is highly regulated, especially the Chattahoochee River that has 5 federal dams and upwards of 6 private full river dams (Johnson et al., 2013). Since the Flint River has only 2 small, run-of-the-river dams, it is relatively unaffected by water control structures. Therefore, unregulated streamflow gauging stations on the Flint River were selected to develop the relation between climate variability and baseflow variations. Daily streamflow data in cubic feet per second were collected from six United States Geological Survey (USGS) gauging stations with historical data of approximately 69 years (Table 2.1).

Table 2.1. Streamflow gauging stations showing the USGS station ID, their assigned names used in the manuscript, and their respective date ranges used for the study.

Station ID	Given Name	Data Range (Year)
02344500	**A**	1950-2008
02347500	**B**	1950-2008
02349500	**C**	1950-2003
02349605	**D**	1950-2008
02352500	**E**	1950-2008
02353000	**F**	1957-2008

Baseflow was separated from streamflow using Web-based Hydrograph Analysis Tool (WHAT) which uses two digital filter methods for baseflow separation. These two digital filter methods are the BFLOW and Eckhardt (Lim et al., 2005). In this study, Eckhardt filter method (Eckhardt, 2005), which is used for perennial rivers, with baseflow index 0.9, was used for baseflow separation (Lim et al., 2005). The equation used for the Eckhardt filter method is presented below.

$$b_t = \frac{(1 - BFI_{max}) \times \alpha + b_{t-1} + (1 - \alpha) \times BFI_{max} \times Q_t}{1 - \alpha \times BFI_{max}} \quad (1)$$

where, BFI_{max} is the maximum value of long term ratio of base flow to total streamflow; b_{t-1} is the filtered base flow at the time step t-1; b_t is the filtered base flow at the time step t; α is the filter parameter; and Q_t is the total streamflow at the time step t.

2.3.3. Oceanic-atmospheric climate variability indicators

2.3.3.1. Interannual climate variability (ENSO)

There is no single measurement that is universally accepted for the definition of ENSO indices (Beebee and Manga, 2004; Tootle et al., 2005). In general, ENSO indices are calculated based on SST (e.g. the Niño 3.4 index) (Trenberth, 1997; Trenberth and Stepaniak, 2001), based on atmospheric observations such as the Southern Oscillation Index (SOI) (Troup, 1965; Chen, 1982; Ropelewski and Jones, 1987), and combination of both ocean and atmospheric parameters such as the Multivariate ENSO Index (MEI) (Wolter and Timlin, 1993). In this study, the Niño 3.4 SST index (ERSST.v3b) is used. The Niño 3.4 indices were obtained from the National Oceanic and Atmospheric Administration's (NOAA) Climate Prediction Center (CPC). This index is based on a 3-month running average beginning with December–February SST anomalies in the Niño 3.4 region (5^0N–5^0S, 120^0–170^0W). The monthly Niño 3.4 indices were obtained by assigning the 3-month running average of Niño 3.4 index values to the middle months. When Niño 3.4 index value is between -0.5ºC and +0.5ºC, ENSO is considered to be in Neutral phase and indices above +0.5 ºC and below -0.5ºC values indicate that ENSO is in El Niño and La Niña phase, respectively (Kiladis and Diaz, 1989; Ropelewski and Halpert, 1986).

2.3.3.2. Decadal and Interdecadal climate variability (PDO, AMO and NAO)

The PDO index is defined as the major principal component of monthly SST anomalies in the North Pacific Ocean, poleward of 20^0N (Mantua et al., 1997). Based on the positive and negative values of SST anomalies, the phases of PDO index were defined as warm/positive and cold/negative phase, respectively (Tootle et al., 2005; Johnson et al., 2013). The PDO index values were obtained from the Joint Institute for the Study of the Atmosphere and Ocean, University of Washington (JISAO, 2012).

The AMO index is identified as the coherent pattern of SST variability in North Atlantic Ocean (0^o–70^oN) (Schlesinger and Ramankutty, 1994; Enfield et al., 2001; Tootle, 2012). The phases of AMO (i.e., warm/positive and cold/negative) were defined based on the positive and negative numerical values from 121-month smoothed index values, and each phase lasts for about 20-40 years. AMO index values were obtained from the Physical Sciences Division of the Earth Systems Research Laboratory, NOAA (ESRL, 2012; Johnson et al., 2008, 2013).

NAO is the leading pattern of atmospheric variability in the North Atlantic region that measures the strength of the westerly winds blowing between 40^oN and 60^oN. The NAO index is defined as the difference between the normalized mean sea level pressure (SLP) anomalies at Lisbon, Portugal and Stykkisholmur, Iceland during winter (December to March) (Hurrell, 1995). A lowpass filter was applied to the yearly NAO index values to remove fluctuations of less than four years, and the phases of NAO were defined based on dominant negative and positive numerical values. The NAO index obtained from the National Center for Atmospheric Research (NCAR) website and validated against those reported by Tootle et al. (2005) are shown in Table 2.2.

Table 2.2. The years identified as positive and negative phases of Pacific Decadal Oscillation (PDO), Atlantic Multidecadal Oscillation (AMO), and North Atlantic Oscillation (NAO).

Phases	PDO	AMO	NAO
Positive	1977–1998, 2003–2007	1950–1963, 1995– 2008	1950– 1951, 1973– 1976, 1981–2008
Negative	1950–1976, 1999–2002, 2008	1964–1994	1952– 1972, 1977–1980

2.3.4. Statistical Method

Linear mixed effect models (LMEs) were used to study and quantify the individual and coupled impacts of climate variability phenomena on baseflow. Two statistical procedures were used to fit the LMEs: the parametric maximum likelihood (ML) and the non-parametric Joint Rank Fit (JRFit). Baseflow data display monthly clustering and LMEs are suitable models for the analysis of clustered data. In other words, each month exhibits similar baseflow patterns irrespective of year. For example, the month of April is likely to have more baseflow than the month of May each year in the ACF River Basin.

Several studies have used the Wilcoxon rank-sum (WRS) test as the preferred test over the classical *t* test for the analysis of climate data due to the presence of possible outliers in the data and heavy tails or skewness in the data-generating distributions (Tootle et al., 2005; Johnson et al., 2013). In such studies, investigators have typically used the difference in medians to quantify effect sizes, although the natural estimator associated with the WRS test is the so-called Hodges-Lehmann estimator defined as the median of all pair-wise differences (Hettmansperger and McKean, 2011). However, studying the coupled effects of climate variables (e.g., ENSO and AMO) on baseflow directly using the WRS test has proven elusive and researchers have resorted to data segmentation before applying WRS as a two-sample procedure (Tootle et al., 2005;

Johnson et al., 2013). The use of fewer observations for such tests leads to lower test power and inefficiency (Lehmann and Romano, 2005). Such difficulties can be addressed by formulating a linear model to perform significance testing and effect size estimation simultaneously. The WRS test and its associated estimator of effect size can be obtained via the Wilcoxon rank-regression estimator (Jaeckel, 1972; Hettmansperger and McKean, 2011) of a linear model.

Effects of an individual climate variability phenomenon (X) on baseflow (Y) were estimated using the linear model

$$Y = \beta_0 + \beta_1 X + \varepsilon, \tag{2}$$

Where, ε represents random errors and $X = 0$ and $X = 1$ represent the two phases of the climate variability phenomenon. The value of β_1 measures the change in baseflow due to change of phase. If the Wilcoxon rank-regression is used to fit the model, then the test for the significance of β_1 is exactly the WRS test and the estimator of β_1 is the Hodges-Lehmann estimator of effect. The estimator of β_0 is the median of baseflow for the $X = 0$ phase.

A major advantage of considering WRS test as a linear model is that it allows us to study the effects of other variables on baseflow by simply including them in the model as independent variables. One such analysis is the study of coupled effects of climate variability phenomena on baseflow. For instance, one may wish to estimate and test the effect of a multi-decadal climate variable, say AMO, as well as its coupled (interaction) effect with ENSO on baseflow. To this end, we create another indicator variable for AMO ($Z = 0$ for AMO Negative and $Z = 1$ for AMO Positive) and consider the statistical model

$$Y = \beta_0 + \beta_1 X + \beta_2 Z + \beta_3 XZ + \varepsilon, \tag{3}$$

Where, β_3 measures the interaction effect of ENSO and AMO. The significance of the interaction effect β_3 indicates that the effect of ENSO on baseflow depends on the phases of AMO and vice versa. In this case, one needs to be careful in interpreting β_1 and β_2. For instance, ENSO effect would have to be compared within the two AMO levels separately and AMO effect would have to be compared within the two ENSO levels. Once again, these models can be estimated using the Wilcoxon rank-regression method (Jaeckel, 1972; Hettmansperger and McKean, 2011). In addition to their robustness, it is known that these estimators are relatively efficient compared to maximum likelihood estimators. For instance, the Wilcoxon estimator is 95.5% as efficient as the maximum likelihood method when the data come from the normal distribution and it is much more efficient than the maximum likelihood method as the tails of the underlying distribution get heavier or there is contamination in the distribution.

Baseflow data exhibit more or less similar patterns on monthly basis irrespective of year; that is, they are clustered by month. Unfortunately, the Wilcoxon rank-regression approach is not suited for dealing with models that contain cluster-correlated responses. Although the Wilcoxon rank-regression estimates remain unbiased, cluster correlation in the responses (and hence the random errors) tends to inflate the standard errors of the estimates from the model fit. This hinders our ability to detect true effects (low test power) of climate variability on baseflow. A recent extension of the Wilcoxon rank-regression method (Kloke et al., 2009), JRFit, uses joint ranking to obtain unbiased estimates of the effect sizes and robust sandwich estimates of the standard errors (White, 1982) for cluster-correlated data. Thus, JRFit provides an ideal approach for constructing robust models for linear processes with cluster correlated responses; hence, a powerful nonparametric technique for studying the dependence of baseflow on climate variability.

2.4. Results and Discussion

Since models with cluster correlated responses can also be thought of as mixed models (Pinheiro, and Douglas, 2000), they can be fitted using the maximum likelihood method in addition to JRFit. Skewness in baseflow data was corrected using the natural logarithmic transformation. Since baseflow data contained outliers and their shape was not Gaussian, JRFit was found to be the more efficient procedure. This was confirmed by comparing the estimates and standard errors obtained from the JRFit and maximum likelihood methods. Therefore, only the results of the JRFit procedure are provided and discussed. All results pertaining to baseflow are in the original scale following back-transformations using the exponential function. Results from individual and coupled analyses are provided below.

2.4.1. Individual Analyses

2.4.1.1. ENSO

The results of JRFit estimation for ENSO cycle are presented in Table 2.3. ENSO teleconnection with baseflow was found to be significant for all the selected USGS gauging stations ($p<0.05$). The differences in median baseflows between El Niño and La Niña phases were highly significant ($p<0.01$) except for the downstream station **F** which was not highly significant but significant ($p<0.05$) nonetheless. This could be due to the existence of a dam upstream of station **F**, thus incorporating anthropogenic controls on streamflows. As previously discussed, it is well-established that rainfall and streamflow in southeastern US are highly influenced by ENSO. The phases of El Niño and La Niña are associated with increased and decreased winter precipitation, respectively (Sharda et al., 2012; Johnson et al., 2013; Hoerling et al., 1997; Montroy et al., 1998).

Table 2.3. JRFit estimated median monthly baseflows and p-values of differences in baseflow during El Niño and La Niña phases.

Site Name	El Niño (m^3/s)	La Niña (m^3/s)	$N_{El\ Niño}^{n}$ / $N_{La\ Niña}^{n}$	P-value	% Increase La Niña to El Niño (m^3/s)
A	4.6	3.7	195/194	0.001	24
B	33.2	25.9	195/194	0.000	28
C	57.1	48.0	183/178	0.001	19
D	57.5	48.0	195/194	0.001	20
E	87.7	69.8	195/194	0.002	26
F	104.1	91.9	174/149	0.018	13

[n] Values indicate sample size for each phase

The results obtained from JRFit procedure also asserted a similar impact of ENSO on baseflow, whereby, baseflow increased during El Niño conditions and decreased during La Niña conditions. Across all stations, baseflow during El Niño conditions were approximately 22% higher on average than baseflow during La Niña conditions.

2.4.1.2. PDO

The results of JRFit estimation comparing the negative and positive phases of PDO are given in Table 2.4. Significance of the differences between medians of the two phases of PDO was not consistent across all stations.

Table 2.4. JRFit estimated median monthly baseflows and p-values of differences in baseflow during PDO positive and negative phases.

Site Name	Neg* (m^3/s)	Pos* (m^3/s)	N_{Neg}^{n}/N_{Pos}^{n}	P-value	% Increase positive to negative (m^3/s)
A	4.3	4.0	384/324	0.140	7
B	30.0	28.0	384/324	0.020	7
C	55.1	51.2	372/274	0.014	8
D	54.7	50.3	384/324	0.001	9
E	79.3	76.9	384/324	0.311	3
F	102.6	96.5	300/324	0.023	6

**Neg=Negative; Pos=Positive*
[n] Values indicate sample size for each phase.

Station **D** exhibited a highly significant ($p<0.01$) difference in the median baseflows of PDO negative and positive phases while stations **B**, **C** and **F** exhibited a significant difference ($p<0.05$). Stations **A** and **E** did not show any significant difference at the 10% level of significance. Baseflow generally decreased during PDO positive phases and increased during PDO negative phases showing an average increase of 7% across all stations during PDO negative phases compared to PDO positive phases.

2.4.1.3. AMO

The results pertaining to the comparison of the phases of AMO are presented in Table 2.5. The differences between the median baseflows of positive and negative phases of the AMO were found to be highly significant (Table 2.5). AMO teleconnection with baseflow was found to be consistent for all the stations ($p<0.001$). It is found that the negative phase of AMO results in increased baseflow compared to the positive phase of AMO with median baseflows approximately 23% higher during the negative phase compared to the positive phase. Numerous studies have found that the southern U.S. experiences warmer temperature and decreased precipitation patterns during the AMO positive phase, whereas, an increase in precipitation during the negative phase.

Table 2.5. JRFit estimated median monthly baseflows and p-values of differences in baseflow during AMO positive and negative phases.

Site Name	Neg* (m^3/s)	Pos* (m^3/s)	N_{Neg}^n/N_{Pos}^n	P-value	% Increase positive to negative (m^3/s)
A	4.9	3.4	372/336	0.000	43
B	32.2	25.2	372/336	0.000	28
C	56.0	50.3	372/274	0.001	11
D	56.4	48.4	372/336	0.000	17
E	85.3	70.5	372/336	0.000	21
F	103.7	88.1	372/252	0.000	18

**Neg=Negative; Pos=Positive*

[n] Values indicate sample size for each phase.

In a study by Enfield et al. (2001), the ACF River Basin has shown mostly negative correlations with summer precipitation during the AMO positive phase leading to dry summers in this region. Tootle et al. (2005) also found similar patterns in streamflow in southeastern United States. The JRFit results show that the same pattern holds for baseflow in the ACF River Basin.

2.4.1.4. NAO

Significant differences were observed between median baseflows of the positive and negative phases of NAO (Table 2.6).

Table 2.6. JRFit estimated median monthly baseflows and p-values of differences in baseflow during NAO positive and negative phases.

Site Name	Neg* (m^3/s)	Pos* (m^3/s)	N_{Neg}^n/N_{Pos}^n	P-value	% Increase positive to negative (m^3/s)
A	4.9	3.7	300/408	0.000	31
B	33.7	26.8	300/408	0.000	26
C	58.3	50.2	300/346	0.000	16
D	58.7	48.8	300/408	0.000	20
E	84.2	73.8	300/408	0.004	14
F	108.0	92.1	240/384	0.000	17

**Neg=Negative; Pos=Positive*

[n] Values indicate sample size for each phase.

It was found that the NAO negative phase results in approximately 23% higher median baseflow compared to the NAO positive phase. Hurrell et al. (2003) made a similar observation regarding southeastern US winter precipitation which showed a significant decrease during the positive NAO phase.

Figure 2.2 contains a visual description of the p-values for the different stations, where the height of the bars are computed as the respective p-values subtracted from one. Therefore, the

higher the bar, the more significant the effect of the phenomenon is. The significance of the effect of PDO on baseflow was found to be inconsistent across stations.

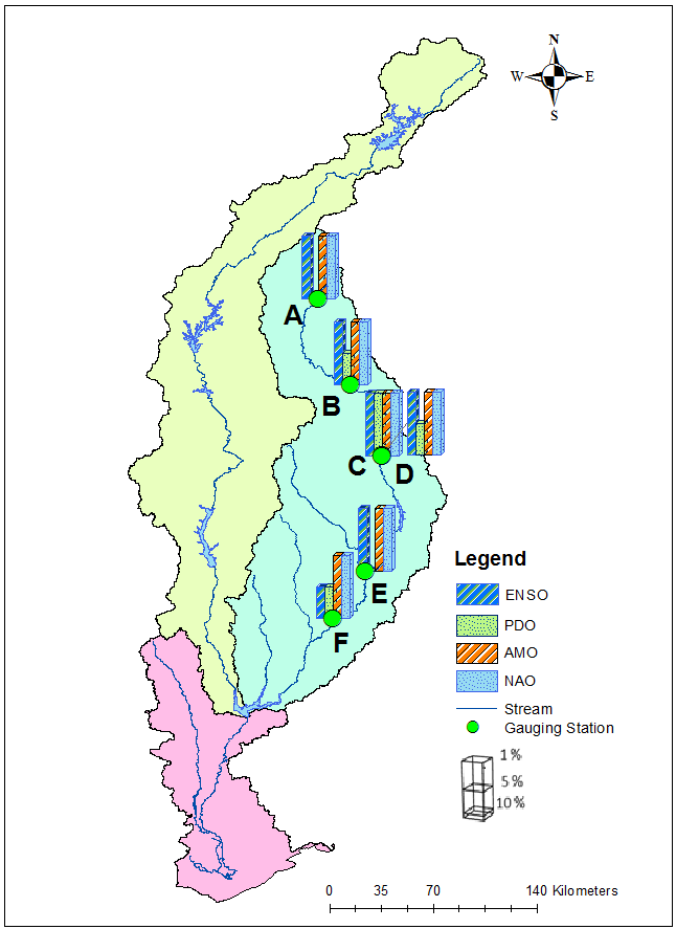

Figure 2.2. Significance of individual analyses for phases of ENSO, PDO, AMO and NAO at the level of 1%, 5% and 10% for each station. Taller bars represent smaller p-values.

2.4.1.5. Graphical Summary of Individual Analyses

Figure 2.3 provides comparison box and whisker plots describing the percentage change in median baseflow of the phases of ENSO, PDO, AMO and NAO for the six stations as compared to the respective station medians. It was found that baseflow decreased by approximately 10% during La Niña and negative phases of AMO and NAO while increased by 10% during El Niño and positive phases of AMO and NAO as compared to the long term medians.

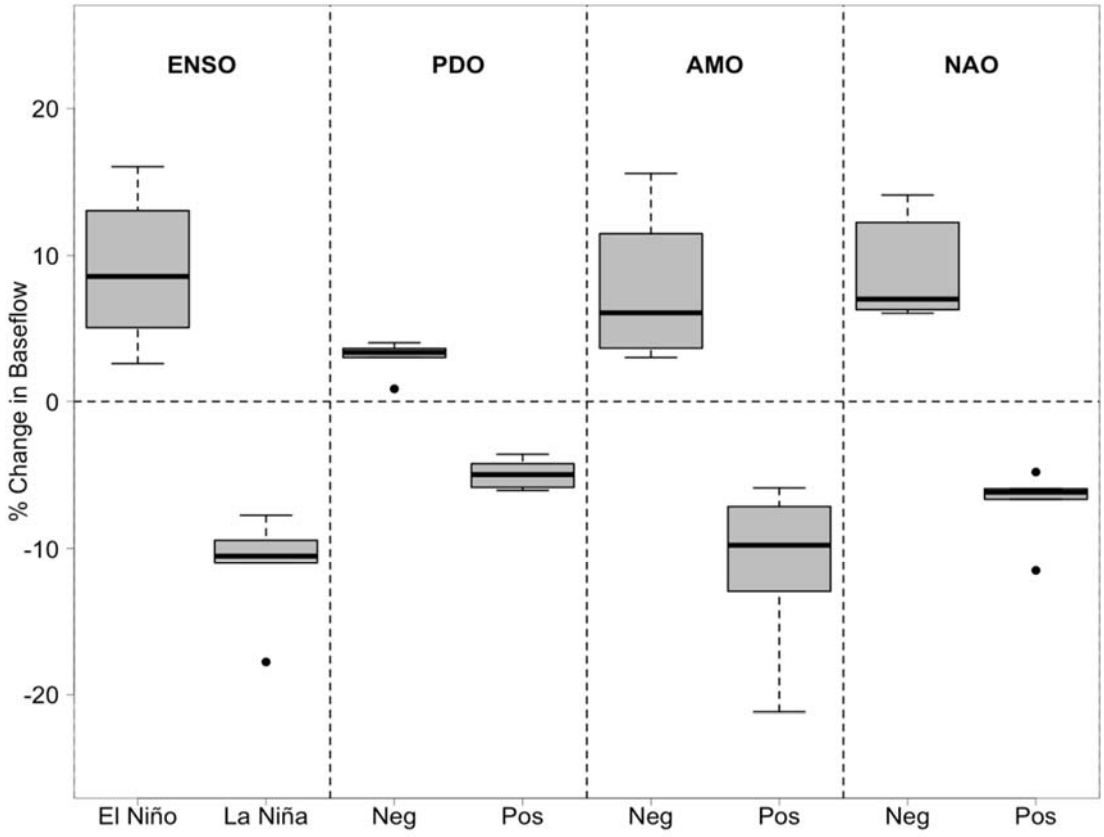

Figure 2.3. Box and whisker plots of percent increase/decrease in baseflows across all six stations due to individual effects of the phases of ENSO, PDO, AMO and NAO. The boundaries of the box represent the first (Q1) and third (Q3) quartiles and the whiskers extend from the boundaries of the box to the extreme data points which are no more than 1.5 times the interquartile range (Q3 - Q1).

It is also observed that baseflow medians of phases of ENSO, AMO and NAO are significantly different from the long term median while individual PDO phases did not show substantial difference from long term median. However, the significant differences obtained from different phases of PDO, AMO and NAO might be due to their interaction with ENSO. Therefore, coupled analyses were performed examining the interactive effect of ENSO with PDO, AMO and NAO in order to understand the fluctuations of El Niño and La Niña phases during the phases of decadal and multi-decadal climate variability.

2.4.2. Coupled Analyses

2.4.2.1. PDO – ENSO Interaction

To verify the interactive effect of PDO and ENSO on baseflow, linear models with PDO-ENSO interaction term (see, for example, eq. (3)) were estimated using the JRFit procedure. The estimated coefficients of the interaction term in the linear model and its significance tests (interaction tests) showed strong interaction ($p<0.01$) of PDO and ENSO for all stations except station **A** (significant at the 10% level). The statistical significance of the interaction of PDO and ENSO found here confirms observations made by several studies that PDO and ENSO exhibit similar spatial pressure, wind, temperature and precipitation patterns but possess vastly different temporal patterns (Mantua and Hare, 2002). The presence of significant interaction indicates possibly heterogeneous modulation of the phases of ENSO by negative and positive phases of PDO. Thus, following the interaction test, simple-main effect comparisons were performed by comparing the phases of PDO for each phase of ENSO using JRFit. Table 2.7 contains the results of these simple-main effect comparisons. The results showed no significant differences between the median baseflow of PDO negative and PDO positive associated with El Niño for the four upstream stations. Contrary to the result in individual analysis, it was found that El Niño baseflows were higher during positive phase of PDO for the remaining two downstream stations. However, significant differences ($p<0.05$) were found across all stations between the median baseflows of negative and positive phases PDO associated La Niña where baseflows were higher during negative phases of PDO. The lack of significant PDO-ENSO interaction for station **A** could perhaps be explained by the slightly elevated p-value ($p=0.028$) that is not in line with all the other stations ($p<0.01$). It is found that La Niña phase associated with positive PDO showed greater decrease in baseflow, approximately 28%, than average/individual La Niña (Figure 2.4).

Table 2.7. Simple-main effect comparisons of baseflow medians for El Niño and La Niña phases combined with positive and negative phases of PDO.

Site Name	Interaction p-value	PDO									
		El Niño					La Niña				
		Neg[a] (m^3/s)	Pos[a] (m^3/s)	N_{Neg}[b]/ N_{Pos}[b]	P-value	Neg/ Pos	Neg[c] (m^3/s)	Pos[c] (m^3/s)	N_{Neg}[d]/ N_{Pos}[d]	P-value	Neg/ Pos
A	0.0929	4.8	4.8	107/88	0.983	1.00	3.7	3.1	140/54	0.028	1.21
B	0.0010	32.3	33.8	107/88	0.344	0.96	27.5	20.2	140/54	0.000	1.36
C	0.0015	56.6	61.2	107/76	0.072	0.92	50.7	40.0	134/44	0.001	1.27
D	0.0005	56.6	58.6	107/88	0.365	0.97	51.4	38.8	140/54	0.000	1.32
E	0.0003	81.9	97.7	107/88	0.001	0.84	74.2	57.5	140/54	0.001	1.29
F	0.0000	92.9	114.9	86/88	0.000	0.81	103.1	70.4	95/54	0.000	1.46

[a] *El Niño phase baseflows associated with negative and positive phases of PDO.*
[b] *Sample sizes for negative and positive phases of PDO associated with El Niño phase baseflows.*
[c] *La Niña phase baseflows associated with negative and positive phases of PDO.*
[d] *Sample sizes for negative and positive phases of PDO associated with La Niña phase baseflows.*

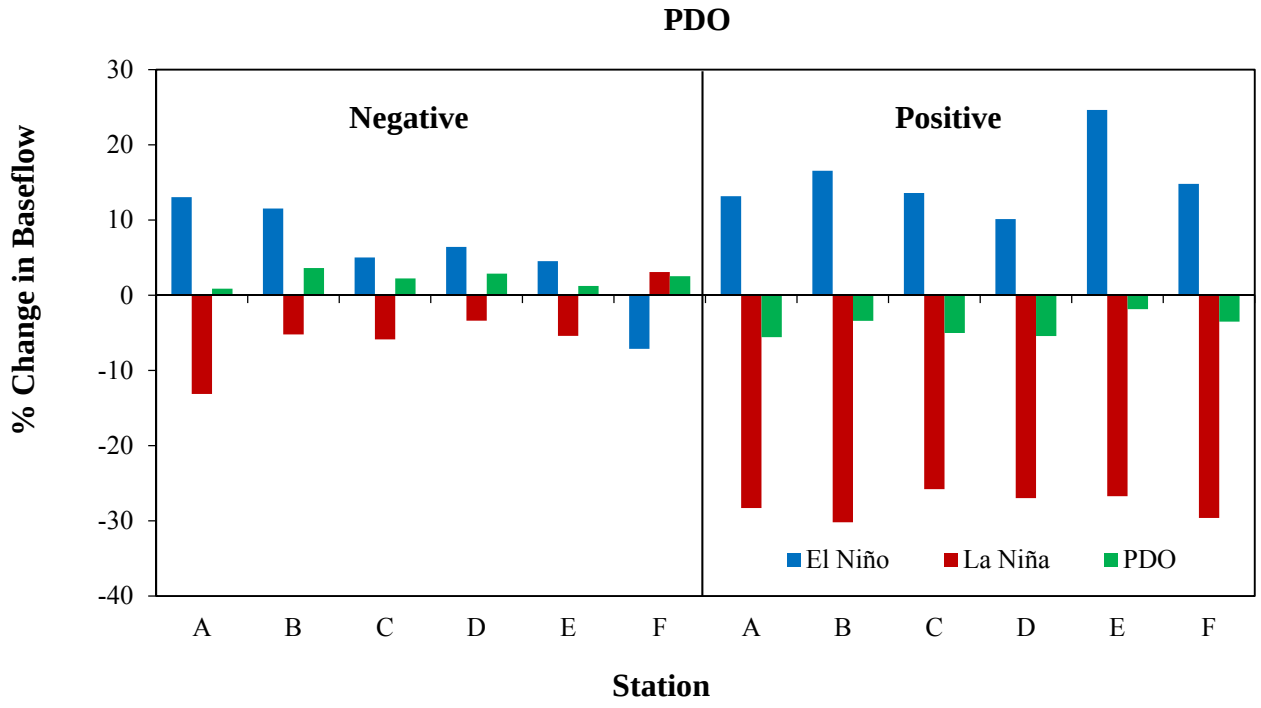

Figure 2.4. Percent change in median baseflows for El Niño and La Niña phases when they are associated with positive and negative phases of PDO. Also shown (green bars) are the median baseflows associated with PDO phase alone.

The modulation of La Niña during PDO positive phase might be due to the southerly shift of the jet stream during PDO positive phase that affects the southern United States (Mantua and Hare, 2002). Significant differences were not seen between El Niño and La Niña baseflows during PDO negative phase for stations **C**, **D** and **E** (results not provided) since PDO negative/El Niño and PDO negative/La Niña baseflow values were low.

2.4.2.2. AMO – ENSO Interaction

JRFit was used to estimate the linear model (equation 3) and test the AMO-ENSO interaction. The estimated interaction coefficients were significant ($p<0.05$) for all stations. This suggests that the effect of the phases of ENSO on baseflow is heterogeneous depending on the phases of AMO. The results obtained from simple-main effect comparisons using JRFit are presented in Table 2.8.

Table 2.8. Simple-main effect comparisons of baseflow medians for El Niño and La Niña phases combined with positive and negative phases of AMO.

Site Name	Interaction p-value	AMO									
		El Niño					La Niña				
		Neg[a] (m^3/s)	Pos[a] (m^3/s)	N_{Neg}[b]/ N_{Pos}[b]	P-value	Neg/ Pos	Neg[c] (m^3/s)	Pos[c] (m^3/s)	N_{Neg}[d]/ N_{Pos}[d]	P-value	Neg/ Pos
A	0.0000	4.9	4.6	106/89	0.279	1.07	5.1	2.5	93/101	0.000	2.05
B	0.0000	33.6	33.2	106/89	0.780	1.01	32.6	18.3	93/101	0.000	1.78
C	0.0000	55.2	60.0	106/77	0.118	0.92	57.3	38.2	93/85	0.000	1.50
D	0.0001	55.4	58.3	106/89	0.260	0.95	57.9	37.9	93/101	0.000	1.53
E	0.0003	86.2	87.2	106/89	0.862	0.99	84.0	53.6	93/101	0.000	1.57
F	0.0134	104.5	96.9	106/89	0.208	1.08	106.3	69.8	93/56	0.002	1.52

[a] *El Niño phase baseflows associated with negative and positive phases of AMO.*
[b] *Sample sizes for negative and positive phases of AMO associated with El Niño phase baseflows.*
[c] *La Niña phase baseflows associated with negative and positive phases of AMO.*
[d] *Sample sizes for negative and positive phases of AMO associated with La Niña phase baseflows.*

No significant differences in baseflows were observed between the phases of AMO associated with El Niño phase. That is, El Niño phase baseflows were not influenced by the phases of AMO. However, highly significant differences ($p<0.01$) were found across all stations between the median baseflows of AMO negative and AMO positive associated with La Niña. This implies that median baseflow of La Niña is highly influenced by the phases of AMO.

La Niña events that occurred during AMO positive phase resulted in below normal baseflow, approximately 33%, than average/individual La Niña phase (Figure 2.5). However, AMO negative phase associated with La Niña resulted in above normal baseflows for all the stations by modulating the effect of La Niña (Figure 2.5). It was also determined that, during the negative phase of AMO, there was no significant difference between El Niño and La Niña phase baseflow patterns.

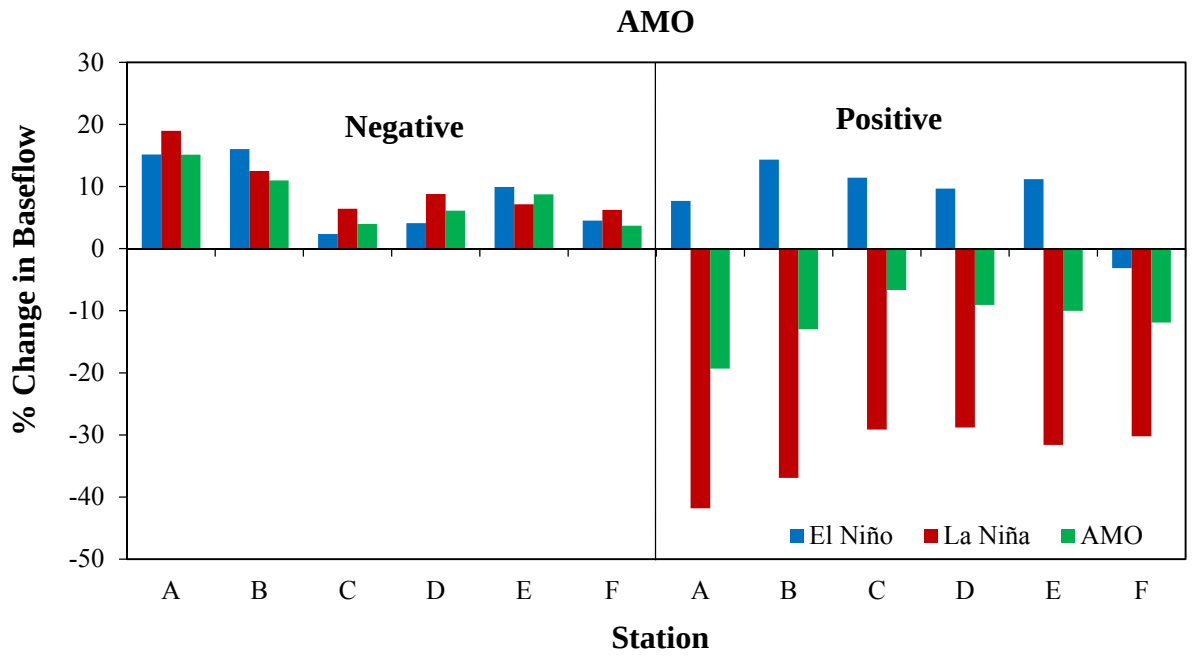

Figure 2.5. Percent change in median baseflows for El Niño and La Niña phases when they are associated with positive and negative phases of AMO. Also shown (green bars) are the median baseflows associated with AMO phase alone.

Tootle et al. (2005) have also noticed a similar pattern of influence of the phases of AMO on the effect of La Niña on streamflow in the southeastern US and acknowledged that La Niña events which occurred during the positive phase of AMO resulted in below normal precipitation and streamflow, thus increasing the severity of droughts in the southeastern US. They also observed that the AMO negative phase dominates the effect of La Niña where above normal streamflow is seen even during La Niña phases. This modulation of La Niña during the negative phase of AMO in the southeastern US might be due to greater impact of SST variability in the Atlantic Ocean which is located adjacent to the region.

2.4.2.3. NAO – ENSO Interaction

Similarly, the interactive effects of NAO and ENSO on baseflow were examined across all six stations by estimating the interaction term in the linear model (eq. (3)). The results obtained from significance test of estimated coefficients of the interaction term showed that NAO and ENSO do not interact with each other except for stations **A** and **F** (at 5% and 1% level of significance, respectively) (Table 2.9). The coupled effects of NAO and ENSO were evaluated by performing simple-main effect comparisons between the negative and positive phases of NAO within the phases of ENSO (Figure 2.6). The results obtained from the simple-main effect comparisons between positive and negative phases of NAO within El Niño were not consistent across all the stations.

Table 2.9. Simple-main effect comparisons of baseflow medians for El Niño and La Niña phases combined with positive and negative phases of NAO.

Site Name	Interaction p-value	NAO									
		El Niño					La Niña				
		Neg[a] (m^3/s)	Pos[a] (m^3/s)	N_{Neg}[b]/ N_{Pos}[b]	P-value	Neg/ Pos	Neg[c] (m^3/s)	Pos[c] (m^3/s)	N_{Neg}[d]/ N_{Pos}[d]	P-value	Neg/ Pos
A	0.0180	5.4	4.4	94/101	0.003	1.22	3.5	3.5	60/134	0.987	1.00
B	0.3611	34.8	29.45	94/101	0.029	1.18	27.9	25.3	60/134	0.241	1.10
C	0.1151	58.7	52.7	94/89	0.080	1.11	49.3	48.1	60/118	0.664	1.03
D	0.2008	59.5	52.7	94/101	0.039	1.13	50.9	48.0	60/134	0.343	1.06
E	0.9141	88.2	85.2	94/101	0.561	1.04	70.5	68.9	60/134	0.790	1.02
F	0.0000	98.2	107.8	79/95	0.088	0.91	142.2	86.5	28/121	0.000	1.64

[a] *El Niño phase baseflows associated with negative and positive phases of NAO.*
[b] *Sample sizes for negative and positive phases of NAO associated with El Niño phase baseflows.*
[c] *La Niña phase baseflows associated with negative and positive phases of NAO.*
[d] *Sample sizes for negative and positive phases of NAO associated with La Niña phase baseflows.*

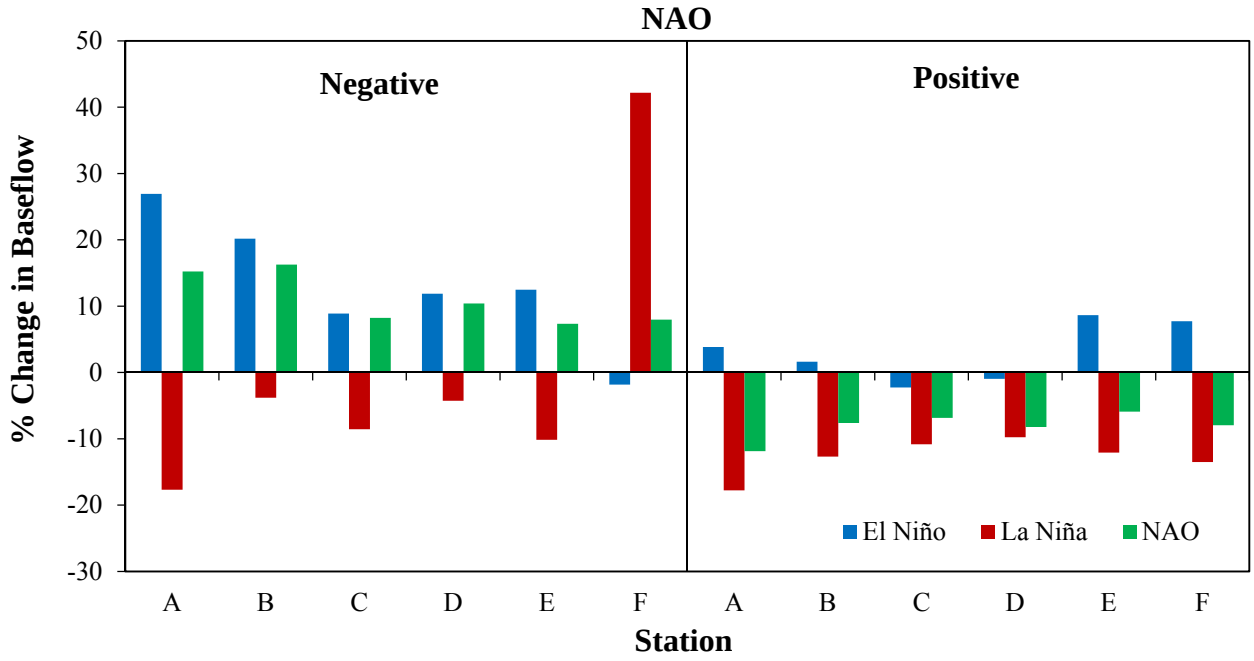

Figure 2.6. Percent change in median baseflows for El Niño and La Niña phases when they are associated with positive and negative phases of NAO. Also shown (green bars) are the median baseflows associated with NAO phase alone.

However, no significant differences were found between negative and positive phases of NAO associated with La Niña baseflows across all the stations. Therefore, the estimation of negative and positive phases of NAO obtained from individual analysis might be accurate due to the absence of NAO-ENSO interaction in this region.

2.4.2.4. Graphical Summary of Coupled Analyses

Figure 2.7 represents the percentage change (relative to station median baseflow) in El Niño and La Niña baseflow medians coupled with the phases of PDO, AMO, and NAO for all six stations.

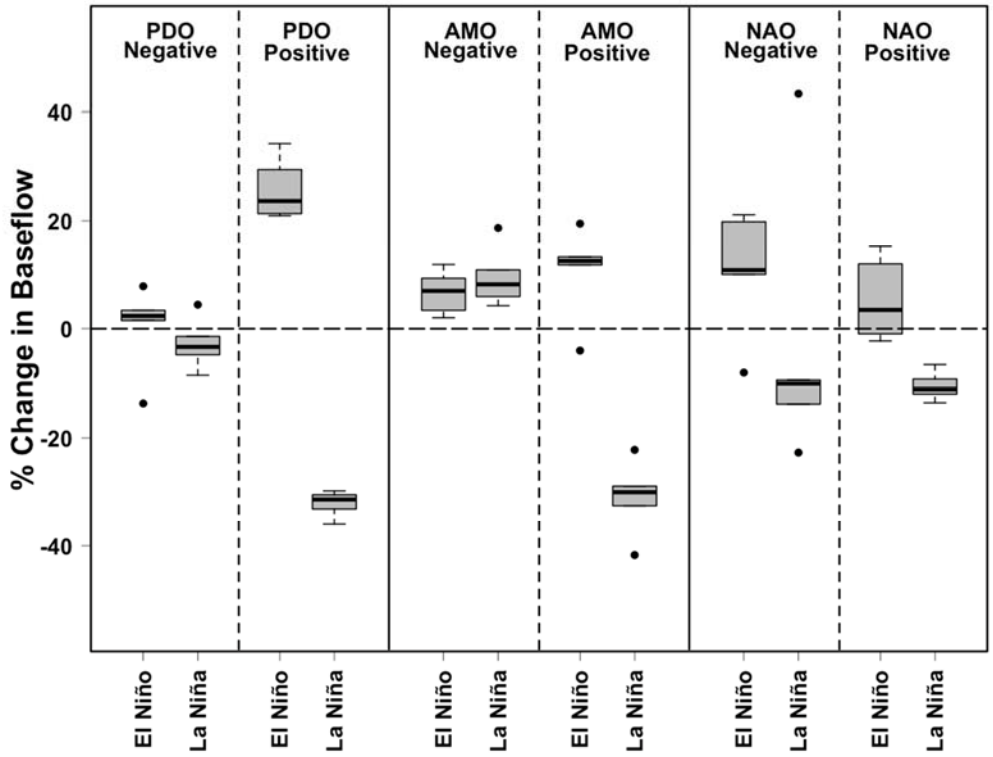

Figure 2.7. Box and whisker plots of the percent increase/decrease in baseflows for all six stations. The boundaries of the box represent the first (Q1) and third (Q3) quartiles and the whiskers extend from the boundaries of the box to the extreme data points which are no more than 1.5 times the interquartile range (Q3 - Q1).

This figure clearly depicts how El Niño and La Niña are influenced by decadal/interdecadal climate variability. It was observed that La Niña coupled with the positive phases of AMO and PDO results in greater decrease in baseflow and such periods are associated with severe droughts in this region. La Niña coupled with the negative phase of AMO, however, results in an above normal baseflow pattern which is a departure from the usual effect of La Niña on baseflow. The modulations of El Niño and La Niña baseflow are displayed in figures 2.8(a) and 2.8(b), respectively.

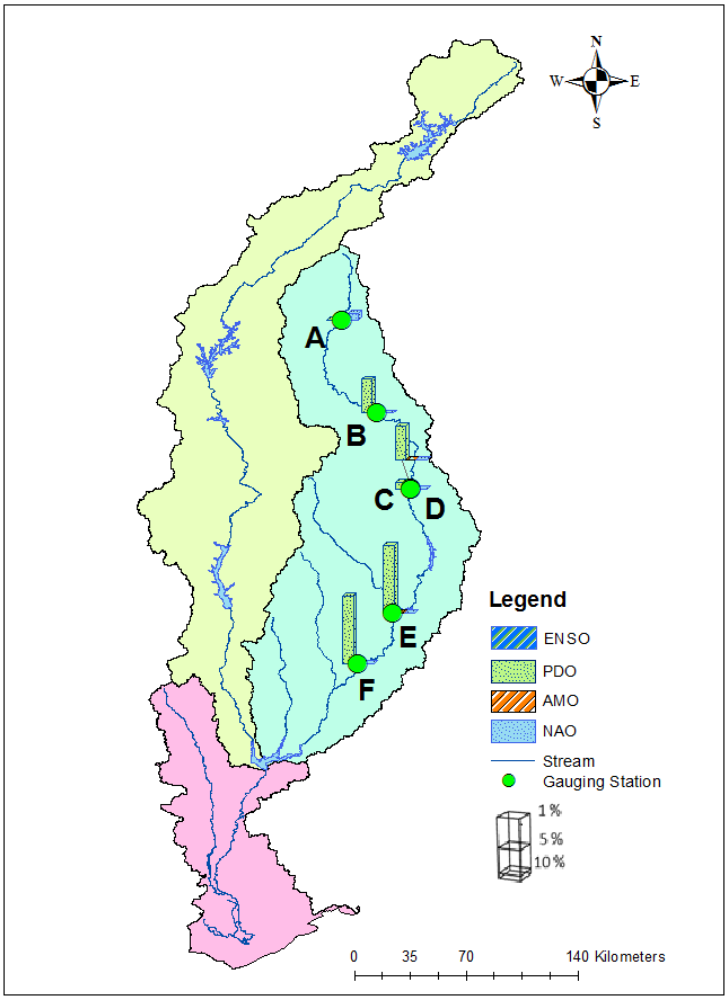

Figure 2.8(a). Significance of differences in El Niño baseflows during the positive and negative phases of PDO, AMO and NAO at the level of 1%, 5% and 10% for each station. Taller bars represent smaller p-values.

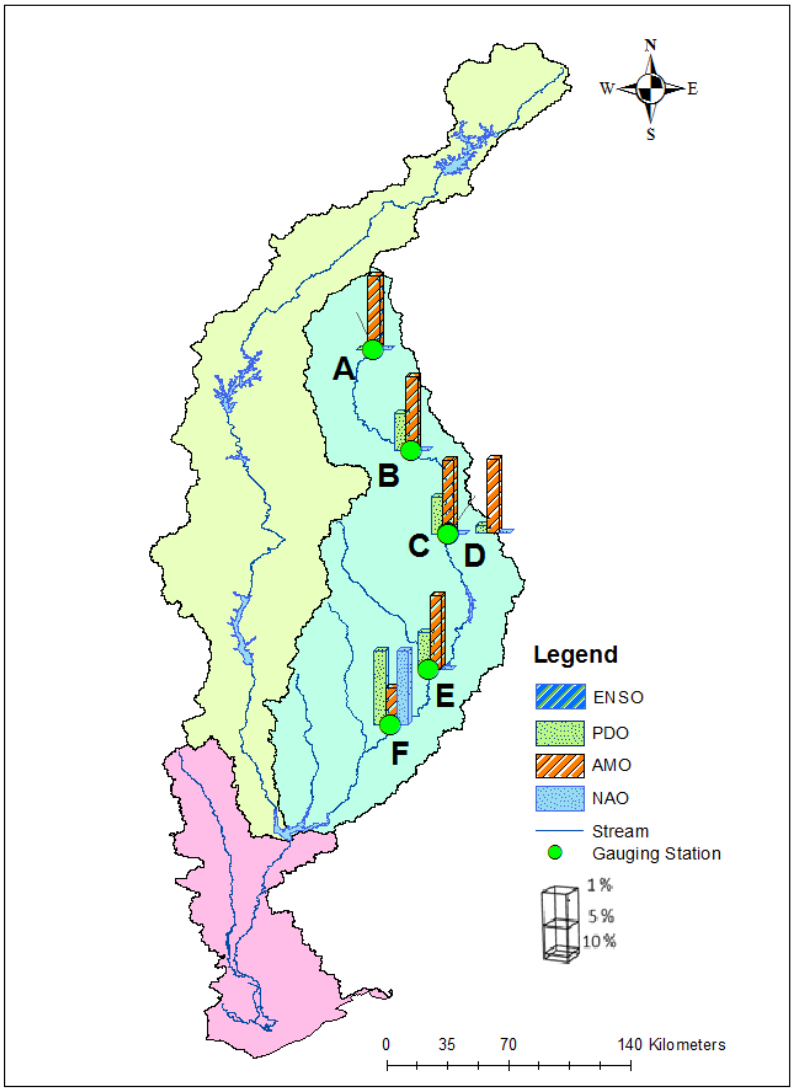

Figure 2.8(b). Significance of differences in La Niña baseflows during the positive and negative phases of PDO, AMO and NAO at the level of 1%, 5% and 10% for each station. Taller bars represent smaller p-values.

2.5. Conclusions

This study explored the relationships between interdecadal and interannual climate variability phenomena on basin level baseflow. The non-parametric JRFit procedure was used to identify and quantify the individual and coupled effects of climate variability phenomena on historic baseflow of the Flint River. Study of the individual effects of ENSO, PDO, AMO and

NAO showed that the phases of ENSO, AMO and NAO had significant impact on baseflow; however, the effect of the phases of PDO was not statistically significant. It was found that baseflow decreased by approximately 10% during La Niña as well as negative phases of AMO and NAO while it increased by approximately 10% during El Niño and positive phases of AMO and NAO as compared to long term median baseflows measured at each station.

Coupled analysis of the effect of ENSO-PDO, ENSO-AMO and ENSO-NAO on baseflow provided interesting relationship patterns. The interactive effect of the phases of ENSO-PDO and ENSO-AMO on baseflow was found to be highly significant. However, the interactive effect of the phases of NAO and ENSO on baseflow was not found to be statistically significant. In particular, during the PDO positive phase, occurrence of La Niña results in greater decrease in baseflow and this can cause severe drought in the ACF River Basin. Similarly, the occurrence of a La Niña event during an AMO positive phase leads to greater decrease in baseflow, thus causing drought in the ACF River Basin. Therefore, the study indicates that the effect of La Niña in the ACF River Basin is intensified by the positive phases of PDO and AMO. However, although La Niña periods are generally associated with below normal baseflow, this was found to not be the case when La Niña occurred during the negative phase of AMO. The negative effect of La Niña on baseflow appeared to have been mitigated by the effects of the negative phase of AMO resulting in above normal baseflows. During the AMO negative phase, baseflow exhibited similar patterns regardless of the fact that the period was El Niño or La Niña, suggesting that AMO suppresses the effect of ENSO.

The above results give credence to the importance of examining the coupled effect of ENSO and inter-decadal climate variability phenomena. Incorporating accurate information on the phases of multidecadal cycles in the analyses of ENSO-induced droughts can help provide a clearer

picture of the severity of droughts and their impact on baseflow. This can in turn help inform water management policy and promote severity-based water restrictions in the study area. Therefore, policy makers trying to resolve the Tri-State Water Conflict may benefit from considering both interannual (i.e., ENSO) as well as multidecadal (i.e., PDO and AMO) climate variability phenomena.

Chapter 3

Powerful Nonparametric Analysis for Cluster-Correlated Climate and Hydrologic Data

3.1. Abstract

Analysis of climatic and hydrologic datasets such as temperature, precipitation, streamflow and baseflow are presently done using the non-parametric Wilcoxon-Rank Sum (WRS) test since these datasets do not follow Gaussian distribution due to the presence of outliers and heavy tails. However, these datasets exhibit monthly and/or seasonal clustering which is not accounted for in the WRS non-parametric test. Therefore, in this study, a novel non-parametric procedure called Joint Rank Fit (JRFit) has been studied for cluster correlated data and compared with traditional methods of restricted maximum likelihood, least absolute deviations, and the nonparametric Wilcoxon rank-sum method. The results show that JRFit provides more efficient result than all three other methods for clustered data with heavier tails (or data with outliers) or strong correlation. This novel procedure JRFit can be used in future to account for the clustering of the data and possibly avoid erroneous conclusions that might be derived through WRS tests.

3.2. Introduction

Natural ocean-atmospheric climate variability phenomena such as ENSO, PDO, AMO and NAO affect temperature and precipitation on interannual, decadal, multidecadal time scale. These climatic oscillations are also responsible for extreme events such as floods, droughts, hurricanes,

and cold waves (IPCC, 2001) across the world. Several studies have found strong influence of climate variability phenomena on meteorological variables and components of hydrologic cycle in many parts of the world. Therefore, understanding the climate variability phenomena and their interactions with metereological and hydrologic processes is essential to mitigate their adverse effects on water resources (Climate Research Committee and National Research Council, 1995).

These climatic oscillations are the periodic warming and cooling of SST and have strong influence on temperature and precipitation across the world including the Southeast US (Diaz and Markgraf, 1992; Chiew et al., 1998; Keener et al., 2007; Roy, 2006). Moreover, several studies have shown that these climatic oscillations exhibit strong tele-connections with precipitation, streamflow, baseflow and groundwater in the Southeast USA.

Most of these studies use non-parametric analysis procedures such as WRS test since they make no assumption on data normality and they are resistant to adverse effects of outliers. Since hydrologic data sets are not typically normally distributed and exhibit outliers, non-parametric procedures provide a promising approach to minimize the influence of outliers and for non-normality. However, as Galbraith et al. (2010) demonstrated, despite its robustness, the performance of WRS is suboptimal when the data exhibit clustering. In practice, in addition to outliers and heavy tails, meteorological variables such as temperature and precipitation and hydrologic components such as streamflow, baseflow and groundwater exhibit monthly or seasonal clustering. Their values tend to be similar on a monthly or seasonal basis, irrespective of year, leading to intra-cluster correlations that tend to be positive.

The common approach employed for studying phenomena that include correlated responses including cluster-correlation is through the use of linear mixed effect (LME) models. This approach was followed in this study to quantify and test the impact of individual and coupled

climate variability phenomena on baseflow. Typically, the fitting of LMEs involves the use of the parametric restricted maximum likelihood (REML) method under the assumption that the responses are derived from the Gaussian distribution. REML is appealing since it allows one to not only test for significance of effects but also estimate effect sizes simultaneously by fitting a mixed linear model. As discussed above, the assumption that the responses follow the Gaussian distribution may not be appropriate for climate related data prompting the use of WRS for testing impact. However, since clustering leads WRS to perform poorly, there is a need for techniques that are robust like WRS while handling the within cluster correlation appropriately. For this reason, Datta and Satten (2010) proposed a WRS test for cluster-correlated data. While this test is appropriate for clustered responses and is as robust as WRS for non-Gaussian data, it does not allow us to test for coupled effects or include other explanatory variables, as there is no model estimated.

Joint Rank Fit (JRFit) gives a genuine nonparametric alternative to REML for fitting LME models. It evolved from the formulation of the WRS method as a linear model to allow for simultaneous estimation and testing of effects. Hodges and Lehmann (1963) defined a rank-score point estimate of effect for two-sample problems whose test of significance is equivalent to WRS. Adichie (1967) studied an extension to the simple linear regression of the Hodges-Lehmann estimate. Jureckova (1971) and Jaeckel (1972) further extended this to multiple linear regression models with independent data. Jaeckel (1972) also showed that the model fitting procedure involve minimization of a convex objective function. This was later extended to LME models by Kloke et al. (2009) under the name JRFit. In the discussion below, a brief review of this progression is given while focusing on efficiency considerations. For a more detailed and technical approach regarding

rank methods, one may refer to the manuscript by Hettmansperger and McKean (2011). An R language implementation is given in Kloke and McKean (2014).

The results of a Monte Carlo simulation experiment is presented in this study that demonstrates the efficiency of JRFit. This experiment is set up to mimic the baseflow data but with seasonal clustering instead of monthly clustering to simplify the discussion.

3.3. Statistical Methods

3.3.1. The Two-Sample Problem

Suppose that we have two samples $U_1, \ldots, U_m$ and $V_1, \ldots, V_n$ from two populations represented by distribution functions $F(\cdot)$ and $F(\cdot - \Delta)$, respectively. That is, the populations differ by location only and we can get the U sample by shifting the V sample by Δ. Assume that the variance of F exists and is given by σ_F^2. Generally, U and V represent untreated and treated populations and the quantity Δ is commonly known as the treatment effect. We are generally interested in testing the null hypothesis $H_0: \Delta = 0$ versus the alternative $H_A: \Delta \neq 0$, $H_A: \Delta > 0$, or $H_A: \Delta < 0$. The classical test for such a problem is the two-sample t-test that uses the test statistic

$$T = \frac{\bar{V} - \bar{U}}{S\sqrt{1/m + 1/n}}$$

where S is the pooled standard deviation of the two samples. Under certain regularity conditions, T has an asymptotic t distribution with $n + m - 2$ degrees of freedom and for large n and m, this is approximated by the standard Gaussian distribution. The associated estimator of the treatment effect Δ is

$$\widehat{\Delta} = \bar{V} - \bar{U}$$

and $\widehat{\Delta}$ is approximately Gaussian with mean Δ and variance $\sigma_F^2\left({}^1/_m + {}^1/_n\right)$.

The *t* test and the associated estimator of Δ are optimal when the data source F is the Gaussian distribution. However, several studies have demonstrated that both the test and estimator are sensitive to outliers and heavy-tails in the data source. Thus, as mentioned above, investigators have proposed to use Wilcoxon rank-sum (WRS) test over the *t* test for the analysis of climate data due to outliers in data and heavy tailed or skewed data-generating distributions that are prevalent in climate data (Tootle et al., 2005; Johnson et al., 2013).

The WRS test proceeds by ranking all the data ($U_1, \dots, U_m$ and $V_1, \dots, V_n$) together from the smallest (rank 1) to the largest (rank $m + n$). The WRS statistic is then the sum of the ranks of the V sample given by

$$W = R(V_1) + \cdots + R(V_n).$$

Similar to the t statistic, W has an asymptotic representation where

$$\frac{W - \frac{n(m+n+1)}{2}}{\sqrt{\frac{mn(m+n+1)}{12}}}$$

follows an asymptotic standard Gaussian distribution. The estimator of the treatment effect associated with the WRS is the Hodges-Lehmann estimator given by

$$\tilde{\Delta} = median\left(V_i - U_j\right), \qquad 1 \le i \le n;\ 1 \le j \le m$$

and $\tilde{\Delta}$ is approximately Gaussian with mean Δ and variance $\tau_F^2\left({}^1/_m + {}^1/_n\right)$, where

$$\tau_F^2 = \frac{1}{12}\left(\int f^2(t)dt\right)^{-2}$$

and, $$f(t) = \frac{dF(t)}{dt}.$$

Based on the asymptotic distributions of T and W ($\widehat{\Delta}$ and $\tilde{\Delta}$), we can study the asymptotic relative efficiency (ARE) of W ($\tilde{\Delta}$) with respect to T ($\widehat{\Delta}$). The ARE represents the relative sample size required by the t test to attain the same power as the WRS test in detecting the same treatment effect. More efficient tests will use smaller samples to achieve the same test power. The ARE is represented as the reciprocal of the variance ratio of the two test statistics. Thus, the ARE of the WRS test with respect to the t test is

$$ARE(W,T) = \frac{\sigma_F^2}{\tau_F^2}$$

If F is Gaussian with mean 0 and variance σ_F^2, then we can compute

$$\tau_F^2 = \frac{\pi}{3}\sigma_F^2$$

and

$$ARE(W,T) = \frac{3}{\pi} \approx 0.955.$$

Thus, under ideal situations where the underlying distribution is Gaussian, the t test needs 95.5% of the sample size the WRS needs to attain the same test power. That is, the t test is slightly more efficient. However, the AREs of WRS to the t test under the logistic and *t* distribution with 5 degrees of freedom error distributions are 1.096, and 1.241, respectively. Thus, with heavier tails, the WRS is more efficient.

3.3.2. Linear Models

3.3.2.1. The Two-Sample Problem as Simple Linear Regression

Although the two sample WRS test is ideal for dealing with data sources that may be heavy tailed or contain contamination, it is not appropriate for studies that have more than one treatment or that contain covariates in addition to the treatment. We will consider a generalization of the WRS to the linear model first proposed by Jaeckel (1972). To motivate this, we go back to the two-sample problem and express it as a linear model estimation/testing problem. Combine the two samples as $(Z_1, \dots, Z_{m+n}) = (U_1, \dots, U_m, V_1, \dots, V_n)$ and consider the model

$$Z_k = \alpha + \Delta x_k + \varepsilon_k, \qquad 1 \le k \le m + n$$

where ε_k are random errors that are independently and identically distributed (iid) according to F centered at 0 and

$$x_k = \begin{cases} 0, & 1 \le k \le m \\ 1, & m + 1 \le k \le m + n \end{cases}$$

Thus the U sample is centered at α and the V sample is centered at $\alpha + \Delta$.

The most common approach of fitting model is via minimization of a norm based on the model residuals $e_k(\alpha, \Delta) = Z_k - \alpha - \Delta x_k$. If focus is on the estimation and testing of the treatment effect Δ, then one may relax this to a minimization of a pseudo-norm based on the residuals $e_k(\Delta) = Z_k - \Delta x_k$. A pseudo-norm satisfies all the properties of a norm except that the norm becomes zero if all the residuals are equal and not necessarily all zero.

The least squares estimator of (α, Δ) are found by finding minimizing the Euclidean norm on the $m + n$ dimensional space

$$\|\boldsymbol{e}(\alpha,\Delta)\|_2^2 = \sum_{k=1}^{m+n}\{e_k(\alpha,\Delta)\}^2.$$

One can easily find the least squares estimators to be $\widehat{\Delta} = \frac{\sum(x_k-\bar{x})Z_k}{\sum(x_k-\bar{x})^2} = \bar{V} - \bar{U}$ and $\hat{\alpha} = \bar{Z} - \widehat{\Delta}\bar{x} = \bar{U}$.

Similar to the WRS test, Jaeckel's (1972) approach starts out by ranking a combined sample. However, instead of ranking the raw data, it ranks the residuals $e_k(\Delta)$ as $R(e_1(\Delta)), \ldots, R(e_{m+n}(\Delta))$. Of course, these are unobservable since Δ is unknown; however, they can be used to construct a 'norm' similar to the Euclidean norm above. Jaeckel proposed to minimize the *rank dispersion function* given by

$$D_\varphi(\Delta) = \sum_{k=1}^{m+n}\varphi\left(\frac{R(e_k(\Delta))}{m+n+1}\right)e_k(\Delta).$$

Here φ is the so-called score generating function that is a nondecreasing, continuous function defined on (0,1). It is usually standardized so that $\int_0^1 \varphi(t)dt = 0$ and $\int_0^1 \varphi^2(t)dt = 1$.

Jaeckel established that D_φ is positive, continuous, and convex as a function of Δ. Schrader and McKean (1980) showed that $D(\Delta)$ defines a pseudo-norm $\|\boldsymbol{e}(\Delta)\|_*$ on the $m+n$ dimensional space. Because it is a pseudo-norm, $\|\boldsymbol{e}(\Delta)\|_* = \|\boldsymbol{e}(\alpha,\Delta)\|_*$ as it is invariant to constant translations. So, it cannot be used to estimate the intercept term α. Denote the minimizer of $D_\varphi(\Delta)$ by $\widetilde{\Delta}_\varphi$. Since $\int_0^1 \varphi(t)dt = 0$, we estimate α using the median of the estimated residuals as $\tilde{\alpha}_\varphi = median\{e_k(\widetilde{\Delta}_\varphi)\}$. Analogously, one may note that the least squares estimate of the intercept $\hat{\alpha} = \bar{Z} - \widehat{\Delta}\bar{x}$ is the mean of the estimated residuals.

The simplest case is when the score generating function φ is linear given by $\varphi(u) = \sqrt{12}(u - {}^{1}/_{2})$. The resulting estimator is called the Wilcoxon estimator. For this φ, minimizing $D_{\varphi}$is equivalent to minimizing (Sievers, 1983)

$$\sum_{k<t} |e_t(\Delta) - e_k(\Delta)|$$

which is clearly a pseudo-norm. For this case, the estimator of Δ is the Hodges-Lehmann estimator $\tilde{\Delta}$ given in and $\tilde{\alpha}$ is the median of the U sample. Once again, $\tilde{\Delta}$ is approximately Gaussian with mean Δ and variance $\tau_F^2({}^{1}/_{m} + {}^{1}/_{n})$.

3.3.2.2. General Linear Model – R Fit

Jaeckel's rank regression method can be used to fit models involving more than one predictor variable. A general linear model relates a set of p predictors (**X**) collected on n subjects to their response (Y) using a plane. For subject k, this is given by

$$Y_k = \alpha + \beta_1 X_{k1} + \cdots + \beta_p X_{kp} + \varepsilon_k$$

for $k = 1, \dots, n$. This is usually written in matrix form as

$$\boldsymbol{Y} = \alpha \mathbf{1}_n + \boldsymbol{X\beta} + \boldsymbol{\varepsilon},$$

where $\boldsymbol{Y}$ is an $n \times 1$ vector of responses, $\boldsymbol{X}$ is an $n \times p$ matrix of predictors, $\boldsymbol{\varepsilon}$ is an $n \times 1$ vector of random errors, and $\mathbf{1}_n$ is an $n \times 1$ vector of ones. Once again, the main interest is to estimate the $p \times 1$ vector of slope parameters $\boldsymbol{\beta} = (\beta_1, \dots, \beta_p)^T$ to study the manner in which predictors are associated to the response as well as test for the significance of the components of $\boldsymbol{\beta}$. For this we need to estimate $\boldsymbol{\beta}$ and determine the asymptotic distribution of the estimator.

The traditional approach of estimating $\boldsymbol{\beta}$ is the least squares estimator that minimizes the Euclidean norm of the residuals. This estimator can be calculated in closed form as

$$\widehat{\boldsymbol{\beta}} = (\boldsymbol{X}^T\boldsymbol{X})^{-1}\boldsymbol{X}^T\boldsymbol{Y}.$$

If the errors $\varepsilon_1, \dots, \varepsilon_n$ are iid from a distribution F that has variance σ_F^2, then $\widehat{\boldsymbol{\beta}}$ follows an approximate p-dimensional Gaussian distribution with mean $\boldsymbol{\beta}$ and covariance matrix $\sigma_F^2(\boldsymbol{X}^T\boldsymbol{X})^{-1}$. One may use this asymptotic distribution to construct a Wald-type test for the significance of the *j*th slope (or variable X_j) $H_0: \beta_j = 0$ versus $H_A: \beta_j \neq 0$ using the statistic

$$T_j = \frac{\hat{\beta}_j}{\sqrt{\hat{\sigma}^2(\boldsymbol{X}^T\boldsymbol{X})^{-1}_{jj}}}$$

where $(\boldsymbol{X}^T\boldsymbol{X})^{-1}_{jj}$ is the *(j,j)*th entry of the matrix $(\boldsymbol{X}^T\boldsymbol{X})^{-1}$ and $\hat{\sigma}^2 = \frac{(\boldsymbol{Y}-\boldsymbol{X}\widehat{\boldsymbol{\beta}})^T(\boldsymbol{Y}-\boldsymbol{X}\widehat{\boldsymbol{\beta}})}{n-p-1}$ is the estimate of the model variance. The approximate distribution of T_j is t with $n-p-1$ degrees of freedom; so, the level γ test of significance is performed by comparing $|T_j|$ with upper $\gamma/2$ percentile of the t distribution with $n-p-1$ degrees of freedom.

An alternative estimator is Jaeckel's rank estimator of $\boldsymbol{\beta}$, say $\widetilde{\boldsymbol{\beta}}$, based on Jaeckel's dispersion function is the value that minimizes

$$D(\boldsymbol{\beta}) = \sum_{k=1}^{n} \varphi\left(\frac{R(e_k(\boldsymbol{\beta}))}{n+1}\right) e_k(\boldsymbol{\beta})$$

where $e_k(\boldsymbol{\beta})$ is the *k*th entry of $\boldsymbol{Y} - \boldsymbol{X}\boldsymbol{\beta}$ and $R(e_k(\boldsymbol{\beta}))$ is the rank of $e_k(\boldsymbol{\beta})$ among $e_1(\boldsymbol{\beta}), \dots, e_n(\boldsymbol{\beta})$. Once again, $D(\boldsymbol{\beta})$ is a convex, continuous, and positive function of $\boldsymbol{\beta}$ but as it defines a pseudo-norm in the residual space, it is invariant to constant translations. Therefore, it cannot be used to

estimate the intercept term α. However, when φ is odd about $1/2$ as in the linear score case and since $\int_0^1 \varphi(u)du = 0$, a natural estimator of the intercept is the median of the estimated residuals $e_1(\widetilde{\boldsymbol{\beta}}), \ldots, e_n(\widetilde{\boldsymbol{\beta}})$. We will denote this estimator by $\tilde{\alpha}$. Heiler and Willers (1988) have shown that the $\widetilde{\boldsymbol{\beta}}$ follows an asymptotic p dimensional Gaussian distribution given by $N(\boldsymbol{\beta}, \tau_\varphi^2(\boldsymbol{X}'\boldsymbol{X})^{-1})$, where τ_φ^2 is defined as

$$\tau_\varphi^2 = \left[\int_0^1 \varphi(u)\left\{-\frac{f'(F^{-1}(u))}{f(F^{-1}(u))}\right\}du\right]^{-1}$$

and represents a scale parameter that is analogous to the standard deviation in least squares estimation. The quantity τ_φ^2 reduces to τ_F^2 defined above for the linear score case given by $\varphi(u) = \sqrt{12}(u - 1/2)$. A consistent estimator of τ_φ^2 is given in Koul, Sievers and McKean (1987). We can use this estimator $\tilde{\tau}^2$ of τ_φ^2 along with the asymptotic distribution to construct test statistics for testing various types of hypotheses. For instance, a Wald type *t* test for the significance of the *j*th individual slope, $1 \leq j \leq p$, can be as

$$W_j = \frac{\tilde{\beta}_j}{\sqrt{\tilde{\tau}^2(\boldsymbol{X}'\boldsymbol{X})^{-1}_{jj}}}$$

and the null hypothesis $H_0: \beta_j = 0$ is rejected in favor of $H_A: \beta_j \neq 0$ if $|T_j| > t_{n-p-1}(\gamma/2)$, $t_{n-p-1}(\gamma/2)$ is the upper $\gamma/2$ percentile of the t distribution with $n - p - 1$ degrees of freedom.

Notice that the asymptotic distributions of the least squares estimator $\widehat{\boldsymbol{\beta}}$ and the rank estimator $\widetilde{\boldsymbol{\beta}}$ differ only in their scale parameters σ_F^2 and τ_φ^2, respectively. It is, thus, obvious that the ARE of the rank estimator with respect to the least squares estimator is

$$ARE\left(\widetilde{\boldsymbol{\beta}}, \widehat{\boldsymbol{\beta}}\right) = \frac{\sigma_F^2}{\tau_{\varphi}^2}.$$

3.3.2.3. Linear Models with Cluster Correlation – JRFit

Assume that we have a total of $N = n_1 + \cdots + n_m$ observations in *m* clusters, where cluster *k* has n_k observations. Within cluster *k*, let $\boldsymbol{Y}_k$, $\boldsymbol{X}_k$, and $\boldsymbol{\varepsilon}_k$ denote the $n_k \times 1$ vector of responses, the $n_k \times p$ design matrix, and the $n_k \times 1$ vector of errors, respectively. Let $\mathbf{1}_{n_k}$ denote a vector of n_k ones. Then the model for $\boldsymbol{Y}_k$, $k = 1, \ldots, m,$ is

$$\boldsymbol{Y}_k = \alpha \mathbf{1}_{n_k} + \boldsymbol{X}_k \boldsymbol{\beta} + \boldsymbol{\varepsilon}_k,$$

where α and $\boldsymbol{\beta}$ represent the intercept and slope parameter, respectively. We do not assume that the errors in the same cluster are independent but different clusters are assumed independent. Thus $Cov(\boldsymbol{\varepsilon}_k) = \sigma^2 \boldsymbol{\Omega}_k$, an $n_k \times n_k$ positive definite matrix not necessarily equal to the $n_k \times n_k$ identity matrix $\boldsymbol{I}_{n_k}$. Note that this case reduces to the independent general linear model if $\boldsymbol{\Omega}_k = \boldsymbol{I}_{n_k}$ for all k. Although not necessary, for this study, we will make the assumption that $\boldsymbol{\Omega}_k$ is compound symmetric (exchangeable structure); that is, all the off-diagonal elements are equal and all the diagonal elements are also equal. This will ensure that we do not give up too many degrees of freedom in estimating the covariance matrix. Moreover, in this study the clusters are monthly and there is no indication that the underlying correlations will be different for different years.

The traditional approach involves using linear mixed-models estimated using the maximum likelihood approach. The likelihood equation is constructed based on the assumption that $\boldsymbol{\varepsilon}_k$ follow an n_k dimensional Gaussian distribution with mean $\mathbf{0}$ and variance-covariance matrix $\boldsymbol{\Omega}_k$. Estimation is performed using the restricted maximum likelihood (REML) method by first using regression to estimate the fixed effects residuals and using these residuals to estimate

the variance components. The REML estimator of $\boldsymbol{\beta}$, denoted by $\boldsymbol{\beta}_{ML}$, has an asymptotic Gaussian distribution with mean $\boldsymbol{\beta}$ and variance-covariance matrix

$$\boldsymbol{V} = \sigma^2 \left(\sum_{k=1}^{m} \boldsymbol{X}_k^T (\boldsymbol{I}_{n_k} + \boldsymbol{X}_k^T \boldsymbol{\Omega}_k \boldsymbol{X}_k)^{-1} \boldsymbol{X}_k \right)^{-1}$$

Joint ranking (JR) estimation starts by stacking $\boldsymbol{Y}_k$ into an $N \times 1$ response vector $\boldsymbol{Y}$. Similarly define the $N \times p$ matrix $\boldsymbol{X}$ by stacking $\boldsymbol{X}_k$. The residuals for the stacked model are defined by the vector $\boldsymbol{e}(\boldsymbol{\beta}) = \boldsymbol{Y} - \boldsymbol{X}\boldsymbol{\beta}$ with ith element $e_i(\boldsymbol{\beta})$, $i = 1, \ldots, N$. JRFit defines Jaeckel's dispersion function using $\boldsymbol{e}(\boldsymbol{\beta})$ as

$$D_{JR}(\boldsymbol{\beta}) = \sum_{i=1}^{N} \varphi \left(\frac{R(e_i(\boldsymbol{\beta}))}{n+1} \right) e_i(\boldsymbol{\beta})$$

Thus, JRFit is exactly the minimization of Jaeckel's dispersion for linear models with cluster-correlated errors. We will denote the resulting estimator by $\widetilde{\boldsymbol{\beta}}_{JR}$. Kloke et al. (2009) show that this procedure results in an efficient estimator of $\boldsymbol{\beta}$ that has an asymptotic Gaussian distribution. In particular, $\widetilde{\boldsymbol{\beta}}_{JR}$ follows an asymptotic Gaussian distribution with mean $\boldsymbol{\beta}$ and covariance matrix given by

$$\boldsymbol{V}_{\varphi} = \tau_{\varphi}^2 (\boldsymbol{X}^T \boldsymbol{X})^{-1} \left(\sum_{k=1}^{m} \boldsymbol{X}_k^T \boldsymbol{\Sigma}_{\varphi,k} \boldsymbol{X}_k \right) (\boldsymbol{X}^T \boldsymbol{X})^{-1}$$

where $\boldsymbol{\Sigma}_{\varphi,k} = Cov(\varphi(F(\boldsymbol{\varepsilon}_k)))$ is the $m \times m$ score intra-cluster covariance matrix. This asymptotic distribution is used to derive significance tests of the estimated parameters.

The computation of the ARE involving $\widetilde{\boldsymbol{\beta}}_{JR}$ is generally complicated. We shall study this using a Monte Carlo simulation experiment. That said, one may compute the ARE in closed form

for very simple cases. For example, for the linear score function $\varphi(u) = \sqrt{12}(u - 1/2)$, the ARE for comparing the JR estimator with the LS estimator is given by

$$ARE(\widetilde{\boldsymbol{\beta}}_{JR}, \widehat{\boldsymbol{\beta}}_{LS}) = \frac{1-\rho}{1-\rho_{\varphi}} 12\sigma^2 \left(\int f^2(t)dt \right)^2$$

where ρ is the within cluster correlation and ρ_{φ} is the within cluster score correlation $cov(\varphi(F(\varepsilon_{11}), \varphi(F(\varepsilon_{12}))$, both of which are constant due to the compound symmetry structure. In the ideal Gaussian error case, the ARE can be computed as

$$ARE(\widetilde{\boldsymbol{\beta}}_{JR}, \widehat{\boldsymbol{\beta}}_{LS}) = \frac{3(1-\rho)}{\pi - 6\, sin^{-1}(\rho/2)}$$

This ARE lies in [.866, .955] for $0 < \rho < 1$, decreasing as $\rho \to 1$, and in [.955, .966] for $-1 < \rho < 0$, increasing as $\rho \to 0$. They also demonstrated that the AREs can be much larger than one for contaminated Gaussian distributions. As expected, this ARE is equivalent to the ARE of the two sample Wilcoxon Rank Sum case when $\rho = 0$. The Monte Carlo simulation experiment will evaluate the effect of tail thickness and correlation on the efficiency of JRFit versus REML. This is not known as of now.

3.3.3. Monte Carlo Evaluation of JRFit

In the Monte Carlo simulation experiment, we will consider 60 years climate data where 30 years are assumed to be under phase A and the remaining 30 are assumed to be phase B. We also assume that the responses (eg. baseflow, streamflow, precipitation, etc.) are measured seasonally; that is, we have four measured responses per year corresponding to each season. Responses measured in the same season are expected to be similar. So, we impose a season cluster

with correlation ρ. To account for heavy tailed nature of climate data, we used the t distribution with various degrees of freedom to generate the responses. The tails of the t distribution are heavy for small degrees of freedom and they approach the tails of the Gaussian distribution for degrees of freedom approaching infinity. Thus, a single set of responses under the two climate phases A and B is generated as

$$Y_A = T_{30}(d, \rho) + S$$

$$Y_B = T_{30}(d, \rho) + \Delta + S$$

where $T_{30}(d, \rho)$ is a random variate from the 30-dimensional t distribution with degrees of freedom d and correlation ρ, Δ is the B phase effect, S is the season effect. Therefore, the expected difference $Y_B - Y_A = \Delta$. Different techniques are judged by how precisely and accurately they are able to recover the true value of Δ in this noisy setting. In our simulation, we took several values combinations of (d, ρ, Δ). However, the value of Δ did not have much effect on the relative efficiencies. So, we only report the results for $\Delta_0 = 3$. The values of d and ρ considered are $d = (3, 4, 5, 10, 15, 20, 30, 60, 100)$ representing decreasing tail-thickness and $\rho = (0, .05, .1, .2, .3, .4, .5)$ representing increasing degrees of seasonal correlation.

To evaluate the performance of JRFit versus traditional approaches, we fit JR, REML, and the Hodges-Lehmann estimator (WRS) on the anomalies (Tootle et al., 2005; Johnson et al., 2013) as well as the least absolute deviation (LAD) regression (Koenker and Basset, 1978) without respecting the correlation structure. We performed M =10,000 iterations and calculated the mean square errors of the estimate of Δ. For example, for JR we have $\tilde{\Delta}_{JR,1}(d, \rho), \ldots, \tilde{\Delta}_{JR,M}(d, \rho)$. The Monte Carlo estimate of the MSE is

$$MSE_{JR}(d,\rho) = \frac{1}{M}\sum_{i=1}^{M}\left(\tilde{\Delta}_{JR,i}(d,\rho) - \Delta_0\right)^2.$$

We similarly computed $MSE_{REML}(d,\rho)$, $MSE_{LAD}(d,\rho)$, and $MSE_{WRS}(d,\rho)$. The MSEs are the L_2 distance measuring the closeness of the phase effect estimate in each iteration to the true phase effect Δ_0. Lower values indicate high efficiency.

The relative efficiencies (REs) of JR, LAD, and WRS versus REML are then given by $\frac{MSE_{REML}(d,\rho)}{MSE_{JR}(d,\rho)}$, $\frac{MSE_{REML}(d,\rho)}{MSE_{LAD}(d,\rho)}$, and $\frac{MSE_{REML}(d,\rho)}{MSE_{WRS}(d,\rho)}$, respectively. If RE = 1, then the two methods are equally efficient whereas RE > 1 indicates the competitor is more efficient that REML in estimating phase effect.

3.4. Results

The RE values are reported for various combinations of (d,ρ) in Figure 1 below. The methods that do not respect the cluster structure (WRS and LAD) are inefficient compared to JR. They are also inefficient compare to REML especially as the tails of the distribution approach the tails of the Gaussian distribution (increasing d). However, they tend to perform better than REML for distributions that have tails substantially thicker than Gaussian tails especially when the correlation is high (large ρ). JR performs better than WRS and LAD in all the cases considered. While we simultaneously estimate and test the significance of effects, Galbraith et al. (2010) have also discussed WRS for clustered data (Datta and Satten, 2005) from a testing perspective. They have reported the perils of ignoring clustering from the perspective of inflated Type I error rates of tests.

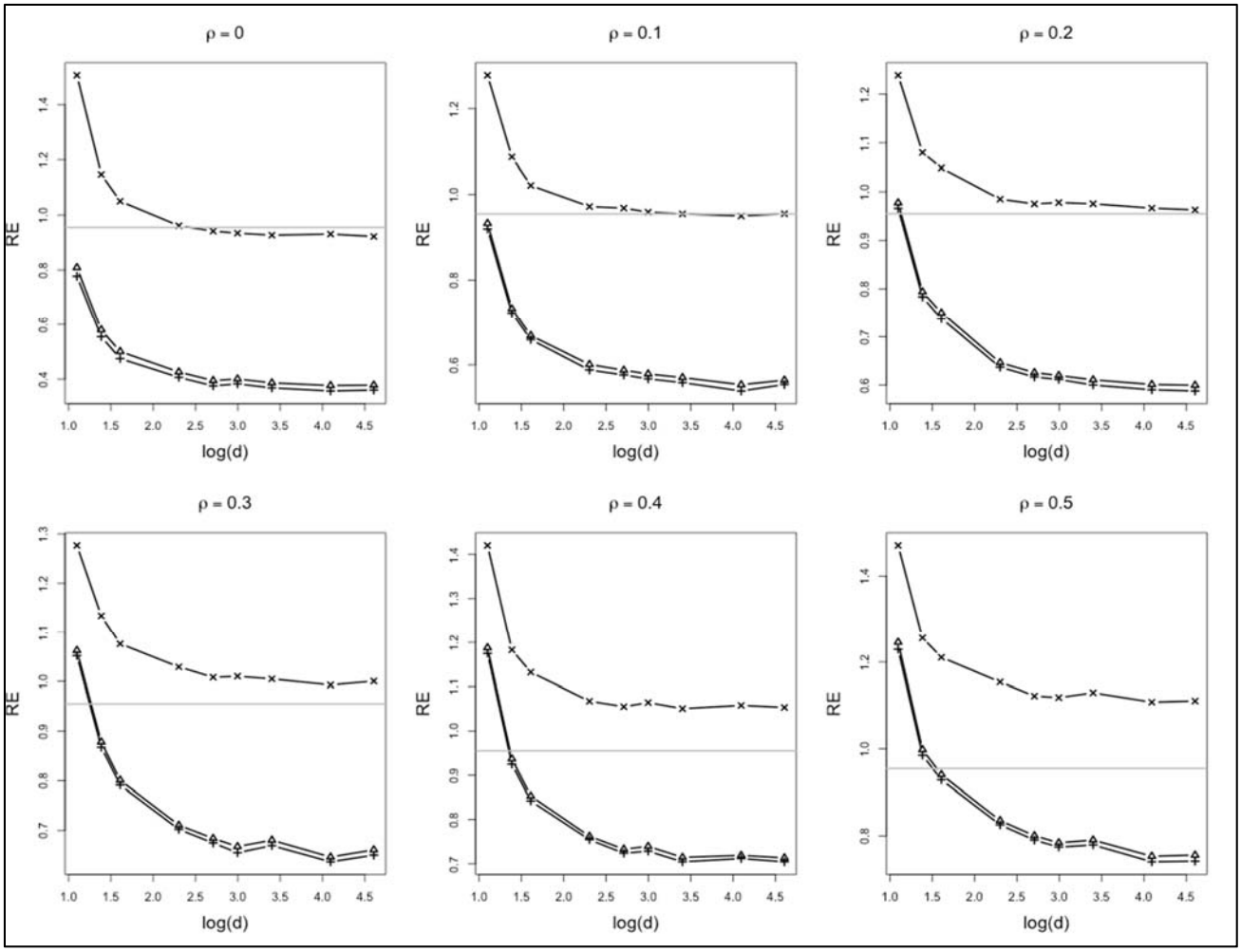

Figure 3.1. Estimated relative efficiencies versus REML; $-\times-$ JR, $-\Delta-$ LAD, $-+-$ WRS. Solid line represents the theoretical ARE $3/\pi$ of JR vs LS for Gaussian ($d=\infty$) case when $\rho=0$.

JR is more efficient that all the methods considered for heavy tailed data (small d). It is less efficient that REML for lighter tails and weak cluster correlation. However, JR becomes more efficient versus REML with increasing correlation. Similar observation has been made for JR versus least squares by Kloke et al. (2009) where they considered errors that follow contaminated Gaussian distributions using the so-called Huber contamination (Tootle et al., 2005; Johnson et al., 2013) of standard Gaussian with a Gaussian that has a higher variance. Considering general

nonlinear models with independent errors, Bindele and Abebe (2012) have shown that rank methods have higher efficiency than least squares based methods for when the errors are drawn from t distribution with small degrees of freedom. Our result here confirms that the pattern remains to hold for linear models with cluster-correlated errors. We also observe that rank methods tend to perform better than REML when the cluster structure exhibits strong correlation. This result has not been reported in the past.

3.5. Conclusion and Recommendations

The purpose of this chapter is to evaluate the fidelity of the JRFit procedure that was used to estimate effect sizes as well as test their significance in our analysis of baseflow data. This was done via a Monte Carlo simulation experiment where data are generated under various scenarios. The efficiency of JRFit was compared to three other methods: the traditional methods such as restricted maximum likelihood and least absolute deviations as well as the nonparametric Wilcoxon rank-sum method. The results confirm that JRFit provides more efficient result than all three for clustered data with heavier tails (or data with outliers) or strong correlation. These are both common characteristics in climate related data. Researchers have applied the WRS method in past studies. However, as our results show, this tends to be inefficient for clustered data leading to possibly erroneous conclusions.

If one is interested in only testing, then the WRS method of Datta and Satten (2005) that is specifically designed for clustered data may be used. However, if one is also interested in measuring effect sizes, then we recommend the use of JRFit that simultaneously provides estimation and testing.

Chapter 4

Combined Effect of Irrigation and Droughts on Surface and Baseflow Levels in the Lower Flint River Basin

4.1. Abstract

Water resources around the world are being stressed due the combined impacts of climate variability and human interactions. The Apalachicola-Chattahoochee-Flint River Basin in the Southeast USA is a classic example where the population growth in the city of Atlanta and increased irrigated agriculture in southwest Georgia is affecting surface flows and aquatic ecosystems in the Flint River and the Apalachicola Bay. Since the 1970s, there has been extensive implementation of center pivot irrigation systems in southwest Georgia. This study was conducted to understand the effect of irrigation water withdrawal during droughts on flow levels in the lower Flint River and its tributaries. Streamflow data collected from four USGS gauging stations were sorted according to non-irrigation (NI) and irrigation (IR) periods. A statistical procedure called JRFit was used to test and quantify the significant difference in streamflow, baseflow and low flows between the NI and IR periods. Moreover, El Niño Southern Oscillation (ENSO) phases associated with the NI and IR periods were analyzed using JRFit to quantify the combined effects of droughts and irrigation withdrawal on the selected flow parameters. Flow levels during the growing and non-growing periods were also analyzed to provide evidence of irrigation induced depletion of flow levels in the lower Flint River basin. The results of the study suggests that streamflow levels have decreased by approximately 20% after the introduction of irrigation in the

study area. The results also show that lowering of flow levels mainly occur during La Niña phases and gets exacerbated during growing periods where the flow levels decreased by as much as 50% as compared to growing seasons of NI periods. Additionally, analysis of presumptive standard flow showed that in recent drought events flow levels repeatedly violated the standards and can result in impairment of aquatic ecosystems.

4.2. Introduction

Natural ocean-atmospheric climate variability phenomena affect temperature and precipitation on interannual, decadal, and multidecadal time scales and are also responsible for extreme events such as hurricanes, floods, droughts, and cold waves (IPCC, 2001) around the world. Studies have found strong influence of climate variability phenomena on components of hydrologic cycle in many parts of the world, thus affecting water resources around the world. Therefore, understanding the climate variability phenomena and its effect on water resources is essential to mitigate their adverse effects on water resources. In addition to natural short term climate variability induced stresses on water resources, an ever growing global population with increasing need for irrigated agriculture is putting tremendous stress on freshwater bodies such as lakes, streams, and aquifers. In the past 50 years, the demand for water consumption for human use has increased by almost three-folds, and it is projected that by 2025, five out of eight people will be living under water scarce condition across the world including USA (Postel et al. 1996). To be able to cope and better manage future water shortages resulting due to climate variability induced droughts and human induced water scarcity, it is important to study the impact of the climatic oscillation on hydrology and their effects on water resources.

El Niño Southern Oscillation (ENSO) phenomenon is the fluctuation of sea-surface temperature (SST) caused by the interaction between large-scale ocean and atmospheric circulation in equatorial Pacific Ocean with a periodicity of 2-7 years. ENSO has three phases such as El Niño, La Niña and Neutral. The terms "El Niño" and "La Niña" refer to the warming and cooling of SST off the shores of the West Coast of South America that lead to changes in climatic conditions around the world (Quinn 1994; Aceituno 1992). ENSO is one of the major modes of climate variability affecting temperature and precipitation around the world (Diaz and Markgraf, 1992; Chiew et al., 1998; Keener et al., 2007; Roy, 2006). Several studies have found that ENSO have strong influence on droughts, streamflow, groundwater, flood frequency, monsoon, water quality, and crop yield in different parts of the world (Kahya and Drakup, 1993; Chiew et al., 1998; Rajagopalan and Lall, 1998; McCabe and Dettinger 1999; Piechota and Dracup, 1999; Kulkarni, 2000; Hansen et al. 2001; Tootle et al., 2005; Roy, 2006; Keener et al., 2007; and Gurdak et al., 2007).

Moreover, several other studies have shown that ENSO exhibits strong tele-connections with precipitation, streamflow, baseflow and groundwater in the Southeast USA. The Southeast often suffers from low surface water availability due to frequent occurance of La Niña, which brings warm and dry conditions between the months of October and April (Kiladis and Diaz, 1989; Hansen and Maul, 1991; Schmidt and Luther, 2002; Mearns et al., 2003), making the region vulnerable to ENSO-induced droughts. Furthermore, water shortages in this region get exacerbated due to very high evaporation rate during summer months and increased demand for water due to growth in population, urbanization and irrigated agriculture in the past few decades. Since 1980, the Southeast has experienced recurring droughts that have caused losses in agricultural productivity, prompted water use restrictions on municipal and irrigated waters uses, and induced

interstate water conflicts in this region. This combined stress of climate variability induced droughts, population growth, and irrigation withdrawal on water resources has led to "Tri-State Water Conflict" among the neighboring states of Georgia, Alabama and Florida (Jordan et al., 2006). This conflict has been marked by costly, time consuming and still ongoing litigations where the sparring parties have failed to reach a common ground on the partitioning of water resources of the Apalachicola-Chattahoochee-Flint (ACF) River Basin, thereby making the ACF as one of the most contentious river basins in the United States. The freshwater resources of the ACF provide support to rapidly growing population, urban sprawl, industrial, municipal and rural water supplies, power facilities, irrigated agriculture, shellfish industry, and estuarine ecosystem. One of the major issues related to the ongoing conflict is the irrigation induced lowering of flow levels in the Flint River.

Agriculture in the lower Flint River Basin (FRB) (in southwest Georgia) is heavily dependent on irrigation water withdrawal from surface and groundwater sources. Since the mid-1970s, groundwater withdrawals for irrigation has increased dramatically in the lower Flint River (LFR) Basin (Appendix B.1) due to extensive installation of center pivot irrigation systems (Hicks et al. 1987; Pierce et al., 1984) where the ratio of groundwater sites to surface water sites is 5:1. During a drought year (typically caused by La Niña), groundwater withdrawal from the Upper Floridan Aquifer (UFA), which is the major groundwater bearing unit in the area, can run into hundreds of millions of gallons per day. The flow in the LFR is hydro-geologically connected with UFA through direct connections with many sinkhole ponds, karst sinks and conduits and trough incised streambeds, and indirect connections through vertical leakage from overburden (Mosner, 2002; Opsahl et al., 2007). Therefore, the major objective of this study was to understand and quantify the effect of irrigation in southwest Georgia on flow levels in the Flint River.

The hydrologic connectivity/interaction of groundwater with surface water has become issue of interest among researchers worldwide since it supports baseflow and serves as a major water resource unit (Shah et al., 2000; Woessner, 2000; Stanford and Ward, 1993; Winter et al., 1998; Boulton and Hancock, 2006). Intensive groundwater removal near stream channels has been linked to alterations in quantity and quality of surface waters which leads to changes in channel morphology, altered stream temperature, lower assimilative capacity, reduced nutrient loading to downstream communities (Pringle and Triska, 2000; Bunn and Arthington, 2002), and threatened aquatic biota (Golladay et al., 2004). To achieve the goal of this study, streamflow and baseflow levels for the pre and post irrigation periods were compared and quantified along with ENSO.

4.3. Methodology

To attain the research goal, the nonparametric Joint Rank Fit (JRFit) procedure (Kloke et al., 2009) was used to test and estimate the ENSO induced drought and irrigation impacts on streamflow, baseflow, and one- and seven-day low flow levels. Additionally, presumptive standard water level for lower Flint River were estimated and compared during La Niña-induced severe drought events. This study is the part of a bigger project that aims to understand the relationships among droughts, irrigation, and streamflow levels in the study area with the final goal of identifying critical reaches and tributaries of the lower Flint River that are responsible for lowering of flow levels in the river. The comprehensive outcomes of this study can be used to help the state of Georgia better manage drought-induced streamflow reductions in the Flint and Apalachicola rivers.

4.3.1. Study Area

The study area is the LFR Basin located in southwestern Georgia (Figure 4.1). The climate in the lower FRB is hot and humid with long summers (temperature ranges from 18 to 35 °C) and mild winters (temperature ranges from 2 to 13 °C). The average annual precipitation is 1200 mm which vary spatially across the region.

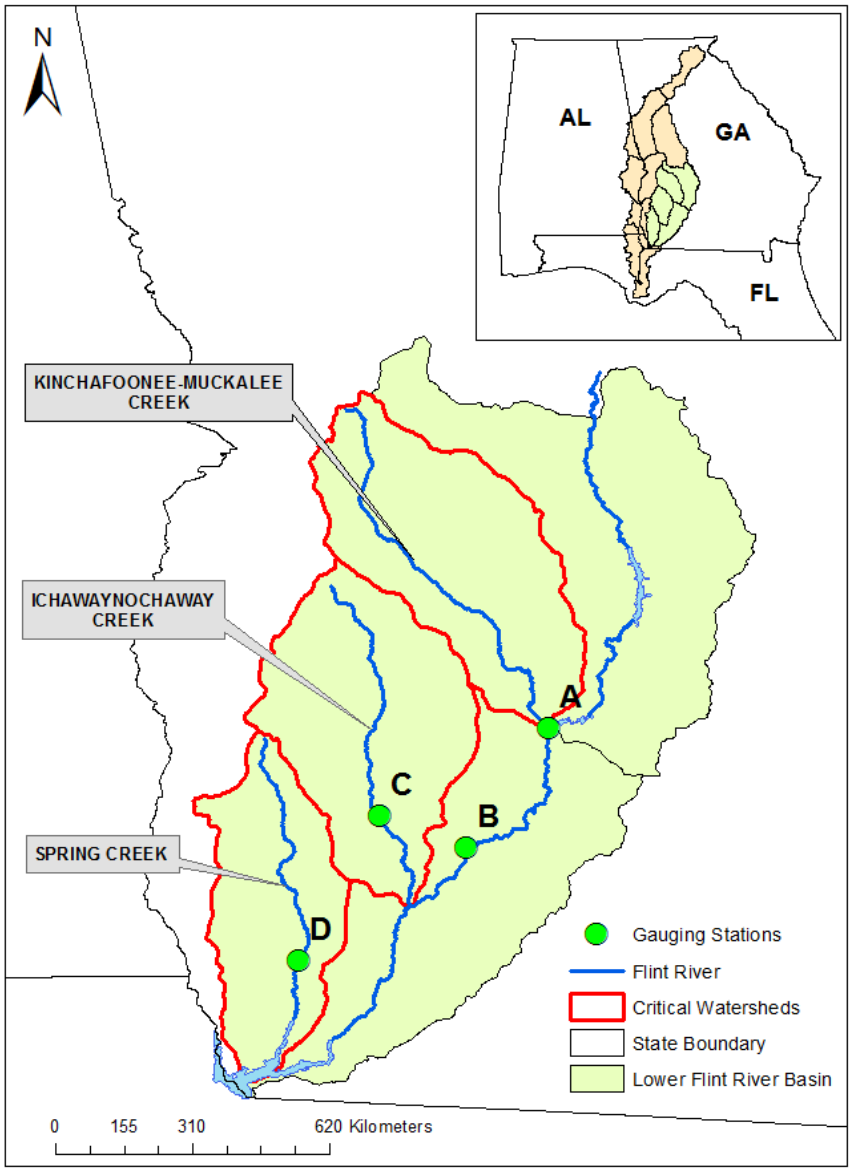

Figure 4.1. The lower Flint River Basin (FRB) showing the critical sub-watersheds. The stream flow gauging stations selected for this study are shown as green circles.

The ACF river basin contains karstic and fluvial plains and predominantly karst limestone which contribute to the exchange of ground water and surface water in the stream-lake-aquifer flow system. The tributaries and principal rivers of lower Flint River are hydraulically connected to Upper Floridan aquifer (UFA) which is the principal water bearing hydrologic unit in the study area. The land use of lower FRB is largely agriculture (50%) with row crop farming of cotton, corn, wheat, soybeans, and peanuts. The farming systems in the lower FRB are primarily supported by center pivot irrigation technique which withdraws water from surface and groundwater (i.e., UFA) resources.

4.3.2. Data

To understand the impact of irrigation and drought on Flint River flow levels, streamflow data from four United States Geological Survey (USGS) gauging stations and climate variability (ENSO) data from NOAA were used (Appendix A.2).

4.3.3. Climate Variability (ENSO) Data

There are several types of indices which are universally accepted for the definition of ENSO cycles (Tootle et al., 2005). In general, ENSO indices are calculated based on atmospheric observations such as the Southern Oscillation Index (SOI), based on sea surface temperatures (SST) (e.g. the Niño 3.4 index) (Trenberth, 1997; Trenberth and Stepaniak, 2001), and combination of both ocean and atmospheric parameters such as the Multivariate ENSO Index (MEI). Each of these indices are a slightly different definitions of ENSO cycles that are based on coordinates and regions selected for the index calculation. However, there is no agreement within the scientific community over the best index to define ENSO years or the strength, timing, and

duration of events. In this study, the Niño 3.4 SST index (ERSST.v3b) is used to define ENSO phases and durations. The Niño 3.4 indices are the SST anomalies in the Niño 3.4 region (5^0N–5^0S, 120^0–170^0W) which were obtained from the National Oceanic and Atmospheric Administration's (NOAA) Climate Prediction Center (CPC). The Niño 3.4 index value of above +0.5ºC corresponds to the occurance of El Niño event and a value below −0.5ºC represents La Niña. When Niño 3.4 index value is between -0.5ºC and +0.5ºC, ENSO is considered to be in Neutral phase.

4.3.4. Streamflow Data

Four USGS stations (Figure 4.1) were selected based on length of data available, where two stations namely **A** and **B** are on Flint River and other two are on the tributaries namely Ichawaynochaway Creek (**C**) and Spring Creek (**D**) (Station ID: 02353500 and 02357000 respectively) (Table 4.1 and Figure 4.1).

Table 4.1. The selected streamflow gauging stations used in this study showing the USGS station ID, location, their assigned names used in the manuscript, and their respective date ranges.

Station ID	Location	Given Name	Data Range (Year)
02352500	Flint River, Albany, GA	**A**	1930-2014
02353000	Flint River, Newton, GA	**B**	1957-2014
02353500	Ichawaynochaway Creek, Milford, GA	**C**	1940-2014
02357000	Spring Creek, Iron City, GA	**D**	1938-1970 and 1983-2014

Ichawaynochaway Creek is a fifth-order tributary and Spring Creek, a third-order tributary of the Flint which flows directly to Lake Seminole. At Lake Seminole, the Flint and Chattahoochee Rivers join to form the Apalachicola River. Daily streamflow data in cubic feet per second were collected from these USGS gauging stations with historical data of approximately 75 years except

station **D** (Table 4.1). The daily values were changed into monthly cubic meters per second (cms) and were sorted according to ENSO phases and growing seasons.

4.3.5. Baseflow Data

Baseflow was separated from daily streamflow data using Web-based Hydrograph Analysis Tool (WHAT). This tool uses two digital filter methods for baseflow separation such as, BFLOW and Eckhardt (Lim et al., 2005). In this study, Eckhardt filter method with baseflow index 0.9 (Eckhardt, 2005) was used for baseflow separation (Lim et al., 2005) since it is used for perennial rivers. The equation used for the Eckhardt filter method is shown below.

$$b_t = \frac{(1 - BFI_{max}) \times \alpha + b_{t-1} + (1 - \alpha) \times BFI_{max} \times Q_t}{1 - \alpha \times BFI_{max}} \quad (1)$$

where, BFI_{max} is the maximum value of long term ratio of base flow to total streamflow; b_{t-1} is the filtered base flow at the time step t-1; α is the filter parameter; b_t is the filtered base flow at the time step t; and Q_t is the total streamflow at the time step t.

4.3.6. Statistical Method

Streamflow/baseflow data are clustered by month, meaning they exhibit more or less similar patterns on a monthly basis irrespective of year. Therefore, the nonparametric JRFit procedure was used in this study which is an extension of Wilcoxon rank-sum procedure for the analysis of clustered correlated data. The Wilcoxon rank-regression approach is not appropriate for the cluster correlated responses since cluster correlation in the responses inflates the standard errors of the estimation. Since, JRFit uses joint ranking to obtain correct estimates of the effect sizes and standard errors for cluster-correlated data, it is a powerful nonparametric technique for

cluster correlated responses. Kloke et al. (2009) show that this procedure minimizes Jaeckel's dispersion, and results in an unbiased and efficient estimator of the slope parameter with an asymptotic Gaussian distribution. This asymptotic distribution is used to construct efficient significance tests of the model parameters without segregating the data which gives more power to test (Kloke et al., 2009; Hettmansperger and McKean, 2011). The following linear model was used to estimate the effect of climate variability phenomenon (ENSO) or irrigation (X) on streamflow/ baseflow (Y)

$$Y = \beta_0 + \beta_1 X + \varepsilon, \quad (2)$$

Where, $X = 0$ and $X = 1$ represent non-irrigation (NI) and irrigation (IR) periods, and ε represents random errors. The value of β_1 measures the change in flow levels due to change of phase from NI to IR.

4.3.7. Non-irrigation and irrigation flow comparison

In this study, streamflow/baseflow data sets were divided into two time periods non-irrigation (≤ year 1975) (NI) and irrigation (> year 1975) (IR) periods. The NI period for the Spring Creek gauging station was defined from 1940 to 1969 and IR period started from 1983 to 2014 due to unavailability of data during the missing period (from 1970 to 1982) (Table 4.1). The significant difference of median streamflow/baseflow for each gauging station was tested and estimated using JRFit procedure. The percentage differences of estimated medians of streamflow/baseflow were calculated while moving from NI to IR period. The significant difference of median streamflow/baseflow between NI and IR periods during El Niño and La Niña phases were also estimated to understand the individual impact of climate variability, and the combined effect of irrigation and climate variability cycles on lower Flint River. To verify the

effect of irrigation on streaflow/baseflow levels, the growing and non-growing season analysis were conducted for overall and ENSO phases associated with IR and NI periods. The growing season is defined as the months from April to October and the remaining months of a year are considered as the non-growing season. The overall median streamflow/baseflow levels of growing and non-growing seasons were compared for non-irrigation and irrigation periods using JRFit procedure.

4.3.8. One-day and seven-day low flows

Low flows (such as 1-day and 7-day) are the most stressful natural events for river biota by constricting the habitat. Low flow levels eventually lead to portions of the channel becoming dry. Aquatic animals try to concentrated in pools where small and large-bodied species are more vulnerable to aquatic predators and terrestrial predators (especially, birds and raccoons), respectively. However, others that are unable to move to the pool perish on the dry stream bed. Extreme low water levels during summer months are associated with higher than normal water temperatures and low dissolved oxygen levels further causing more stress to river flora and fauna. Low flows are more stressful depending on the magnitude, duration and frequency of low flows. Decrease in magnitude and increase in frequency of extreme low-flows have detrimental effects on native riverine biota including mussel and engendered species that reside in the Flint River. Therefore, in this study, 1-day and 7-day low flows were analyzed for the NI and IR periods. One-day low flow is defined as the lowest streamflow in a given month and seven-day low flow is the lowest seven day running average streamflow for that month. The significant differences of median low flows for NI and IR periods were also tested and estimated using JRFit procedure. The significant differences of median low flows between NI and IR periods during El Niño and La

Niña phases were also estimated to understand the individual impact of climate variability, and the combined effect of irrigation and climate variability cycles on low flows that adversely affect the river biota of the Flint River.

4.3.9. Flow duration curve analysis

Flow duration curve (FDC) is a cumulative frequency curve that show the percent of time a flow was equaled or exceeded without regard to the sequence of occurrence during a given period. FDC has different intervals that can be used as a general indicator of the probability of hydrologic conditions such as dry or wet. The intervals are categorized into different zones such as the moist, mid-range, and dry zones at the quartiles (25th, 50th, and 75th percentiles, respectively). In this study, FDCs were constructed from the NI and IR daily flows and analyzed graphically for each station.

4.3.10. Presumptive standard flow level analysis

Around the world, water managers are facing a great challenge virtually everywhere to meet the increasing water needs due to population growth, irrigated agriculture, and urban uses combined with seasonal and interannual climate variability. Nevertheless, society at large (people around the world) are also demanding freshwater to protect the natural ecosystem which is being stressed due to human intervention. Therefore, the "environmental flows" are defined based on the quantity, quality and timings of water flows in the riverine system to sustain the biota and human livelihoods of freshwater and estuarine ecosystems. Basically, there are three approaches that have been used across broad geographies such as states or nations to determine the environmental flow standards. These three approaches are minimum flow thresholds, statistically based standards, and

percent-of-flow (POF). The minimum flow thresholds are the most commonly applied approach around the world. These minimum flow standards that must be maintained are the annual 7Q10, 30% of the mean annual flow (MAF), and variation of MAF seasonally, such as 40% of MAF in spring and fall, 30% of MAF in summer, and 60% of MAF in winter (Gillilan and Brown, 1997; IFC, 2001; Richter et al., 2011). The most widely used minimum flow thresholds in the USA is the annual 7Q10, which was originally used to protect water quality under the federal Clean Water Act of 1972. However, by default, it became a rule for the minimum flow standard in many states of USA (Gillilan and Brown, 1997; IFC, 2001; Richter et al., 2011). The annual 7Q10 is defined as the lowest flow for seven consecutive days that has a recurrence interval of 10 years.

Statistically based standards have been used in regulating water use to maintain high flow of a specified magnitude, duration and inter-annual frequency. These standards are estimated by using computerized hydrologic models that simulate the hydrologic changes such as dam operations and water withdrawal on the flow regime without affecting the high flows. If the water managers only need to meet the minimum flow standard, i.e., the annual 7Q10, then they have to only maintain a flat-lined flow since the annual 7Q10 provides specified values that depend on the length of the data used to calculate the annual 7Q10. On the contrary, if the water managers have to maintain the high flows (more flow regime) based on statistical standards then they need to simulate complex statistical models which might be confusing for non-technical stakeholders thus would be difficult to implement (Richter, 2009).

Therefore, a conceptually simple and considerably more protective approach for natural flow variability than minimum flow standard called the POF approach has been widely used across the world including USA in the past few decades. This approach is expressed as percentage alteration of natural (undeleted and unregulated) flow. The standards are set based on a high or

moderate level of ecological protection where riverine ecosystem will be maintained with minimal changes.

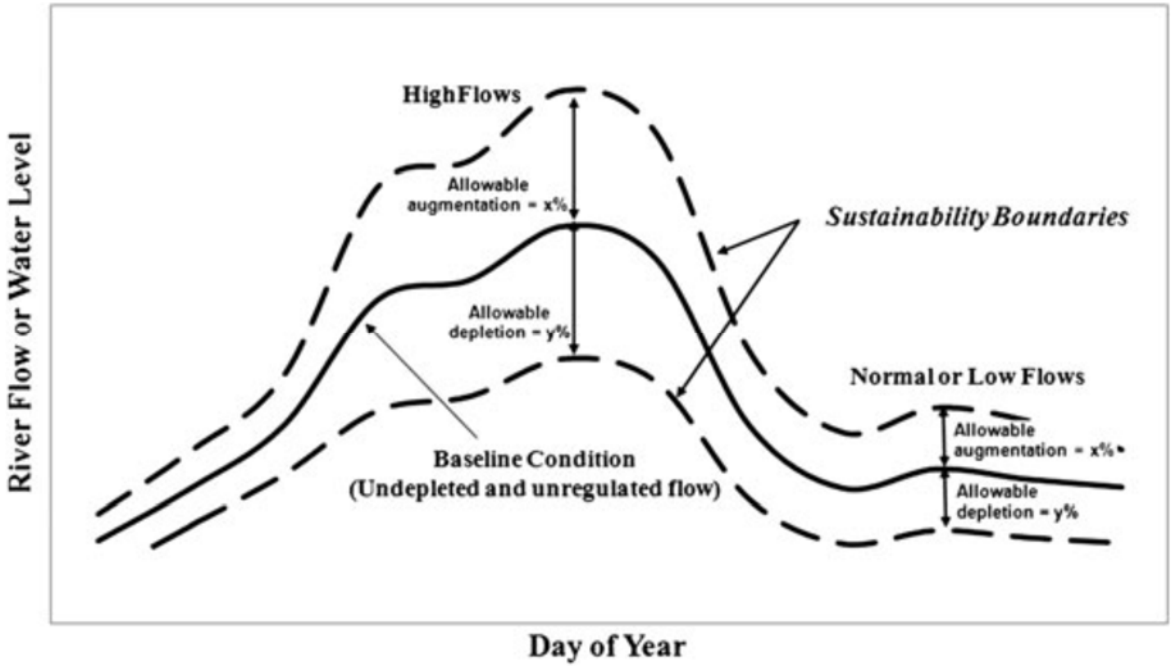

Figure 4.2. Representation of the sustainability boundary approach. The sustainability boundaries are defined as the limits to which natural flows can be altered and are expressed as a percentage of natural flows. (Source: Richter 2009, 2011).

High level of ecological protection means less than 10% alteration of daily flow while moderate level of protection provides alteration of daily flow by 11-20% (Figure 4.2) (Richter et al., 2003, 2006, 2011; Esselman and Opperman, 2010). Hydrologic alterations by greater than 20% of daily flows have resulted in moderate to major changes in natural ecosystem functions (Richter et al., 2003, 2006, 2011). However, studies by Brizga et al. (2002) and Carlisle et al. (2010) have observed biological impairment due to hydrologic alteration of greater than 25% of daily flow. Therefore, in this study POF approach was used with a hydrologic alteration of 25% daily flow during the non-irrigated period. The median daily flow of non-irrigated period was obtained for each day of a year then ±25% daily flow was plotted against the median natural flow. Finally,

drought year (La Niña phase) daily flows during NI and IR periods were plotted to understand the violation of the standards and stress buildup in the ecosystem.

4.4. Results and Discussion

4.4.1. Streamflow Analysis

A comparison of NI and IR period was performed on monthly median streamflows using JRFit procedure to determine if there was significant streamflow depletion during the IR period as compared to the NI period. The results of JRFit estimation for NI and IR are presented in Table 4.2. It was found that the differences in median streamflows between NI and IR period were highly significant ($p<0.01$) except for the station **D** which was not highly significant but significant ($p<0.05$) nonetheless.

Table 4.2. JRFit estimated median monthly streamflows in cms, p-values and percentage differences in streamflows during NI and IR periods.

Station ID	NI	IR	% difference NI to IR	p- value
A	124.48	103.89	-17	0.000
B	150.48	120.59	-20	0.000
C	17.23	13.87	-19	0.000
D	7.50	6.58	-12	0.036

The overall streamflow decreased by approximately 20% during irrigation period (Table 4.2). This might be due to the combined effects of intensive water withdrawal from UFA aquifer, and occurrence of several severe droughts during this period. To rule out changes in streamflow levels due to climate and be certain that the changes are caused by human interactions only, precipitation data for the IR and NI periods were also analyzed. Comparison of precipitation data for IR and NI periods suggests that precipitation did not change during the respective periods and the changes in the streamflow levels are due to human interactions only. Also, the JRFit analysis

of precipitation data for El Niño and La Niña phases suggested no significant difference ($p>0.05$) between NI and IR period median rainfall patterns for the phases of ENSO (Appendix C.1). Similar results have also been asserted by several researchers showing that no significant differences in rainfall amounts were found from 1938 to 2005 in Southeastern USA (Rose, 2009; Seager et al., 2009) and the recent droughts are similar to historic droughts; thus, suggesting that the current water shortages are mainly due to increased water demand in this region (Seager et al., 2009; Rugel et al, 2011). Although repeated droughts have occurred in the last decade, the study done by Rugel et al. (2011) on PDSI and precipitation showed that there has been no reduction in average precipitation or no increase in severity of drought during irrigation years.

Since the La Niña and El Niño phase precipitation pattern and amount have not been altered during NI and IR periods, the streamflow levels associated with El Niño and La Niña periods were analyzed to understand and quantify the effect of irrigation on the respective phases. The results pertaining to the comparison of the NI and IR periods during El Niño and La Niña phases are presented in Table 4.3. The results showed no significant differences between the median streamflows of NI and IR periods associated with El Niño, however, the differences between the median streamflows were found to be highly significant ($p\leq0.01$) during La Niña except station **D** ($p>0.05$) (Table 4.3). The streamflow levels in certain stream sections during the IR periods have seen reduction of as much as 34% compared to NI period (Table 4.3). Since there is not much irrigation withdrawal during the El Niño phases, these phases did not show lowering of IR period streamflow levels compared to the NI period (Table 4.3). However, flow levels fell drastically during the IR periods of La Niña (droughts) compared to NI periods which conclusively shows that irrigation and human withdrawal from the Flint River during droughts are primarily responsible for lowering of flow levels.

Table 4.3. JRFit estimated median monthly streamflows in cms, p-values, and percentage differences in streamflows from NI to IR periods associated with phases of ENSO.

Station ID	El Niño				La Niña			
	NI	IR	% change NI to IR	p-value	NI	IR	% change NI to IR	p-value
A	135.81	135.00	-1	0.901	104.96	92.06	-12	0.01
B	144.03	148.43	3	0.479	162.32	106.56	-34	0.00
C	17.27	17.77	3	0.543	15.63	11.68	-25	0.00
D	8.25	10.28	25	0.126	4.20	3.56	-15	0.30

4.4.2. Baseflow Analysis

Similarly, baseflow analysis was performed to account for the stream-aquifer interaction response to long-term (intensive) groundwater extraction (Table 4.4). Highly significant differences between NI and IR period median baseflows ($p<0.01$) were found across all stations and baseflow levels were reduced by approximately 18% during IR as compared to NI periods (Table 4.4). Rugel et al. (2011) also found similar patterns in baseflow in the lower Flint River basin.

Table 4.4. JRFit estimated median monthly baseflow in cms, p-values and percentage differences in baseflows from NI to IR periods.

Station ID	NI	IR	% difference NI to IR	p- value
A	84.96	71.94	-15	0.000
B	110.31	89.21	-19	0.000
C	12.90	10.16	-21	0.000
D	5.60	4.77	-15	0.007

Similar to streamflow analysis, baseflow results also showed no significant differences between the median streamflows of NI and IR periods associated with El Niño. However, the differences between the median streamflows were found to be highly significant ($p\leq0.01$) during La Niña except for station D ($p>0.05$) which might be due to less data availability (Table 4.5). Recent studies done by Jones and Torak (2006) also suggested that intensive groundwater

withdrawal has lowered potentiometric surface of groundwater by decreasing potential recharge which explains the results found in Table 4.4 and Table 4.5.

Table 4.5. JRFit estimated median monthly baseflows in cms, p-values and percentage differences in baseflows from NI to IR periods associated with phases of ENSO.

Station ID	El Niño				La Niña			
	NI	IR	% change NI to IR	p-value	NI	IR	% change NI to IR	p-value
A	87.48	87.72	0	0.953	71.60	62.70	-12	0.006
B	99.87	103.52	4	0.353	118.59	78.73	-34	0.000
C	12.39	12.19	-2	0.740	12.14	9.09	-25	0.001
D	5.59	6.84	22	0.169	3.08	2.51	-18	0.182

4.4.3. 1-Day and 7-Day Low Flow Analysis

The results pertaining to the comparison of the NI and IR periods for 1-day and 7-day low flows are presented in Table 4.6 and Table 4.7, respectively. The overall 1-day and 7-day median low flows reduced significantly ($p<0.01$) during the IR period for all the gauges by approximately 20% and 22%, respectively (Table 4.6 and Table 4.7). Analysis of 1-day and 7-day low flows showed no significant difference between low flows of NI and IR periods during El Niño except for station B which was significant at a level of 5% (Table 4.8 and Table 4.9).

Table 4.6. JRFit estimated median monthly one-day low flows in cms, p-values and percentage differences in one-day low flows from NI to IR periods.

Station ID	NI	IR	% difference NI to IR	p- value
A	58.16	51.14	-12	0.003
B	84.51	69.52	-18	0.000
C	10.89	8.11	-25	0.000
D	3.89	2.94	-24	0.000

Similar to streamflow and baseflow results, one-day low flow values were substantially ($p<0.05$) lower during the IR period associated with La Niña except the station **D** (due to less data) (Table 4.8). One-day low flow values during La Niña phases were lower than overall one day low flow values (Table 4.8). Overall, 1-day low flow value for station B during irrigation period was

18% lower than the NI period which further reduced by 29% (approximately one-third of one day low flow) during La Niña phases in the IR period (Table 4.6 and Table 4.8). Similar to 1 day low flows, the differences between the median 7-day low flows of NI and IR periods were not significant during El Niño phase. However, highly significant differences were found during La Niña ($p<0.01$) for all stations except station D ($p>0.05$) (Table 4.9). Moreover, overall 7-day low flow value for station B during irrigation period was 22% lower than NI period and it further reduced by 34% (approximately more than one-third of flow) during La Niña phases in IR period (Table 4.7 and Table 4.9). The above results clearly shows that pumping during droughts can have significant impact on 1-day and 7-day low flows and thereby threaten the aquatic habitat of the stream.

Table 4.7. JRFit estimated median monthly 7-day low flows in cms, p-values and percentage differences in seven-day low flows during non-irrigated and irrigated periods.

Station ID	NI	IR	% difference NI to IR	p- value
A	79.73	63.92	-20	0.000
B	103.66	81.37	-22	0.000
C	11.60	8.80	-24	0.000
D	4.13	3.19	-23	0.000

Table 4.8. JRFit estimated median monthly one-day low flows in cms, p-values and percentage differences in one-day low flows from NI to IR periods associated with phases of ENSO.

Station ID	El Niño				La Niña			
	NI	IR	% change NI to IR	p-value	NI	IR	% change NI to IR	p-value
A	57.30	58.33	2	0.712	49.57	45.29	-9	0.04
B	69.94	79.33	13	0.015	90.90	64.45	-29	0.00
C	10.39	9.81	-6	0.282	10.34	7.50	-27	0.00
D	3.92	4.42	13	0.456	2.49	1.88	-24	0.07

The JRFit estimation of median streamflows, baseflows, 1-day and 7-day low flows are presented in Figure 4.3. It was found that overall and La Niña flows during irrigation period have reduced substantially for all the stations. However, flow has not changed during the El Niño phase

(Figure 4.3). Figure 4.3 also shows that flows during La Niña have substantially reduced in the IR period which suggests that drought and irrigation water withdrawal from the aquifer lead to decreased flow levels during IR periods.

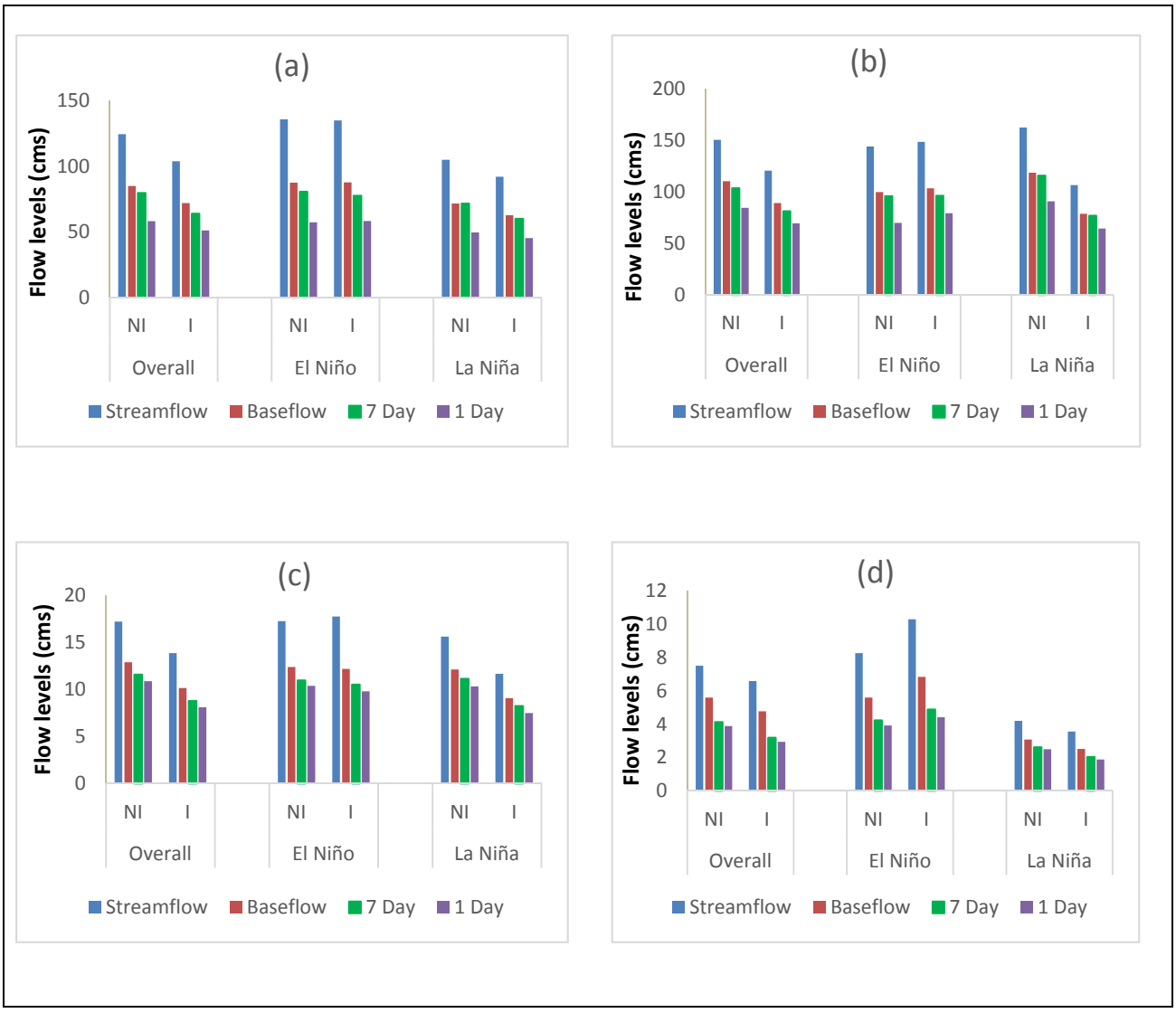

Figure 4.3. JRFit estimation of median streamflows, baseflows, 1-day and 7-day low flows for (a) station A, (b) station B, (c) station C, and (d) station D.

Table 4.9. JRFit estimated median monthly seven-day low flows in cms, p-values and percentage differences in seven-day low flows from NI to IR periods associated with phases of ENSO.

Station ID	El Niño				La Niña			
	NI	IR	% change NI to IR	p-value	NI	IR	% change NI to IR	p-value
A	80.71	77.55	-4	0.449	71.69	60.02	-16	0.00
B	95.87	96.26	0	0.934	115.77	76.90	-34	0.00
C	10.98	10.54	-4	0.524	11.15	8.26	-26	0.00
D	4.23	4.88	15	0.394	2.62	2.03	-22	0.12

4.4.4. Growing and Non-Growing Period Analysis

4.4.4.1. Streamflow Analysis

The results of JRFit estimation comparing the NI and IR periods during non-growing and growing seasons are presented in Table 4.10. During non-growing seasons, no significant differences were found between median NI and IR periods except for the station **C** (Table 4.10). However, highly significant differences ($p<0.01$) were found during growing seasons across all stations between the median streamflows of NI and IR periods and streamflow levels decreased by approximately 26% during IR periods (Table 4.10).

Table 4.10. JRFit estimated median monthly streamflows in cms, p-values and percentage differences in streamflows from NI to IR periods associated with non-growing and growing seasons.

Station ID	Non-Growing				Growing			
	NI	IR	% change NI to IR	p-value	NI	IR	% change NI to IR	p-value
A	180.58	169.77	-5.99	0.093	105.83	79.66	-24.74	0.000
B	208.86	182.46	-12.64	0.073	130.12	96.82	-25.59	0.000
C	23.81	22.06	-7.36	0.013	14.97	10.86	-27.47	0.000
D	11.12	12.12	9.02	0.279	6.31	4.55	-27.86	0.001

The results of JRFit estimation comparing the NI and IR periods during ENSO phases associated with non-growing seasons are presented in Table 4.11. It is found that no significant

differences were observed during La Niña for all the stations and El Niño as well except for the stations **C** and **D** (Table 4.11). This suggests that streamflow levels in non-growing seasons do not vary significantly between NI and IR periods even during La Niña phases.

Table 4.11. JRFit estimated median monthly streamflows in cms, p-values and percentage differences in streamflows from NI to IR periods associated with non-growing season for the phases of ENSO.

Station ID	El Niño				La Niña			
	NI	IR	% change NI to IR	p-value	NI	IR	% change NI to IR	p-value
A	195.04	216.79	11.15	0.055	123.71	125.87	1.75	0.823
B	192.09	217.12	13.03	0.215	205.81	151.98	-26.15	0.101
C	22.21	25.56	15.09	0.019	17.75	15.79	-11.08	0.086
D	12.54	21.23	69.28	0.006	3.95	5.33	34.96	0.173

However, interesting results have been found during the growing period when NI and IR periods have been compared (Table 4.12). No significant ($p>0.05$) differences were observed between the median streamflows of NI and IR periods associated with El Niño phase except for station **A** significant ($p<0.05$) (Table 4.12). However, the differences between the median streamflows of NI and IR periods were found to be highly significant ($p<0.01$) associated with La Niña phase (Table 4.12). During the La Niña cycle streamflow levels are lower by approximately 50% in the irrigation period except for the station **A** which is lower by approximately 30%. The comparison of results in Table 4.11 and Table 4.12 confirm that streamflow levels in the Lower Flint River and its tributaries are being impacted by irrigation water withdrawal and streamflow levels in certain stream sections have been reduced by as much as 50% since the introduction of irrigation in the mid-1970s.

Table 4.12. JRFit estimated median monthly streamflows in cms, p-values and percentage differences in streamflows from NI to IR periods associated with growing season for the phases of ENSO.

Station ID	El Niño				La Niña			
	NI	IR	% change NI to IR	p-value	NI	IR	% change NI to IR	p-value
A	101.62	88.71	-12.71	0.026	93.69	63.34	-32.40	0.000
B	120.00	106.70	-11.08	0.067	155.01	75.36	-51.39	0.000
C	13.12	11.71	-10.76	0.127	14.65	8.07	-44.90	0.001
D	5.68	5.98	5.29	0.606	4.40	2.07	-52.97	0.001

4.4.4.2. Baseflow Analysis

Similar to streamflow analysis, baseflow results have also shown significant differences between NI and IR periods during growing season and showed no significant difference during non-growing periods except for the station **C** ($p<0.05$) (Table 4.13). During non-growing seasons, no significant differences were observed between NI and IR periods associated with La Niña (across all the stations) and El Niño as well (except for station C) (Table 4.14). During growing seasons, no significant differences were observed between NI and IR periods associated with El Niño except for station C.

Table 4.13. JRFit estimated median monthly baseflows in cms, p-values and percentage differences in baseflows from NI to IR periods associated with non-growing and growing seasons.

Station ID	Growing				Non-Growing			
	NI	IR	% change NI to IR	p-value	NI	IR	% change NI to IR	p-value
A	72.19	56.19	-22.16	0.000	121.73	113.64	-6.65	0.127
B	97.86	74.70	-23.66	0.000	147.87	130.63	-11.66	0.081
C	11.40	8.01	-29.72	0.000	16.87	15.43	-8.55	0.047
D	5.07	3.61	-28.81	0.000	7.24	7.64	5.61	0.449

However, highly significance differences were found between NI and IR periods associated with La Niña (Table 4.15). Moreover, overall baseflow levels during growing seasons decreased

substantially by approximately 26% (Table 4.13) in the IR period which further lowered by approximately 50% during La Niña (Table 4.15). These results again confirm that stream-aquifer interaction gets affected by intensive irrigation during droughts.

Table 4.14. JRFit estimated median monthly baseflows in cms, p-values and percentage differences in baseflows from NI to IR periods associated with non-growing season for the phases of ENSO.

Station ID	El Niño				La Niña			
	NI	IR	% change NI to IR	p-value	NI	IR	% change NI to IR	p-value
A	133.29	146.64	10.02	0.093	85.39	86.24	0.99	0.893
B	139.13	151.02	8.54	0.199	127.19	103.12	-18.92	0.282
C	17.47	19.57	11.97	0.025	13.47	12.18	-9.57	0.283
D	9.25	13.59	46.90	0.077	2.93	3.82	30.36	0.087

Table 4.15. JRFit estimated median monthly baseflows in cms, p-values and percentage differences in baseflows from NI to IR periods associated with growing season for the phases of ENSO.

Station ID	El Niño				La Niña			
	NI	IR	% change NI to IR	p-value	NI	IR	% change NI to IR	p-value
A	66.48	60.38	-9.18	0.059	63.31	43.87	-30.70	0.000
B	83.68	76.79	-8.23	0.067	112.47	55.50	-50.65	0.001
C	10.18	8.63	-15.22	0.011	11.20	6.16	-45.01	0.001
D	4.27	4.19	-1.89	0.807	3.66	1.78	-51.47	0.000

4.4.5. Flow Duration Analysis (FDC)

Flow duration curves were produced from the daily flows of non-irrigation and irrigation periods for all the gauging stations that are presented in Figure 4.4. FDCs showed that 80% exceedance flows have been dropped substantially for all the stations (Figure 4.4). This clearly suggests that low flows have been majorly impacted and have reduced substantially during the irrigation period. However, high flows and above first quartile flows were identical to flows during the non-irrigations flows (Figure 4.4).

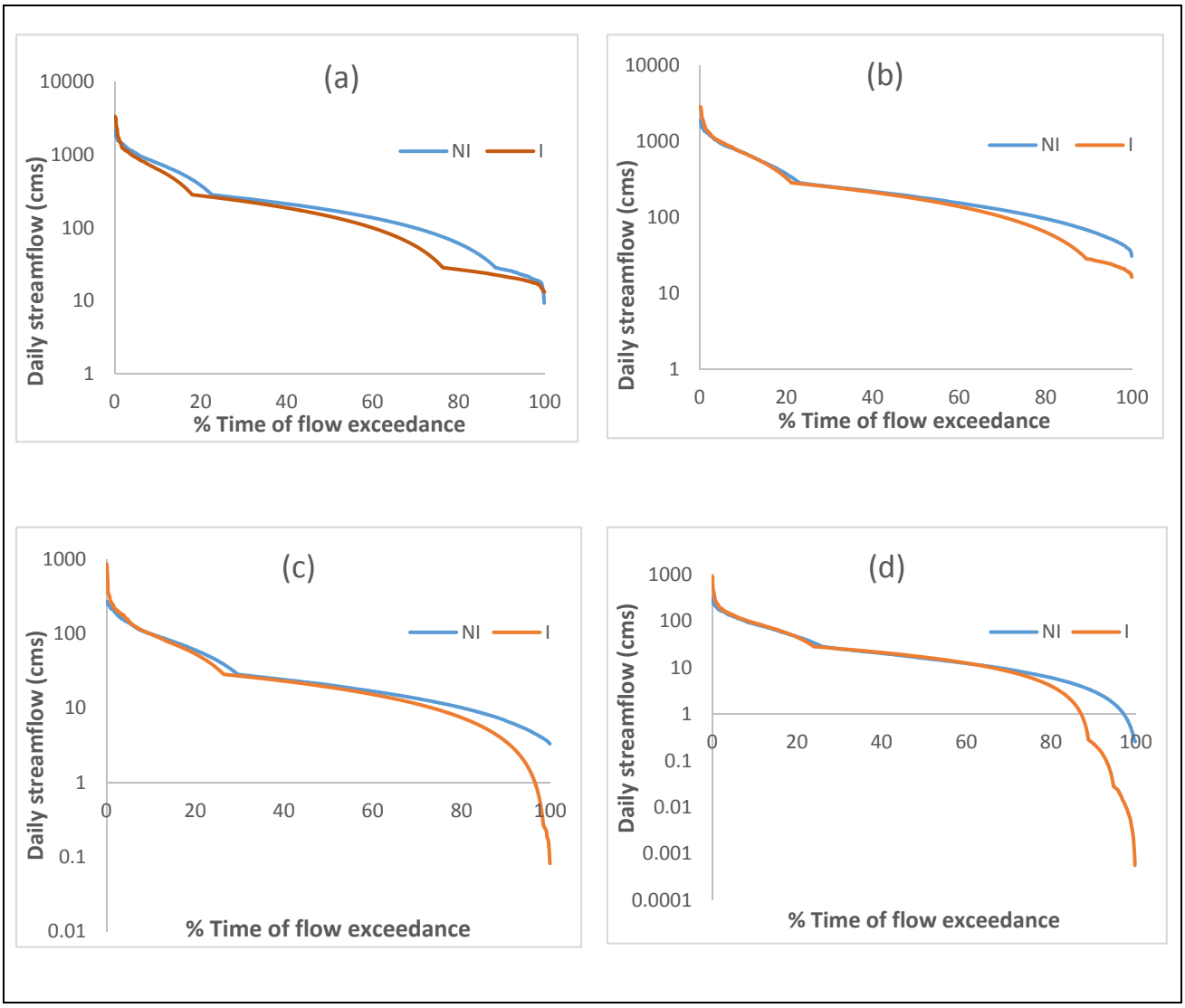

Figure 4.4. Flow duration curve for non-irrigated and irrigated periods for (a) station A, (b) station B, (c) station C, and (d) station D.

The FDC also suggests that in the IR period the occurrence of low flows have increased substantially compared to the NI period. The gauging stations C and D suggests that tributary reaches are severely affected by agricultural irrigation withdrawal since the FDC analysis shows that at times low flows have reduced to zero during the IR period which was not the case during NI period (Figure 4.4(C) and Figure 4.4(D)). The results from FDC analysis shows that irrigation water withdrawal affects the tributaries of the LFR more severely than the main Flint River since

flow ranges in these tributaries are far less than the main Flint River and hence any increase in irrigation can run the streams dry and affect the aquatic habitat severely.

4.4.6. Presumptive Standard Flow (PSF) Level Analysis

The presumptive standard flow (PSF) for station A is presented in Figure 4.5 where blue line shows the long term median flow obtained from non-irrigation period for all the months. The upper and lower red lines show the 25% increased and decreased from the median flow, respectively (Figure 4.5).

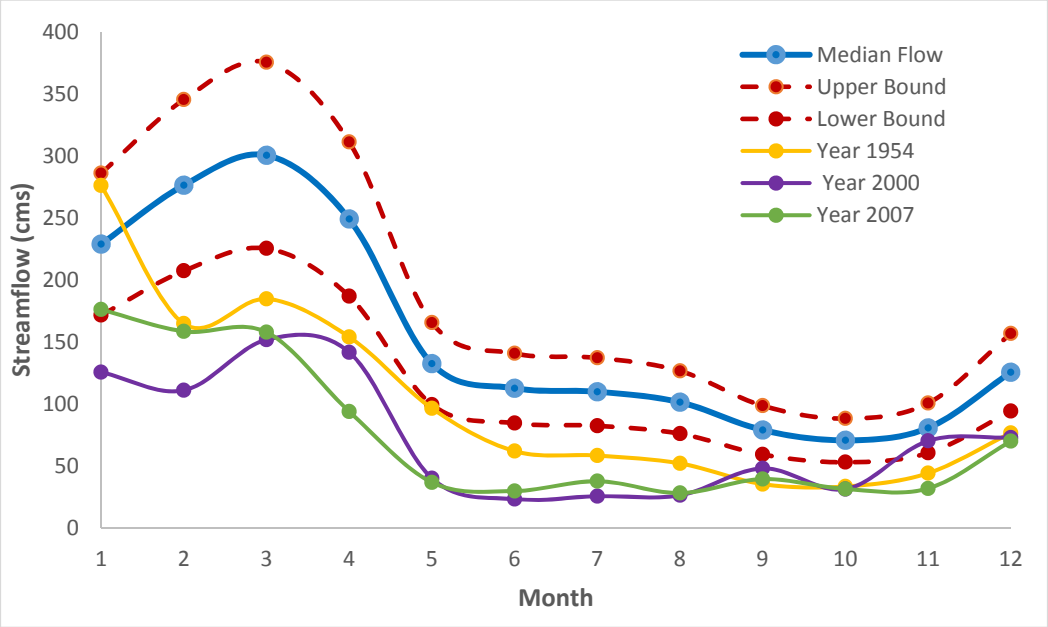

Figure 4.5. Monthly presumptive standard streamflow levels, associated upper and lower bounds, and streamflow levels for the year 1954, 2000 and 2007 for station A.

This band of presumptive flow standard was compared with historic drought events during NI and IR periods. The severe drought event of 1954 that occurred during the non-irrigated period shows that the flow levels for all the months were close to or less than the 25% lower bound of the PSF (Figure 4.5). However, the recent drought events of the irrigation period (year 2000 and 2007)

were much lower than the 25% lower bound of the PSF (Figure 4.5). The 25% lower bound of the PSF value for the month of June was 112.5 cms, while the flow value for that month for year 1954 was 61.76 cms which is approximately 27% lower than the 25% lower bound PSF value (Figure 4.5). Flow levels during the similar months for year 2000 and 2007 reduced drastically to 23 cms and 29.6 cms, respectively, which is approximately 72% and 65% lower than the 25% lower bound PSF value for that month (Figure 4.5). The results of this PSF analysis shows that during the drought events in the IR period flow levels are in violation of the PSF standards which will result in greater changes in stream ecosystem functions and associate greater risk to the habitat due to greater levels of alteration in daily flows.

4.5. Conclusions

This study estimated the effect of ENSO induced drought and irrigation on flow levels of lower FRB using non-parametric JRFit procedure. The results of the study indicated that ground-water withdrawal from the UFA within the Dougherty Plain of southwestern Georgia resulted in decrease of streamflow/baseflow in the lower FRB since the underlying riverbed is hydraulically connected to the karstic UFA. Especially during droughts (La Niña phases), when ground water levels are already low (Mitra et al., 2014), increased irrigation water withdrawal leads to further lowering of groundwater levels and are hence responsible for greater decrease in the stream-aquifer flow. The analysis of non-irrigation and irrigation period showed that since 1970s overall streamflow/baseflow has reduced substantially in the LFR and its tributaries. Moreover, the analysis of 1-day and 7-day low flows and FDC showed that frequency of low flows has increased during IR period and tributaries (gauging station **C** and **D**) have changed from perennial stream to

intermittent, which suggests that groundwater withdrawal has intensified the extreme low flows in this region.

The analysis of NI period to IR period flow levels during growing and non-growing seasons has provided interesting results where non-growing season flow levels were similar during both the phases of ENSO. However, during the growing period flow levels has reduced substantially during La Niña phases, which suggests that the combination of groundwater removal (irrigation pumpage) and La Niña induced drought have significant impact on flow levels of the lower FRB causing stream reaches to go dry. Lowering of flow levels in stream reaches due to drought and pumpage may result in anoxic conditions that threatens the federally protected mussel species and other aquatic species residing in the lower FRB. The analysis of presumptive water use also demonstrated that the flow levels are always lower than the presumptive flow band during the drought events in the IR period and flow levels have reduced substantially during the growing season.

The above findings provides an insight on the lowering of the flow levels in the lower FRB by studying the natural and anthropogenic hydrologic stresses. Understanding the climate induced droughts and resulting lowering of the flow levels can provide a clear picture of hydrologic droughts which might be further exacerbated in future by increased water demand by growth in population, increased irrigated agriculture and urban sprawl. In addition to anthropogenic stress (such as population growth) on fresh water resources, it is projected that natural stresses such extreme climatic events, including drought, are going to be a common phenomenon under global climate change scenarios (Easterling et al., 2000). Therefore, policy makers and water managers in this region should try to make a better policy where definite fresh water resources can be shared between human and aquatic biota of the ecosystem.

Chapter 5

Effects of Groundwater Pumpage on Stream-Aquifer Interaction during Droughts in the Lower ACF River Basin

5.1. Abstract

Groundwater is the ultimate source of freshwater and also primary buffers against episodic El Niño Southern Oscillation (ENSO) induced droughts in the Southeast for agriculture, municipal, and industrial water supply. The lower Apalachicola-Chattahoochee-Flint (ACF) River Basin is a major agricultural area and is underlain by a highly productive karstic aquifer called the Upper Floridan Aquifer (UFA) which is in hydraulic connection with the Flint River. This hydrologic connectivity between surface water and groundwater leads to lowering of flow levels in the Flint River due to intensive agricultural withdrawals during droughts. The lowering of flow levels in the Flint River leads to changes in quantity and quality of surface waters and threatens the endangered species. This study was conducted to quantify the compounding effect of climate variability induced drought and human induced irrigation pumpage on stream-aquifer flux in the Flint River to identify critical reaches and tributaries of the Flint River that are sustained by baseflow and are majorly responsible for lowering of flow levels in the river. The groundwater model MODular Finite-Element Model (MODFE) developed by USGS was used to simulate the effect of irrigation on stream-aquifer flux during the drought years of 2010 to 2012. Sensitivity analysis was performed to identify the sensitive reaches where stream-aquifer connection is strongest and lowering of flow levels are prone to irrigation water withdrawal. The effectiveness

of the proposed various water restrictions scenarios on irrigation withdrawal were also analyzed by comparing the percentage recovery of simulated stream-aquifer fluxes. Moreover, acreage buyout under various water restrictions scenarios were studied. The results of the study indicated that increased ground-water withdrawal in the WY 2011 resulted in decrease in the stream-aquifer flux in the lower ACF. Particularly, in the Spring creek, increased pumpage during the months of April, June and July resulted in significantly decrease in stream-aquifer flux that changed the stream characteristics from gaining to losing stream. The results from sensitivity analysis and simulated water restrictions suggested that stopping irrigation pumpage in sensitive areas is more effective measure in streamflow recovery than reducing irrigation intensity (15% or 30%) throughout the study area. Moreover, analysis of acreage buyout suggested that restrictions on irritation withdrawal can have significant impact on stream-aquifer flux in the study area, especially in critical watersheds of Spring creek and Ichawaynochaway creek.

5.2. Introduction

The compounding effect of climate variability induced droughts and anthropogenic activities such as irrigation can have detrimental effects on all the components of hydrologic budget (White et al., 2008; Hopkin, 2007; Thuiller, 2007) including surface water and ground water interactions. Aquifers that host groundwater are sensitive to climatic oscillations such as El Niño Southern Oscillation thereby regulating the fluctuation of groundwater system (Mitra et al., 2014). In the Southeast US, La Niña induced droughts are responsible for lowering of groundwater levels which sometimes take few years to recover keeping the region under water stressed condition (Mitra et al., 2014). Moreover, these water stresses gets exacerbated increase in irrigated agriculture in southwest Georgia. This has led to growing interest of studying the combined effect

of climate and anthropogenic impacts on coupled hydrologic system where recharge/discharge from groundwater interact to affect both groundwater and surface water in the region.

The hydrologic connectivity between surface water and groundwater has become an importance issue among scientific community due to increased dependency on groundwater withdrawals. Groundwater is the ultimate source of freshwater and less prone to pollution than surface water and also the primary buffers against episodic drought in the Southeast for agriculture, municipal, and industrial water supply. The lower ACF River Basin (Figure 5.1), a major agricultural area, is mostly located in the southwest Georgia. This region is underlain by a highly productive karstic aquifer called the Upper Floridan Aquifer (UFA). The UFA is the major water bearing unit and the primary source of groundwater in the lower ACF basin, which is heavily exploited due to widespread irrigation water withdrawal for row crop agriculture. The UFA is a limestone aquifer and the hydraulic connection with surface water has been well documented (Hayes et al, 1983; Bush and Johnston, 1988; Toral et al., 1996; Torak and McDowell, 1996; Torak and Painter, 2006). Therefore, groundwater withdrawal from UFA would affect the stream flows in this region, particularly, where stream reaches are directly connected to UFA through sink holes and fractures.

Southwest Georgia had witnessed tremendous expansion of agricultural water usage between 1970 and 1980, during which the total irrigated acreage increased from 130,000 to 261,000 (Pollard et. al, 1978), mainly due to extensive implementation of centre pivot irrigation systems (Pierce et al., 1984). By 1980s, irrigated farmland had increased many folds to more than 452,000 acres, and the annual combined surface water and groundwater use was greater than 290 million gallons per day (Mgals/day) (Pierce et. al, 1984), out of which, approximately 80% of water used for irrigation was extracted from the UFA (Hicks et al., 1987; Litts et. al., 2001).

Presently, in the lower ACF river basin (Figure 5.1), about half-a-million acreage is irrigated by nearly 4000 irrigation wells pumping from the UFA. Since the mid-1970, climate variability induced droughts and intensive irrigated agriculture have caused unprecedented decline in groundwater levels and resulted in lowering of baseflow levels in the lower Flint River Basin (Chapter 3).

Numerous studies have shown that excessive withdrawal of groundwater has been responsible for changes in quantity and quality of surface waters, loss of riparian communities, land subsidence, and damage to the ecosystem and economy of various regions across the world (Postel, 1999; Glennon, 2002; Chen et al., 2003; Zektser et al., 2005; Shi et al., 2007). Moreover, overextraction of groundwater removal near stream channels leads to depletion of streamflow levels (Sophocleous, 2002) by altering the stream characteristics (gaining to loosing stream) and temperature, threatening aquatic habitats (Golladay et al., 2004), and reduction of nutrient loading to downstream areas (Pringle and Triska, 2000; Bunn and Arthington, 2002). Therefore, the increased irrigation groundwater withdrawals in southwestern Georgia have raised concern of sustainability of streams and rivers in the lower ACF Basin.

The freshwater resources of the ACF basin (Figure 5.1), which is located in Alabama, Georgia, and Florida, provides great support to human needs, urban sprawl, industrial, municipal and rural water supplies, power facilities, irrigated agriculture, shellfish industry, and estuarine ecosystem. Since 1980, ACF basin has experienced water shortages due to recurring droughts in the Southeast, rapid growth in population, increased urbanization. Irrigated agriculture has put tremendous stress on freshwater resources and threatens the availability of freshwater to the shellfish industry present in the downstream Apalachicola Bay. This water shortage has prompted water use restrictions on municipal and irrigated waters uses and has instigated interstate water

conflicts in this region. These combined stresses of climate variability induced droughts, irrigation and population growth on water resources has led to "Tri-State Water Conflict" among the neighboring states of Georgia, Alabama and Florida (Jordan et al., 2006). Over the last two decades, this conflict has been marked by costly, time consuming, ongoing litigations and failed negotiations where the sparring parties have failed to reach a common ground on the partitioning of water resources of the ACF River Basin, thereby, making the ACF as one of the most contentious river basins of the USA. One of major issues related to the ongoing conflict is the lowering of streamflow levels in the Flint River during droughts due to increased demand for water for irrigation, municipal and industrial purposes from surface and groundwater resources in Georgia.

Numerous modeling studies have reported the connection between ground water and surface water (through streams and the UFA) in the study area and the effect of natural and/or anthropogenic stress on ground water (GW) levels and stream-aquifer flows (Hayes et al., 1983; Faye and Mayer, 1990, 1996; Torak et al., 1996; Torak and McDowell, 1996). However, in this study, a groundwater model called Modular Finite Model (MODFE), developed by United States Geological Survey (USGS) was used to evaluate the impact of pumping groundwater from the UFA on stream aquifer interaction in the lower ACF region (Torak and Paniter, 2006; Jones and Torak, 2006). The model was applied to recent drought period of two water years; 2011 and 2012 including a 6-month of irrigated season and a 6-month off-season having relatively little or no irrigation pumping. This study was focused specifically on La Niña events that existed from May 2010 to September 2012. Therefore, the overarching goal of this study is to understand the relationships among droughts, irrigation, and flow levels in the study area and to identify critical reaches and tributaries of the Flint River that support baseflow and are responsible for lowering of

flow levels in the river due to drought and pumpage. Moreover, various possible simulated water restrictions suggested by the Flint River Drought Protection Act (FRDPA) (Georgia General Assembly), Environmental Protection Division (EPD) policies, and Flint River Basin Regional Water Development and Conservation Plan (the Flint Plan) were also analyzed to study the effectiveness of possible future water restrictions. Apart from that, cost analysis was done based on buyback program for different water restriction scenarios. The FRDPA mandates the state to introduce buyback program that compensate farmers for voluntary and involuntary suspension of irrigation during droughts to sustain flows in the FR. During 2001 drought, the buyback program was first implemented, but later in drought year 2012, the state of GA did not implement the program due to lack of funds and citing ineffectiveness of the policy. Therefore, in this study, a cost benefit analysis of the buyback program is studied for various suggested water restriction scenarios. The results from this research provides useful information to decision-makers in evaluating policies or management strategies and can also help the State of Georgia to better manage groundwater in order to protect surface water from irrigation-induced streamflow reduction during droughts in the lower ACF.

5.3. Methodology

5.3.1. Study Area

The ACF basin is located in the southeastern United States where much of the basin lies in western Georgia, and some in eastern Alabama and northern Florida (Figure 5.1). The total area of the ACF river basin is approximately 50,800 square kilometers. The ACF basin has mild winters and long summers with the average annual precipitation and temperature of 50 in and 64^0F, respectively. The headwater of Chattahoochee and Flint Rivers are located in the north of Lake

Sidney Lanier and south of Atlanta, respectively. Both the Chattahoochee and Flint Rivers converge together at Lake Seminole to form the Apalachicola River which drains into the Gulf of Mexico. The lower ACF River Basin contains karst UFA which mainly supports the groundwater resources and eventually contributes to surface water in the ACF River Basin. The streams in this basin have gaining and losing characteristics depending on the location and season of the year.

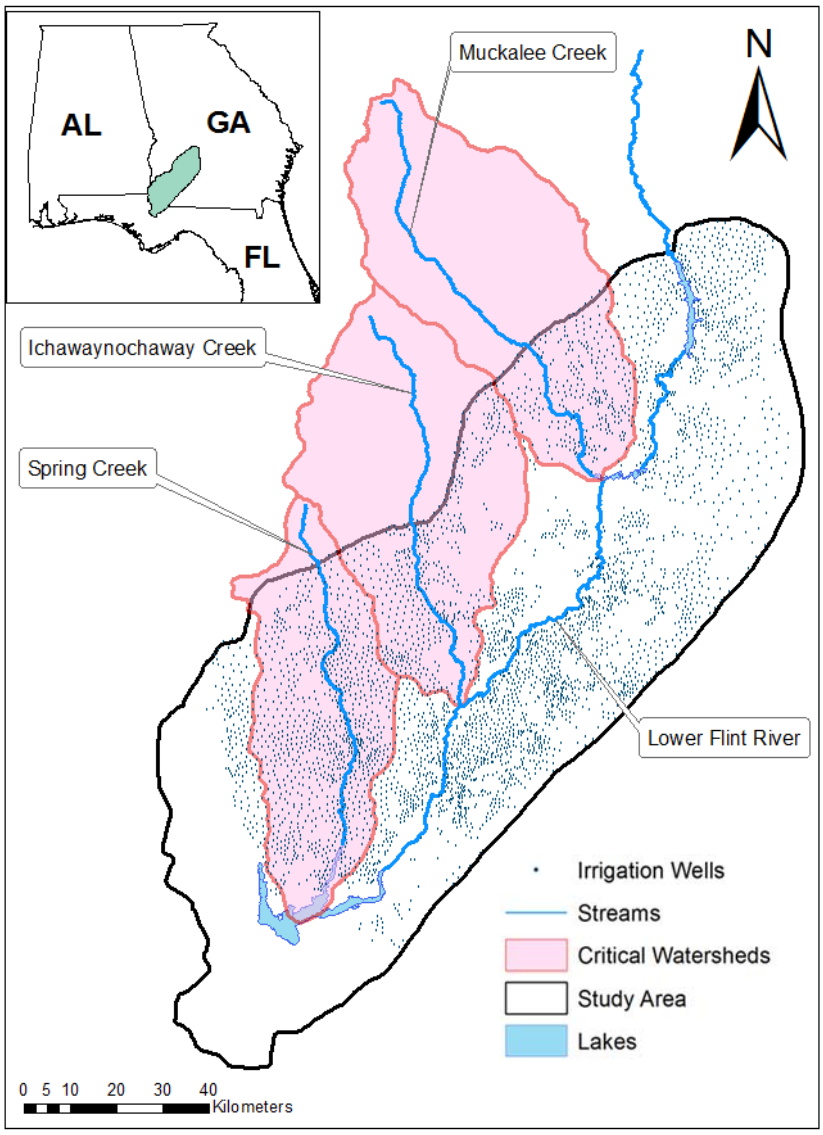

Figure 5.1. Location of the study area showing location of irrigation wells in Spring Creek, Ichawaynochaway Creek, Muckalee creek and lower Flint River Basins (LFRB).

5.3.2. Upper Floridan Aquifer and Stream-Aquifer Flow

The UFA is the primary water-bearing hydrologic unit in the lower ACF basin. The UFA has strong hydraulic connection with streamflows through direct connections with many sinkhole ponds, karst sinks, and conduits and trough incised streambeds and indirect connections through vertical leakage from overburden. UFA is comprised of four hydrologic units namely surficial aquifer system (SAS), upper semi-confining unit (USCU), aquifer (UFA), and lower confining unit (LCU) (Torak and Painter, 2006) and these hydrologic units are created by the differences in hydrologic and lithologic characteristics within a geologic unit. The surficial aquifer system is undifferentiated (surficial) overburden or weathered residuum deposits that contain water-bearing zones. However, for this MODFE groundwater model all the sediment (overburden) overlying the UFA are lumped together and called the USCU, and the underlain unit of the UFA made by the Eocene Lisbon Formation is called LCU. The UFA mainly consists of the karst Ocala Limestone which becomes thin as it nears the outcrop (Figure 5.3) and has high transmissivity value of 1.4 x 10^4 m^2/day (Hicks et al, 1987). The USCU lying above the UFA is the major source of vertical leakage to the UFA and consists of sandy (above) layers and clayey layers (below). The upper sandy layer completely dries up during drought while the lower clayey layer acts as a source of recharge to UFA.

Stream-aquifer flow is the flow of water across the streambed (Torak and McDowell, 1996) and is responsible for either increase or decrease of baseflow at any point along a stream. Every point along a stream reach has a set of Stream–aquifer flow characteristics that determine the volumetric flow at that point and these are stream dimensions, hydraulic conductivity of streambed materials, streambed thickness, stage of the stream, and head in the aquifer. However, stream stage and aquifer head are the most dynamic of all the factors listed above that cause changes in GW

levels and stream-aquifer flows. Both, GW levels and the stream-aquifer flux in the UFA respond to seasonal climatic effects of precipitation, droughts, lake level changes and stream-stage fluctuations in water levels in the UFA. Fluctuation of GW levels in the UFA depend on proximity to surface streams or lake systems, location specific hydraulic characteristics and thickness of the overlying confining unit, and groundwater irrigation withdrawal for agricultural, industrial, and municipal purposes.

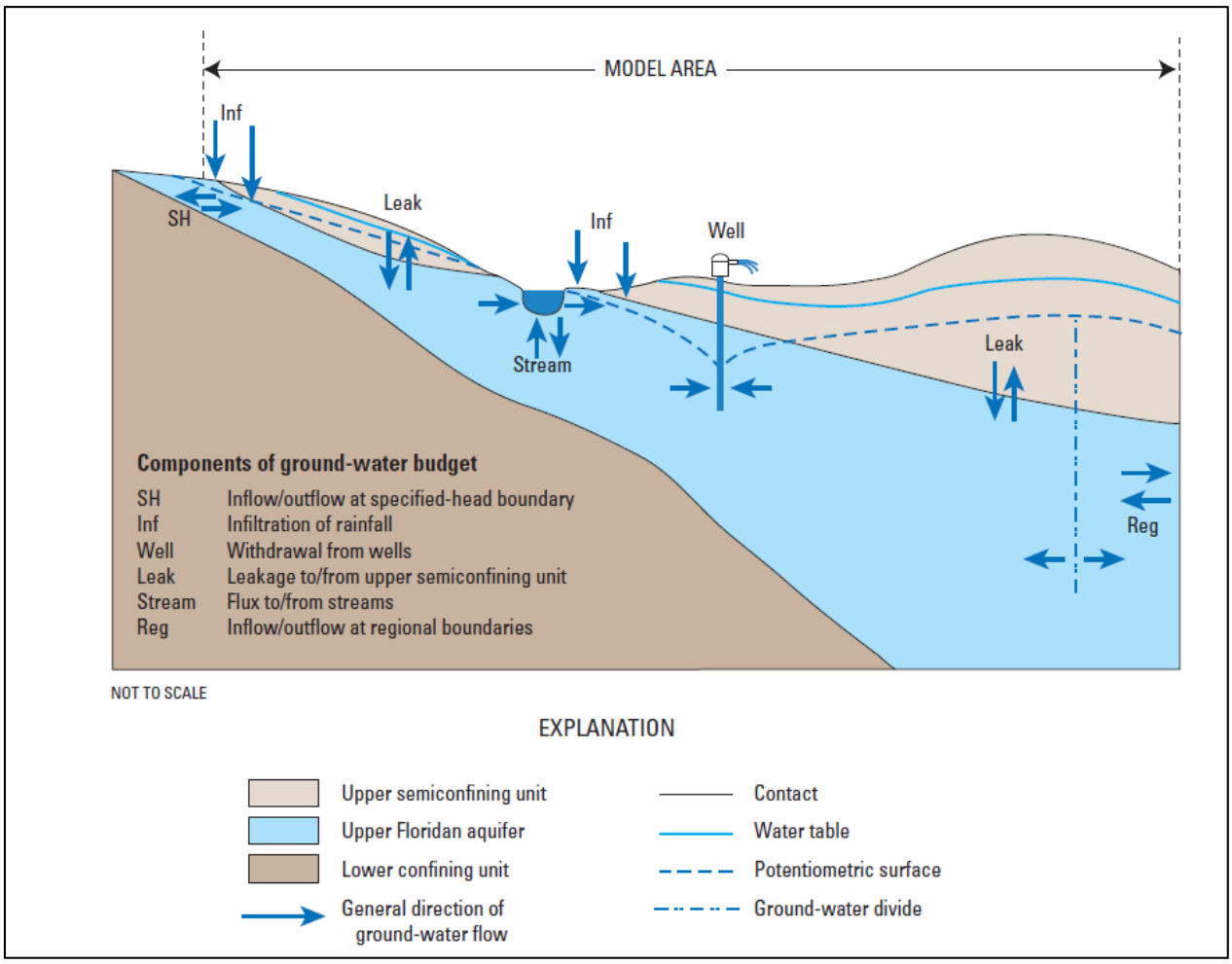

Figure 5.2. Stream and Groundwater flow system of the Upper Floridan aquifer in the lower Apalachicola-Chattahoochee-Flint River Basin showing components of the ground-water budget simulated by the model (Jones and Torak, 2006).

5.3.3. MODular Finite-Element (MODFE) Model

To understand and quantify the effect of climate variability induced droughts and irrigation pumpage on stream-aquifer interaction (flux), the MODular Finite-Element (MODFE) model (Cooley, 1992; Torak 1993a, b; Jones and Torak, 2004) was used. The MODFE model (Cooley, 1992; Torak 1993a, b) was developed by USGS for the lower ACF river basin. The model has been used by researchers in the past to simulate and understand the complex and interconnected streamflow, groundwater levels, and boundary flows in the lower ACF (Figure 5.3).

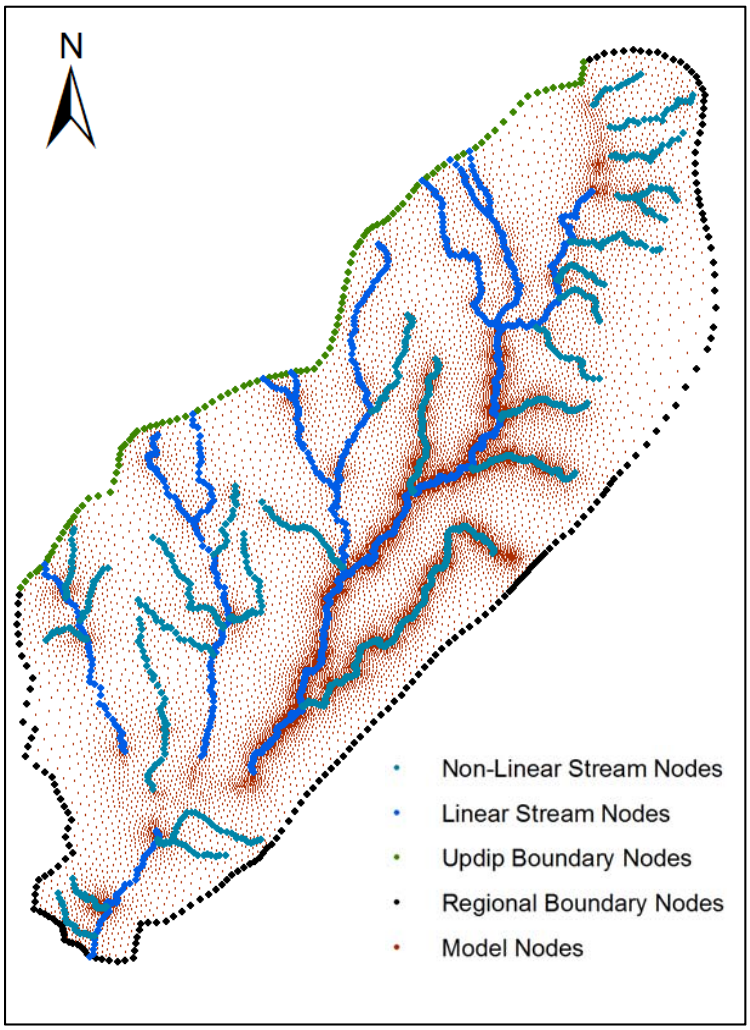

Figure 5.3. MODFE model set up in the study area showing the types of boundary, stream and finite element mesh nodes.

However, in this study MODFE was used to simulate different hypothetical climatic and pumpage scenarios to understand their effect on streamflow, baseflows, and stream-aquifer interaction and to identify the vulnerable areas where streams and the UFA exhibit greater hydraulic connection, i.e., the areas majorly responsible for streamflow depletion during droughts in the lower ACF river basin (Jones and Torak, 2004; Mitra et al., 2014). Moreover, the individual impacts of irrigation (anthropogenic factor) and climate variability (natural phenomena) have been quantified as well.

5.3.3.1. Finite Element Mesh

MODFE model adequately simulates the complex hydrogeology, geometry, and flow boundaries of the lower ACF river basin by using extreme flexible finite-element mesh design (Torak, 1993a, b). A finite-element mesh is the basic component of MODFE that represents the geometry of the study area. The irregular sized finite-element mesh comprises of nearly equilateral triangular planes and element sides that represents the hydrologic characteristics of stream courses, aquifer boundaries, aquifer property zone and computed water-level surface in the model. The model inputs at the intersection of the element sides are called nodes (Figure 5.3). The finite element sides also describe the irregular flow-system geometry, such as solution-enlarged joints and cavities. The mesh used in this study was developed by Jones and Torak (2006) and consists of 37,587 elements and 18,951 nodes. Further details of the finite-element mesh can be found in Jones and Torak (2006).

The MODFE model is far better than the rigid, row-column arrangement of nodes and blocks inherent to finite difference models, such as MODFLOW (Harbaugh et al., 2000). The MODFE model can also easily simulate the changes in anisotropy and preferential directions of

groundwater flow created by cavities and dissolution conduits in the karst Upper Floridan aquifer by allowing the element-by-element assignment of directions of anisotropy which is not possible with finite-difference models.

5.3.3.2. Governing Equation

The governing equation of MODFE uses partial differential equation that consists of appropriate boundary and initial conditions which represents flow through porous media. Groundwater flow in the Upper Floridan aquifer at various physical boundaries of the aquifer in the lower ACF river basin is governed by the following two-dimensional steady-state flow equation (Jones and Torak, 2004):

$$\frac{\partial}{\partial x}\left(T_{xx}\frac{dh}{dx}+T_{xy}\ \frac{dh}{dx}\right)+\ \frac{\partial}{\partial y}\left(T_{yx}\frac{dh}{dx}+T_{yy}\ \frac{dh}{dx}\right)+R(H-h)+W+P=S\frac{\partial h}{\partial t} \qquad (1)$$

where, *t* is time, *(x,y)* are the cartesian coordinate directions, *H(x,y,t)* is the hydraulic head of the USCU, *h(x,y,t)* is the aquifer hydraulic head, *R(x,y,t)* is the vertical hydraulic conductance (vertical hydraulic conductivity divided by thickness) of USCU, *W(x,y,t)* is the unit areal recharge or discharge rate (infiltration), *P(x,y,t)* are point source or sinks, *S(x,y,t)* is the storage coefficient and symmetric transmissivity is written in matrix form as

$$\begin{bmatrix} T_{xx}\ (x,y,t) & T_{xy}\ (x,y,t) \\ T_{yx}\ (x,y,t) & T_{yy}\ (x,y,t) \end{bmatrix}. \qquad (2)$$

MODFE uses the Garlerkin finite-element method with triangular elements and linear coordinate functions in space (Cooley, 1983; Zienkiewicz, 1977) for approximation of the governing equation, boundary and initial conditions. Further information about boundary and initial conditions can be found in Jones and Torak (2006) and MODFE manuals (Torak, 1992).

5.3.3.3. Model Input Parameters

Data into MODFE model are input under various input classes and are categorized based on their respective simulation approaches. For example, inputs relating to flow across streambeds are simulated as head-dependent flux boundaries (class) at the nodes and/or elements (simulation approach), whereas irrigation and springs are simulated as specified-flux boundary (class) at the nodes (simulation approach),

The model input parameters are categorized as static and dynamic. The static input parameters are temporally constant and are representation of the model geometry, the aquifer (e.g., transmissivity and storage coefficients of UFA; specific yield and head at the UFA updip limit), stream-lake system (such as, vertical leakage coefficients of the lakes, streambed conductance) and upper semi confined unit (USCU) (e.g., vertical leakage coefficients of the USCU) properties and their variations spatially. The dynamic input parameters change temporally in the model and consist of the temporal stresses in a transient simulation.

The static input parameters from the Jones and Torak (2006) model were retained for this study. However, two parameters, namely vertical leakage from USCU and aquifer transmissivity, were changed slightly within the limits to attain calibration. The model setup had to be calibrated to account for the change in the calculation procedure of irrigation pumpage to meet the desired calibration criteria.

The dynamic input parameters in the model are temporal stresses in a transient simulation and are representation of the infiltration, municipal and irrigation pumpage, heads at the USCU, and stream and lake stages. The dynamic inputs are the stresses that change on a monthly basis along with boundary and initial conditions to solve for groundwater heads at model nodes using

the governing groundwater equation (Equation 1) in the model. The various input parameters along with their respective input classes are summarized below.

5.3.3.4. Infiltration

Infiltration rates to the UFA in the model vary on a seasonal basis where mean annual recharge is about 10 inches per year (approximately, 20 percent of mean annual rainfall) and during late summer recharge is about 6 inches per year (approximately, 12 percent of mean annual rainfall) (Hayes et al., 1983). Infiltration was estimated from daily precipitation data that was collected from 14 stations inside the study area from the National Climate Data Center (NCDC). MODFE does not have an in-build infiltration calculation mechanism, and therefore, assumptions had to be made that required to input infiltration data directly to the model as a percentage of precipitation.

Infiltration values were calculated from monthly precipitation based on a seasonally varying conversion rate of 10, 20 and 30 percent of precipitation. This allowed the model to simulate variable recharge rates in accordance to the seasonally variable infiltration rates in the study area. A conversion rate of 30% of precipitation was used to simulate infiltration during the months of fall and winter (October to February) (Torak and Painter, 2006 and Jones et al., 2006) due to long duration precipitation from frontal passages and low evapotranspiration occurs.

Similarly, infiltration rates during convective storms of summer months (April to August) with short duration and high intensity rainfall with high evapotranspiration rates was simulated with a conversion rate of 10 percent of average monthly rainfall (Jones et al., 2006). The transition months of March and September in which both types of storms can occur, a 20% conversion rate of average monthly precipitation was used for calculation of infiltration rate (Jones and Torak,

2006) (April to August). It is important to note that the USCU is unable to act as a source of recharge through vertical leakage in areas where the USCU thickness is less than 30 ft or where USCU is absent (Jones and Torak, 1996). In these areas, infiltration from precipitation is the only mode of recharge to the aquifer (in absence of nearby streams or lakes) due to absence or small thickness of the USCU. Therefore, a zero value is assigned to vertical hydraulic conductance simulate zero vertical leakage to/from USCU in these areas, and only at areas where the USCU is absent or less than 30 ft thick can infiltration act as a source of recharge to the UFA.

5.3.3.5. Specified-Head Boundary at UFA Updip Limit

Specified head boundaries (SHB) represent ground-water level and regional flow conditions near the updip limit of the UFA where the hydraulic head remains constant (or change little) on temporal basis. The location of the model boundary near the updip limit (Figure 5.3) represent the area where the aquifer is at the land surface and is thin enough not to be considered as a water source. On a year to year basis water levels in this area do not fluctuate appreciably (Jones, 2006) thereby can be classified as SHB. Thus, the hydraulic head distribution at the updip limit for this study was retained from the Jones (2006) model.

5.3.3.6. Specified-Flux Boundaries

Specified-Flux Boundaries (SFB) were simulated in areas where a specified value (input) can be used to simulate water exchange that remains constant throughout that stress period (month) but might change in the subsequent stress period. Two types of SFB functions were used in the model on the basis of mesh design namely: point functions applied at node points and aerially-distributed functions applied at elemental areas of a mesh. The model input parameters such as

irrigation/municipal pumpage and off-channel spring flow were simulated using nodal SFB and direct infiltration of precipitation was simulated using elemental SFB.

5.3.3.7. Irrigation/Municipal Pumpage and Springs

Irrigation water withdrawal is the major anthropogenic activity affecting groundwater and its interaction with surface flow in the lower ACF region. There are more than 4000 irrigation wells in the model area (USGS) that represent seasonal withdrawal from UFA. The estimation of irrigation pumpage for the model depends on the availability of a reliable and accurate database. This database includes the location of each permitted ground-water irrigation well and the irrigated acres associated with each permitted well. Irrigation withdrawal was simulated at each irrigated acreage (wells) as SFB at the model nodes using irrigation acreage maps and monthly telemetered irrigation depth maps procured from USGS, Georgia. Irrigation flux at the model nodes were calculated by multiplying irrigated acreage with irrigation depths and the resulting irrigation flux values were input to the nearest node in the finite element mesh.

The municipal and industrial pumpage of 26 Mgal/d was applied at several localities within the model and was simulated as SFB point discharge functions in the area. The municipal and industrial pumpage rates were retained from the model conditions of Jones and Torak (2006) for the entire simulation period as they are based on the records of Georgia Environmental Protection Division (GAEPD). Off-channel springs were also simulated in the model as discharge function at a rate of 0.39 Mgal/d which represents springflow in the identical manner as point withdrawals from wells and was input as a constant value (SFB point discharge function) for the entire simulation period owing to the unavailability of time-varying data. Compared to the total irrigation

withdrawal, pumpage for municipal/industrial purposes combined with springflow is extremely small and therefore lack of data is unlikely to introduce significant error to the model.

5.3.3.8. Head-Dependent Flux Boundaries (HDFB)

Recharge and discharge to/from the UFA are primarily through USCU, lakes and streams and are simulated as head-dependent flux boundaries (HDFB). Similar to SFB, there are two general types of HDFB function were used in the model based on the basis of mesh design namely: point functions applied at node points and aerially-distributed functions applied at elemental areas of a mesh. Regional groundwater flow into and out of model area within the UFA (except at the UFA updip) and flow across streambeds were simulated using linear head dependent flux boundaries, whereas, vertical leakage to and from the overlying USCU and lake beds were simulated using aerially-distributed and head-dependent flux boundary.

5.3.3.9. Regional Groundwater Flow

Flow across the regional boundaries (except UFA outcrop) are simulated across element sides corresponding to the model boundaries and is governed by the difference in the computed hydraulic head and the external head (H_B) (controlling head) at the boundary nodes multiplied by the leakage coefficients. The external head for each boundary node represents the head outside the model boundary at a certain distance from that node and helps the model simulate inflow/outflow in the study area. The boundary nodes (except UFA outcrop) represent a groundwater divide represented by the external head and values in the area do not change appreciably on a monthly basis. However, changes in hydraulic heads at the boundary nodes (inside the study area) due to anthropogenic and seasonal stresses control the flow to the study area from the regional

boundaries. It is important to note that the only the flow rate across the area external to the model is calculated and the region external to the model area is not simulated *per se*. The mathematical expression for flow across the model boundary for an element side defined by nodes *k* and *l*, is expressed as:

$$Q_B = (1/2)\ \alpha\ L_{kl}\ (H_{Bi} - h_i),\ i = k\ or\ l \tag{3}$$

L_{kl} is the length of the element side and α is defined as

$$\alpha = \frac{Kb}{L} \tag{4}$$

b and K are thickness and average hydraulic conductivity of the aquifer between the model boundary and H_B. α is the leakage coefficient and the values of α were retained from Jones (2006) model setup. *L* is represented as the distance between the model boundary and the external head (H_B) and for this study *L* was assigned a value of 3 mi. Potentiometric surface maps of the UFA for May 2010 (Kinnaman and Dixon 2011) were used to interpolate the values for the external head.

5.3.3.10. Flow across Streambeds

Flow across streambeds are simulated as HDFB and is similar to the simulation of across regional boundary. However, for streambed flux the value of α is defined as

$$\alpha = \frac{K_r\, W_r}{b_r} \tag{5}$$

where, B_r and W_r is streambed thickness and width, respectively, *and* K_r is vertical hydraulic conductivity of the streambed. For calculation of stream-aquifer flux across streambeds controlling

head, H_{Bi}, (equation 3) is the stream stage (or lake level), for the associate node *i* (=*k or l*) of the element side aligned along the streambed. This linear form of HDFB is applied to stream channels that are perennial in nature and have flow all year long (Figure 5.3).

For intermittent or small streams (that go dry if aquifer levels fall below the altitude of the streambed) a non-linear form of HDFB is used to simulate stream-aquifer flux (Figure 5.3). The boundary condition for such a non-linear function is dependent on the nodal aquifer head, h_i and the relative positions of the altitude of the bottom of the streambed, z_r. Therefore, an element side represented by node *i* (=*k or l*) representing a surface water body as non-linear HDFB, leakage is calculated by

$$Q_{ri} = \begin{cases} C_{ri}\,(h_{ri} - h_i), & h_i > Z_{ri} \\ C_{ri}\,(h_{ri} - z_{ri}), & h_i > Z_{ri} \end{cases} \quad (6)$$

where, C_{ri} is the coefficient, Q_{ri} is the volumetric flow rate, z_{ri} is the altitude of streambed bottom and h_{ri} is stream stage. Most of the α values for the present model were retained from model setup of Jones (2006). α values at certain reaches were changed within limits for stream-aquifer flux calibration. Stream stage values (H_{Bi}), were interpolated from two lake stages and 13 stream gauging stations obtained from U.S. Army Corps of Engineers, Mobile District, Mobile, Alabama, (Appendix B.1) (USCOE and Crisp County Power Commission) based on local variations of slope along the stream channel (calculated from contour maps).

5.3.3.11. Vertical Leakage across USCU and Lake-Beds

Leakage to/from Lake Blackshear, Seminole and USCU were simulated using a non-linear leakage function. The leakage function is expressed as *R(H-h)* in equation 1. Vertical leakage

to/from USCU is simulated in areas where the thickness of USCU is greater than 30 ft. The volumetric flow rate (Q_{ai}), across nodes *i* from/to USCU is expressed as

$$Q_{ai} = \begin{cases} C_{ai}\,(H_{ai} - h_i), & h_i > z_{ti} \\ C_{ai}\,(H_i - z_{ti}), & h_i > z_{ti} \end{cases} \quad (7)$$

where, z_{ti} is the nodal altitude of the top of UFA or base of USCU, H_i is the nodal head in the USCU, h_i is the nodal hydraulic head in the UFA, C_{ai} is the nodal vertical leakage coefficients and Q_{ai} is the flow rate for the steady vertical leakage. The maximum recharge rate to the aquifer is limited by equation 7 and occurs when the hydraulic head of the aquifer drops below the base of USCU. The discharge to USCU from the aquifer is not limited by the non-linear function. At each geo-hydrologic zone (GHZ), USCU hydraulic head at the nodes, H_i, are calculated as a proportion of the thickness of USCU which varies seasonally and are dependent on the characteristics of the GHZ. In the event of a drought, the saturation proportion of the USCU is represented as the thickness of the underlying clay or sandy clay layer for the respective GHZ (Torak and Painter, 2006). This is due to the fact that during droughts the upper sandy layers dewaters completely and only the underlying clay layer acts as a source of recharge (Torak and Painter, 2006). USCU head data from Jones and Torak (2006) (March 2001 – February 2002) were retained due to lack availability of head data in USCU (only 6 wells in the entire study area) and also because the 2001-2002 was a La Niña period and the conditions were similar to the drought conditions of 2010-2012 (simulated in this study).

Spatial interpolation techniques such as conditional simulation and kriging were used by Jones and Torak (2006) for spatial interpolation of the static input parameters such as leakage coefficients of USCU, transmissivity, and specific yields. Data for these static parameters were

collected from measurements at specific points (resulting in a small data pool) which are highly spatially heterogeneous in nature. The spatial interpolation techniques used by Jones and Torak (2006) filled the data gaps in areas where data were not available, but it is important to note that these interpolation techniques might not be able to fully capture the location specific spatial heterogeneity of these parameters, thereby introducing error in the model on a location specific basis while still being consistent on a regional scale. These errors in the model will be manifested in the simulation of location specific hydraulic heads from equation 1. Detailed explanation about the model simulation techniques and input/output parameters can be found in USGS scientific investigation reports by Jones and Torak (2006) and Torak et al, (1996) and the MODFE manual (Torak, 1992).

5.3.4. Transient Simulation (May 2010 - September 2012) and Model Validation

Understanding how the combined effect of climate variability induced drought and agriculture withdrawal from the UFA affect stream-aquifer interaction in the study area, the groundwater model MODFE was simulated for the La Niña event of 2010 (started from mid-2010 and continued until mid-2012). This 2010 drought event was selected because it was responsible for severe drought condition in the Southeast and also due to availability of robust irrigation data during this period. Therefore, for this study, the MODFE model was calibrated and validated for the drought period of May 2010 to September 2012 to understand the effect of irrigation pumpage on stream-aquifer flux.

The model setup developed for the year 2010-2012 was similar to the model setup of Jones and Torak (2006) (which was calibrated). Thus most of the model parameters, except the dynamic stresses were retained, for the year 2010-2012. Even though most of the model parameters were

retained from model setup that was calibrated, it was important to ascertain whether the model is working reliably for the present time period or not. Therefore, for the transient simulation of 2010-2012, observed groundwater hydraulic heads and stream-aquifer flux for the month of July 2011 was compared to the model output of that month to validate the model. July 2011 was selected for calibration and validation as data from 159 wells were available and such extensive data was not available for the rest of the months. Initial conditions were simulated using the published USGS potentiometric surface maps for May - June 2010 was used (Kinnaman and Dixon, 2011).

As mentioned earlier that the interpolation techniques would affect the accuracy of the model setup, additionally measured GW level data (for comparison) also would have uncertainty associated with it. Conservatively, the model input parameters (aquifer geometry) have an accuracy of about 4.7 ft which would be the same for the accuracy of the GW level measurements as well (Jones and Torak, 2006). Combining the two potential errors, the Root Mean Square Error (*RMSE*) of the model setup for year 2010-2012 should be lower than 9.4 ft at the end of July 2011. The *RMSE* is defined as

$$RMSE = \left[\frac{1}{N}\sum_{i=1}^{N}(h_{i\,sim} - h_{i\,mes})^2\right]^{1/2} \quad (8)$$

where, N is the number of residuals (simulated – observed), and $h_{i\,mes}$ and $h_{i\,sim}$ measured hydraulic heads and are the simulated , respectively.

Stream aquifer flow was calibrated at 17 stream reaches using 21 USGS gauging stations. Observed data from the gauging stations were used to calculate target flow at each stream section which was then used as the calibration criteria. The gauge data across the stream section (upstream and downstream) were averaged to obtain observed stream-aquifer fluxes. These model simulated fluxes were compared to the observed at the end of the month after application of an error factor

(EF) to account for the daily fluctuations in stream flow data. The EF was used to calculate target range having an upper limit $Flow_{max}$ and lower limit $Flow_{min}$ of stream-aquifer fluxes. The upper and lower limits of the target range are defined as

$$Flow_{min} = (Q_d - EF \,.\, Q_d) - (Q_u + EF \,.\, Q_u) \quad (9)$$

$$Flow_{max} = (Q_d + EF \,.\, Q_d) - (Q_u - EF \,.\, Q_u) \quad (10)$$

$$qm = (Flow_{max} + Flow_{min}) / 2 \quad (11)$$

where, Q_d and Q_u is the measured streamflow at the downstream and the upstream end respectively. *qm* is the measured flow. The measured fluxes (*qm*) and associate target ranges were compared to simulated fluxes for evaluation of model accuracy. It is important to note that stream-aquifer flux values compared in the model are for a single day (measured flow) which can vary significantly on a daily basis. Therefore, comparison of observed and simulated value of particular day is not recommended. Hence, the concept of target flow range allows the values to vary within a certain range beyond which they are not expected to vary on a daily basis. Further, details about the MODFE model calibration techniques and processes can be obtained from Jones and Torak (2006) and Torak et al, (1996).

5.3.5. Model Scenarios

Various studies have shown that agricultural withdrawals from the UFA results in decreased base flow to streams that are in hydrologic connection to the UFA during droughts. Therefore, various simulated scenarios were analyzed to study the effectiveness of possible future water restrictions in order to maintain the flow levels in the Flint River. These simulated scenarios are described as follows,

1) Scenario I (SI): 15% reduction of current irrigation (i.e., WY 2011 and WY 2012).

2) Scenario II (SII): 30%% reduction of current irrigation (i.e., WY 2011 and WY 2012).

3) Scenario III (SIII): Shutting irrigation in Capacity Use Area (Figure 5.4).

4) Scenario IV (SIV): Shutting irrigation in Restricted Use Area (Figure 5.4).

5) Scenario V S(V): Shutting irrigation in both Capacity Use Area and Restricted Use Area.

6) Scenario VI (SVI): Shutting irrigation in a 3 mile buffer zone along the highly sensitive stream zones.

7) Scenario VII (SVII): Shutting irrigation in a 3 mile buffer zone along the high and moderate sensitive stream zones.

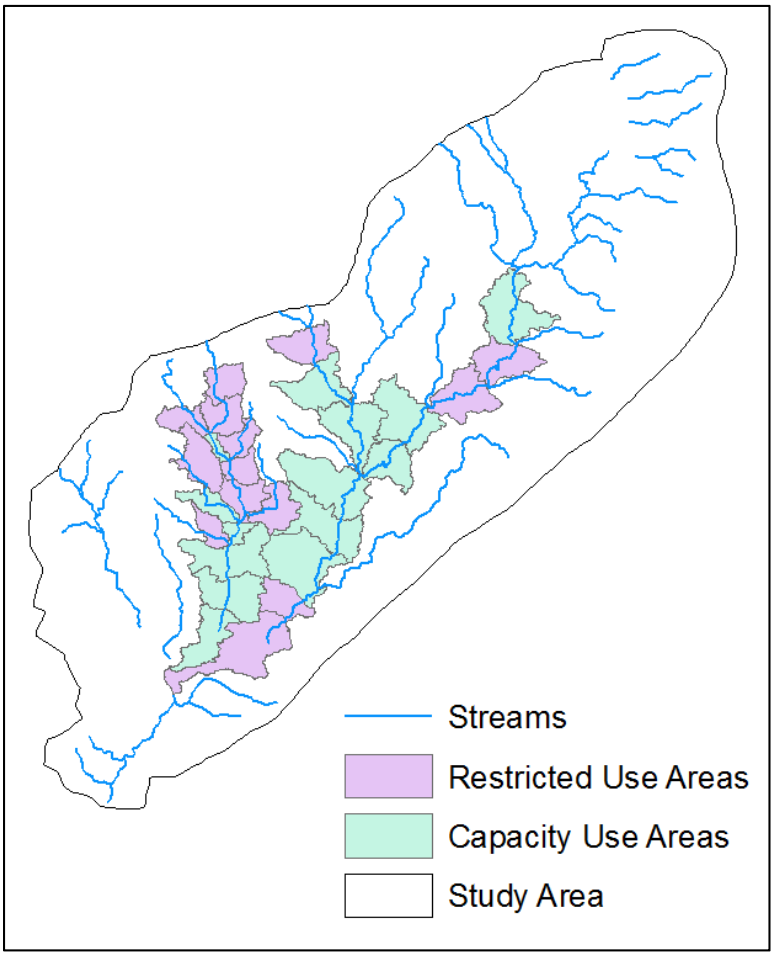

Figure 5.4. Capacity and restricted use watersheds in the study area.

5.3.5.1. Capacity Use Areas (CUA): CAU refers to those watersheds in which hydrologic models indicate that baseflow has been decreased in any month of a drought year (Georgia Department of Natural Resources Environmental Protection Division (GAEPD), 2006) by more than 5 cfs, 10 cfs, and 30 cfs in the Spring Creek, Ichawaynochaway Creek, and Lower Flint River sub-basins respectively. Capacity Use Areas are shown in green on the map (Figure 5.4) in which irrigation withdrawal from UFA is at the maximum permissible capacity.

5.3.5.2. Restricted Use Areas (RUA): RAU refers to those watersheds in which hydrologic models indicate that baseflow has been decreased in any month of a drought year (GAEPD, 2006) by 1-5 cfs, 1-10 cfs, and 3-30 cfs in Spring Creek, Ichawaynochaway Creek, and Lower Flint River sub-basins, respectively. Restricted Use Areas are shown in pink on the map (Figure 5.4). In these areas additional irrigation withdrawal from UFA must be restricted in order to prevent the sub-basins from becoming CUAs.

5.3.6. Sensitivity Analysis

Groundwater withdrawals have a more direct effect on stream-aquifer flux in some sub-basins than others and these reductions account for majority of baseflow reductions in the study area. In other words, depending on the nature of the connection between streams and the aquifer, groundwater withdrawals from UFA in some parts of the LFR Basin are responsible for a greater decrease in stream-aquifer flux (baseflow) than other parts. Therefore, Principal Component Analysis (PCA) and K-means clustering were applied on stream-aquifer fluxes to identify stream zones with high, moderate and low sensitivity.

Principal components analysis (PCA) is a widely used component extraction technique to examine the spatial or temporal variability (Preisendorfer, 1988; Walsh and Mostek, 1980) and has been successfully used in hydrologic sciences (Bartlein, 1982; Lins, 1985). PCA contains principal components (PCs) or latent variables that describe the dominant patterns and the main trends in the data (Jackson, 2003). For example, replacing a group of variables with a smaller set of new variables can make the analysis simple and these new set of variables, are called principal components. PCA uses eigenvector decomposition of the covariance matrix of the original variables. PCA can be described by matrix X and be presented as (Aguado et al., 2008)

$$X = SP^S + E$$

where, S is the PC score, P is the eigenvector of the covariance matrix and E is the residual matrix (error variance that are not captured by the model). PCA maximizes the rate of decrease of variance and usually first few principal components contains more than 70% of the total variance of the original data.

K-means algorithm is used to distinguish the boundaries of PCs and to categorize stream zones in different sensitivity streams sections in the LFRB. The k-means method developed by MacQueen (1967), assigns each data point to the cluster based on the smallest distance between the cluster centroid and the data points. Based on the cluster analysis, stream zones are categorized into sensitive (with regard to irrigation) zones namely high, moderate and low (Figure 5.5). Further, no irrigation was applied to three-mile-buffer to the acreage of the highly and moderate sensitive stream zones and its impacts were studied on stream-aquifer fluxes.

The lower ACF Basin is divided into four sub-basins namely, Spring Creek, Muckalee creek Ichawaynochaway Creek, and lower Flint River Basin (LFRB) (Figure 5.1). The different water restriction scenarios mentioned above were analyzed for the above four sub-basins. The non-

irrigated (NI) scenario was simulated for the 2010-12 drought period and the results from this scenario were compared to current irrigation situation in order to better understand the coupled effects of irrigation and droughts. The simulation of the NI scenario helped us quantify stream-aquifer flux conditions in the absence and presence of irrigation. The irrigation restriction scenarios were analyzed according to water year 2011 (WY 2011) and water year 2012 (WY 2012).

5.3.7. Cost Analysis

Finally, cost analysis was also done for above mentioned scenarios based on 2001 acreage buyout program. In this study, an attempt has been made to identify the most efficient and cost effective scenario that will help water managers maximize stream recovery. The acreage buyout costs applied in the study were $150, $200, and $300.

5.4. Results and Discussion

5.4.1. Model Validation

The simulated stream-aquifer flows obtained from Mitra, (2014) for all the stream reaches were within the target flux range except for reach number 15 and 16 (Figure 5.6) in Muckalee Creek for the month of July 2011 (Table 5.1). The above results are in agreement with the results obtained by Jones and Torak (2006) where the fluxes in the reach 16 also did not meet the required target range for the October 1999 model. Note that the validation results of the stream-aquifer fluxes in Table 5.1 are presented in cubic feet per second (not in SI units) to better comprehend the ranges since these values in SI units would be very low and more difficult to distinguish.

Table 5.1. Simulated stream-aquifer flow, Measured flow and associated target ranges for stream reaches for the month of July 2011 that are used for model stream-aquifer flux validation. All the flow values are in cubic feet per second (Mitra, 2014).

Reach Number	EF[c]	Stream Reach	Estimated Flux[b] (qm)	Simulated Flux (qs)	Target Flux[a]	
					$Flux_{min}$	$Flux_{max}$
1	0.1	Big Cypress Creek near Newton, Ga.	0.00	0.00	0.00	0.00
2	0.1	Big Slough at Ga. 179 near Pelham, Ga.	0.00	0.00	0.00	0.00
3	0.1	Big Slough at Ga. Hwy. 97 near Bainbridge, Ga.	0.00	0.00	0.00	0.00
4	0.1	Long Branch near Colquitt, Ga.	0.00	0.00	0.00	0.00
5	0.1	Aycocks Creek below Colquitt, Ga.	0.00	0.00	0.00	0.00
6	0.1	Gum Creek (U.S. Hwy. 280) at Coney, Ga.	41.80	41.30	37.62	45.98
7	0.1	Cedar Creek near Cordele, Ga.	0.00	0.00	0.00	0.00
8	0.1	Swift Creek near Warwick, Ga.	7.43	7.00	6.69	8.17
9	0.1	Jones Creek near Oakfield, Ga.	1.21	1.10	1.09	1.33
10	0.1	Abrams Creek near Oakfield, Ga.	3.72	3.70	3.35	4.09
11	0.1	Mill Creek near Albany, Ga.	7.56	7.72	6.80	8.32
12	0.1	Cooleewahee Creek near Newton, Ga.	0.32	0.30	0.29	0.35
13	0.1	Spring Creek at Ga. Hwy. 200 at Damascus, Ga.	-2.96	-3.12	-3.26	-2.66
14	0.1	Dry Creek at Hentown, Ga.	33.40	28.70	27.98	38.82
15	0.1	Muckalee Creek below Leesburg, Ga.	-55.00	17.74	-81.50	-28.50
16	0.1	Spring Creek near Reynoldsville, Ga.	76.80	2.92	52.88	100.72

[a] *Target flux, $Flux_{min}$ and $Flux_{max}$ are calculated using equation 9 and 10.*

[b] *Estimated fluxes are derived from USGS streamflow gauging stations.*

[c] *Error factor obtained from Jones and Torak (2006).*

The RMSE of the groundwater level residuals obtained from the present model was 2.40 m (Table 5.2) for the month of July 2011 which acceptable and within the limits of 2.86 m. The RMSE of the present model obtained by Mitra (2014) was close to the RMSE of October 1999 model (RMSE of 2.49 m) by Jones and Torak (2006). The ratio of standard deviation and range were much lower than 0.1 (Table 5.2).

Table 5.2. Validation statistics of the groundwater residuals for the simulated model for the month of July 2011 (Mitra, 2014).

Root Mean Square Error	Standard Deviation (STD)	Range (R*)	STD/R	Average
2.40 m	2.34 m	69.20 m	0.03	0.55 m

**Range of simulated groundwater levels.*

The above validation results showed that the model was performing satisfactorily to simulate stream-aquifer flux and groundwater flow in the lower ACF. The model was able to simulate stream-aquifer fluxes within the respective target ranges for most of the reaches and GW levels within the acceptable error limits.

5.4.2. Sensitivity Analysis

To understand the effect of irrigation on stream-aquifer flux and determine the sensitive stream reaches where the hydraulic connectivity with UFA is stronger than other stream section, sensitivity analysis was performed. The sensitivity of stream sections with irrigation withdrawal were determined based on the stream-aquifer flux response to irrigation by running the model with uniform irrigation across the study area (at all the model nodes) and by keeping other input variable constant. The model was run with 4 different irrigation values. The MODFE model for the WY 2011 was run for the months of May, June and July and irrigated values of 6000 cfd (based on the irrigation value of June, 2011), 3000 cfd, 9000 cfd and 0 cfd were applied uniformly across all the nodes of the study area. The irrigation value of 0 cfd represented no irrigation as a comparison against irrigated runs.

The stream-aquifer flux values from the above scenarios were obtained for all the non-linear and linear zones of stream reaches. The percentage differences of stream-aquifer flux for irrigation values of 3000 cfd, 6000 cfd and 9000cfd were calculated from the non-irrigated run, respectively. PCA was applied to percent change of stream-aquifer fluxes. Prior to applying PCA, the percentage changes of stream-aquifer fluxes was scaled to give equal importance to each attribute/variable subsequently named as variable 1 (V1), 2 (V2) and 3 (V3). Figure 5.5 shows the plot of the percentage of variability explained by each principal component (PCs) of V1, V2, and

V3. The graphical plot shows that the first principal component (Comp. 1) explains almost 98%-100% of the total variability in the standardized data, so that is considered as a reasonable way to reduce the dimension in order to visualize the PC.

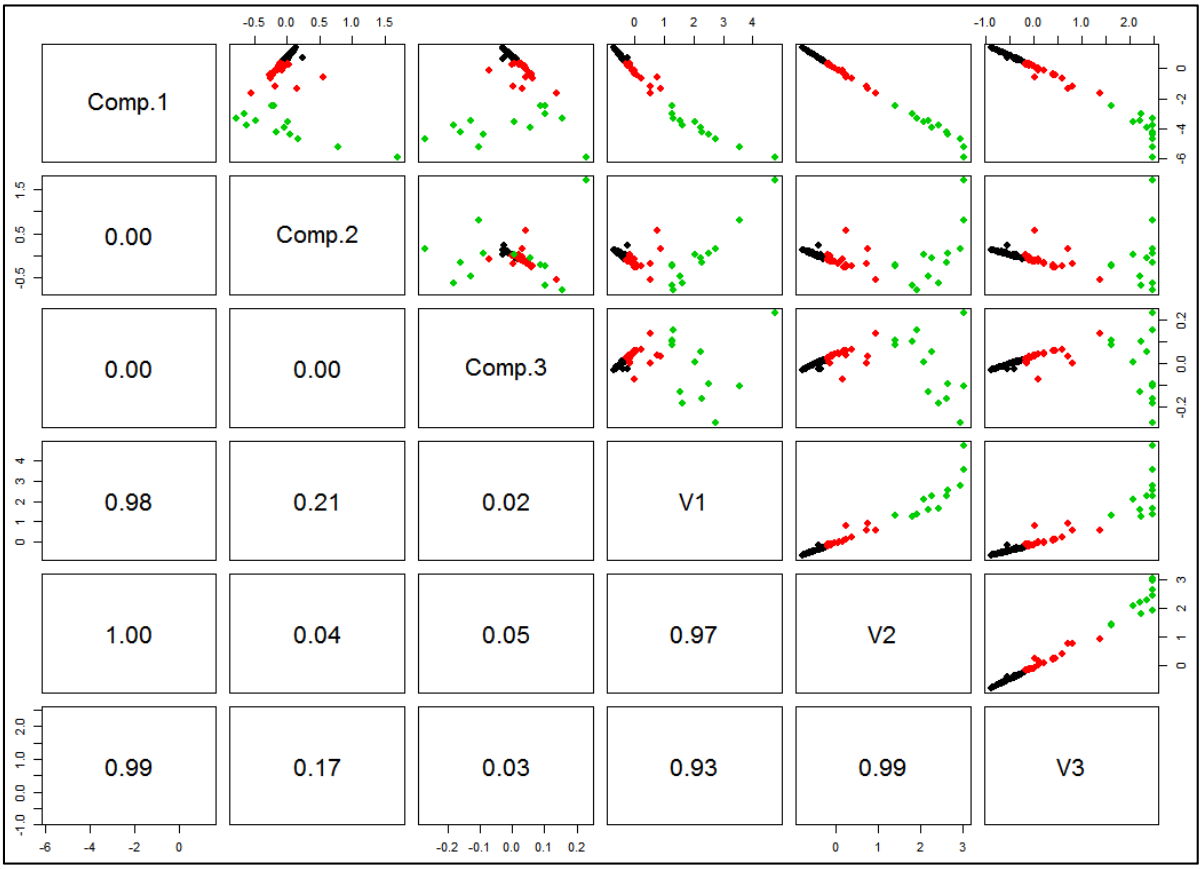

Figure 5.5. Principal component analysis results showing first three principal components and K-cluster analysis showing black, red and green dots indicating high, moderate and low sensitive stream zones.

K-means algorithm was applied to the scores of the cluster of the first principal component to discover groups of stream zones with similar characteristics. K-means partitions the points into K clusters and K=3 is the optimal number of clusters used for the analysis. K=3 is taken as an appropriate number of clusters for simplifying the analysis. K-means algorithm was applied on the first principal components (scores) of stream zones and were classified into three clusters (Figure 5.5). The black, red and green colors of each dot presented in Figure 5.5 indicates high, moderate

and low sensitive stream zones, respectively. A stream reach exhibiting high sensitivity to pumpage is where stream-aquifer flow decreases for all simulations of increased pumpage. Note that, stream-aquifer flux values for non-linear stream zones were zero where no flow was entering this reach from the upstream and were categorized as non-sensitive zone in this study. The figure 5.6 shows different categories of sensitive zones for linear and non-linear streams identified from sensitivity analysis. The categories of stream reach sensitivity can be used as an indicator of the degree to which pumpage affects change stream-aquifer flux in streams containing federally protected mussel species that are mentioned in Chapter 4.

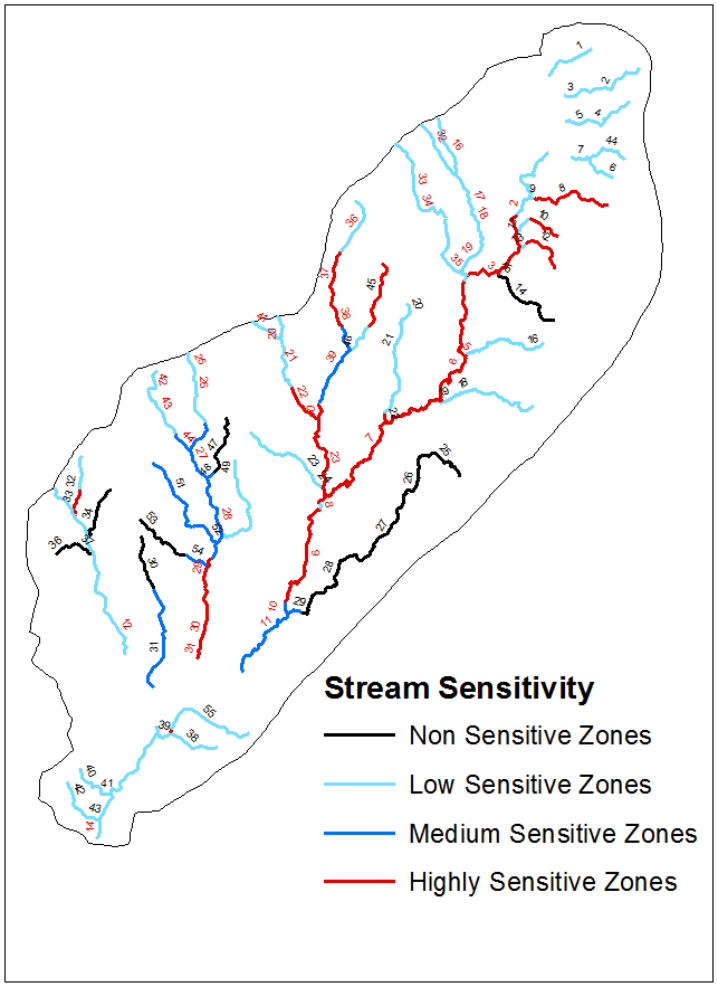

Figure 5.6. High, moderate, and low sensitive zones for linear (number are in red) and non-linear (number are in black) streams.

5.4.3. Simulation analysis for WY 2011 and WY 2012

5.4.3.1. Spring Creek

Understanding the highly complex stream-aquifer dynamics and identifying the locations where increased interactions exist between streams and the underlying UFA are essential in order to adequately allocate limited water resources in the lower ACF. Precipitation, ground-water levels, and stream stage vary seasonally and are interrelated. Seasonal precipitation patterns of the Southeast USA fluctuates and GW levels in the UFA vary accordingly throughout the study area including Sprink Creek (Torak and Painter, 2006; Mitra et al., 2014). GW levels reach a yearly maximum from late winter to early spring due to recharge from high and steady rain and low evapotranspiration which leads to high baseflow (stream-aquifer flux) during this period. Thereafter, GW levels start declining during the growing season due to decrease in recharge (low precipitation), increase in evapotranspiration and irrigation pumpage (Torak and Painter, 2006) which further results in lowering of stream-aquifer flux. This relationship which follows distinct pattern of seasonality is presented in the Table 5.3. In the study area, the growing period is defined as the months from April to October of a WY. The irrigation pumpage varies during a growing season and it peaked during June (Table 5.3) for WY 2011. The net stream-aquifer fluxes from different scenarios discussed above are presented in the Table 5.3. The results show that the irrigation pumpage and the net stream-aquifer flux share an inverse relationship. Table 5.3 shows that increase irrigation pumpage results in lowering of net stream-aquifer flux and during peak irrigation pumpage the net stream-aquifer flux becomes negative which suggests that stream characteristic changes from gaining to losing stream in some of the reaches during the months of April, June, and July in the WY 2011. Simulation results indicate that under dry conditions, some stream reaches would go dry with increase in pumpage rates (April, June, and July).

Unless otherwise noted, the simulated results of stream-aquifer fluxes shown in all the figures and tables are in the units of 1000 cubic meters per day (TCMD).

Table 5.3. Irrigation withdrawal in cfd and simulated stream-aquifer flux for current and different scenarios in TCMD for Spring Creek.

Month	Pumpage	Current Condition	NI	SI	SII	SIII	SIV	SV	SVI	SVII
Oct-10	-101	83	123	87	90	95	90	101	92	101
Nov-10	0	158	172	158	159	159	158	159	158	160
Dec-10	0	142	146	142	142	142	142	142	142	142
Jan-11	0	226	230	226	227	227	226	227	226	227
Feb-11	0	245	250	245	245	245	245	245	245	245
Mar-11	-111	116	144	120	124	126	122	132	124	135
Apr-11	-358	-7	97	8	24	44	17	68	35	70
May-11	-332	14	107	26	39	59	30	77	39	69
Jun-11	-1468	-212	140	-164	-116	15	-171	65	-29	55
Jul-11	-396	-36	140	-12	13	79	-15	103	58	106
Aug-11	-311	40	137	55	71	91	61	108	75	113
Sep-11	-150	122	182	133	145	149	139	158	136	166
Total	**-3227**	**891**	**1867**	**1024**	**1162**	**1430**	**1044**	**1587**	**1303**	**1587**

Table 5.4. Percentage recovery of stream-aquifer flux under different scenarios as compared to current stream-aquifer flux.

Month	Current Condition	Percentage Recovery of Stream-Aquifer Flux						
		SI	SII	SIII	SIV	SV	SVI	SVII
Oct-10	83	3.82	7.75	13.34	7.30	21.11	10.85	20.58
Nov-10	158	0.28	0.65	0.76	0.24	1.07	0.55	1.56
Dec-10	142	0.14	0.25	0.25	0.08	0.31	0.17	0.42
Jan-11	226	0.03	0.05	0.05	0.02	0.07	0.03	0.06
Feb-11	245	0.02	0.04	0.03	0.02	0.05	0.02	0.04
Mar-11	116	3.42	6.84	9.35	5.12	14.48	7.27	16.71
Apr-11	-7	217.83	438.13	735.66	338.24	1079.42	607.86	1100.80
May-11	14	92.51	185.53	330.47	120.98	464.14	188.99	403.59
Jun-11	-212	22.46	45.20	106.99	19.49	130.89	86.52	125.81
Jul-11	-36	67.50	137.34	320.96	58.68	387.55	260.60	394.88
Aug-11	40	37.47	76.52	127.54	51.31	170.51	86.59	181.16
Sep-11	122	9.28	19.18	22.00	14.32	30.17	11.43	36.47

The results of no-irrigation scenario show the fluctuation of net stream-aquifer flux due to climatic variations such as less precipitation and high evaporation rates results in lowering of

recharge to UFA from streams. The results from the scenarios of irrigation reduction by 15% and 30% (scenarios I and II) show the increase in flux from aquifer to stream (flux) as compared to current irrigation scenario. The flow from stream to aquifer in the month of July reversed during for scenario II (compared to SI) thus changing it from a losing stream to a gaining stream. Table 5.4 presents the percentage recovery of net stream-aquifer flux from current scenario. It was found that net stream-aquifer flux recovered higher when irrigation was reduced by 30% than 15% of current irrigation pumpage (Table 5.4).

Similarly, the results from the scenario III: shutting down the irrigation pumpage in the capacity use areas, shows that net stream-aquifer flux is much higher than the scenario I and II (Figure 5.7) and making the Spring Creek gaining stream throughout the WY 2011 (Table 5.3). The total percentage recovery of net stream-aquifer flux during scenario III is much higher than scenarios I and II (Table 5.4). The results from scenario IV: shutting down the irrigation pumpage in the restrictive use areas, indicate that the net flux was more or less similar to the scenario II. The characteristic of Spring Creek was gaining stream except for the month of June in which it became a losing stream. The total percentage recovery of net stream-aquifer flux during scenario IV was lower than scenario III since the irrigated area under scenario IV is lower than scenario III. The results obtained from scenario V: shutting down the irrigation pumpage in both capacity and restrictive use areas, indicate that net stream-aquifer flux is much higher than scenario III or IV since the irrigated area was much lower than other scenarios.

The sensitivity analysis and buffer analysis results also showed interesting results where the results found from scenario VI: shutting down the irrigation pumpage under buffer of 3 mile from the highly sensitive stream zones showed that the net flux was higher than other scenarios except the scenario V. The characteristic of Spring Creek was gaining stream except for the month

of June in which it was a losing stream and the total percentage recovery of net stream-aquifer flux was similar to scenario III. The results obtained from scenario VII: shutting down the irrigation pumpage within a three-mile buffer from both highly and medium sensitive stream zones, showed the highest net stream-aquifer flux than other scenarios (Table 5.3 and Figure 5.7) and resulted in the best recovery of net flux among all the scenarios (Table 5.4).

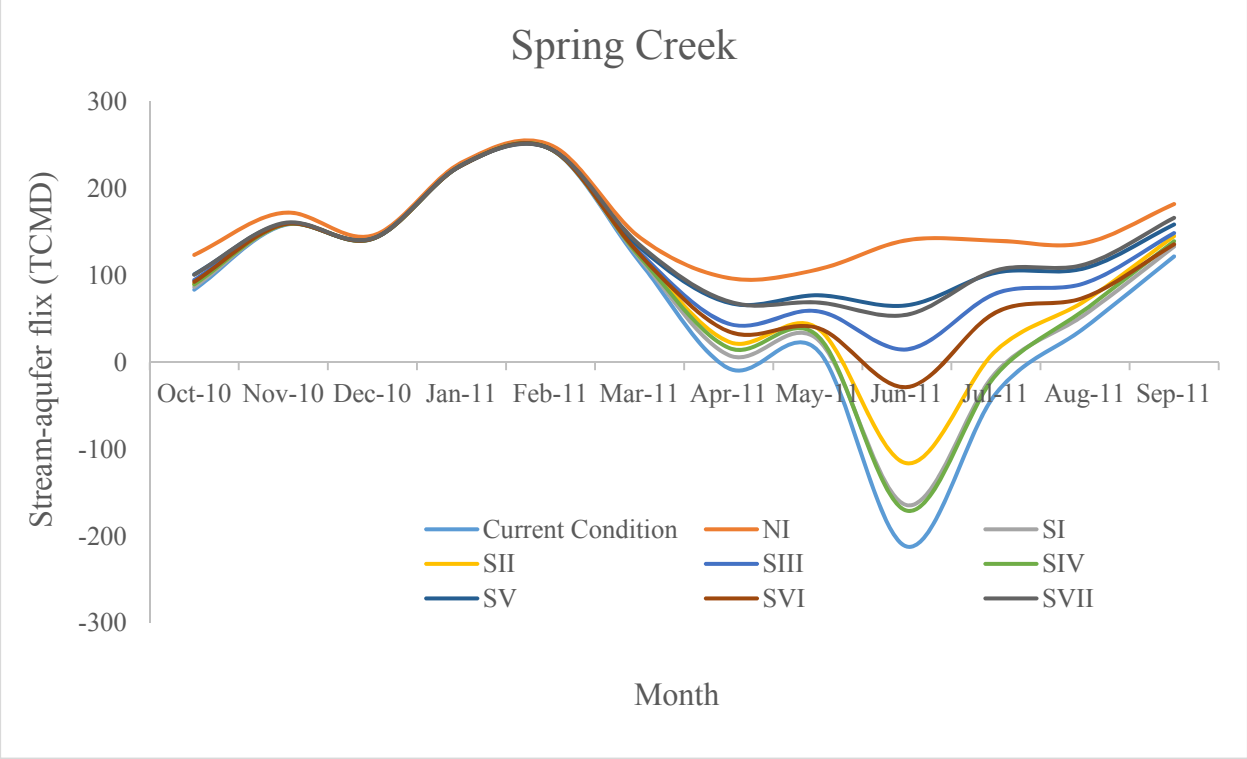

Figure 5.7. Simulated stream-aquifer flux for current and different scenarios in TCMD for Spring Creek.

The net stream-aquifer flux in WY 2012 obtained from different scenarios were similar to the WY 2011, except that the Spring Creek was always a gaining stream throughout the year since the irrigation pumpage was lower during WY 2012 (Appendix D.1).

5.4.3.2. Ichawaynochaway Creek

The net stream-aquifer fluxes from different scenarios discussed above for Ichawaynochaway Creek are presented in the Table 5.5 for the WY 2011. Table 5.5 shows that increase irrigation pumpage results in lowering of net stream-aquifer flux. The net stream-aquifer flux is lowest (135 TCMD) during peak irrigation pumpage in the month of August, however it is a positive value suggesting that Ichawaynochaway Creek remains gaining stream throughout the year unlike Spring Creek, although, the irrigation pumpage and the net stream-aquifer flux also share an inverse relationship in this region as well.

The results of no-irrigation scenario show the fluctuation of net stream-aquifer flux due to variations of recharge to UFA. The results from the scenarios I and II show the increase in flow from aquifer to stream (flux) as compared to flux from current irrigation. Table 5.6 presents the percentage recovery of net stream-aquifer flux from current scenario. It was found that net stream-aquifer flux recovery was approximately 44% and 33% when irrigation was reduced by 30% than 15% of current irrigation pumpage, respectively.

Similarly, the results from the scenario III show that net stream-aquifer flux is much higher than the scenario I and II (Figure 5.8). The total percentage recovery of net stream-aquifer flux during scenario III is much higher (approximately 61%) than scenarios I and II (Table 5.6). The results from scenario IV observed that the net flux were more or less similar to the scenario II. The total percentage recovery of net stream-aquifer flux during scenario IV was lower (approximately 27%) than scenario III since the irrigated area under scenario IV is lower than scenario III The net stream-aquifer flux obtained from scenario V was much higher than scenario III and IV since the irrigation pumpage was stopped in both the capacity and restrictive use areas.

The sensitivity analysis and buffer analysis results in Ichawaynochaway Creek for scenario VI showed that the net flux was higher than other scenarios except for scenario V. The total percentage recovery of net stream-aquifer flux during scenario VI was approximately 82% as compared to net flux obtained from current irrigation situation in WY 2011. The net stream-aquifer flux obtained from scenario VII was similar to scenario V (Table 5.5 and Figure 5.8) and gave the second best recovery of net flux among all the simulated scenarios (Table 5.6).

Table 5.5. Irrigation withdrawal in cfd and simulated stream-aquifer flux for current and different scenarios in TCMD for Ichawaynochaway Creek.

Month	Pumpage	Current Condition	NI	SI	SII	SIII	SIV	SV	SVI	SVII
Oct-10	-67	208	239	209	210	212	210	213	213	213
Nov-10	0	199	225	200	200	200	200	201	200	200
Dec-10	0	171	191	171	172	171	172	172	172	172
Jan-11	0	211	229	211	211	211	212	212	211	211
Feb-11	0	260	277	261	261	260	261	262	261	261
Mar-11	-76	251	271	253	255	256	255	260	258	258
Apr-11	-99	219	239	222	224	227	221	228	229	230
May-11	-131	237	261	240	243	247	239	248	250	251
Jun-11	-378	225	264	230	235	242	231	248	245	246
Jul-11	-207	174	218	180	186	190	185	201	195	195
Aug-11	-517	136	217	147	159	170	146	180	183	187
Sep-11	-94	192	240	198	205	207	201	217	212	213
Total	**-1569**	**2484**	**2870**	**2522**	**2561**	**2593**	**2532**	**2642**	**2628**	**2636**

Table 5.6. Percentage recovery of stream-aquifer flux under different scenarios as compared to current stream-aquifer flux.

Month	Current Model	Percentage Recovery of Stream-Aquifer Flux						
		SI	SII	SIII	SIV	SV	SVI	SVII
Oct-10	208	0.51	1.03	1.56	0.73	2.29	2.05	2.20
Nov-10	199	0.19	0.38	0.28	0.50	0.79	0.38	0.41
Dec-10	171	0.20	0.40	0.27	0.47	0.74	0.36	0.38
Jan-11	211	0.15	0.30	0.18	0.39	0.57	0.24	0.26
Feb-11	260	0.15	0.28	0.13	0.41	0.54	0.22	0.24
Mar-11	251	0.79	1.59	1.95	1.42	3.37	2.76	2.90
Apr-11	219	1.05	2.11	3.47	0.70	4.17	4.44	4.68
May-11	237	1.27	2.55	3.90	0.74	4.64	5.36	5.74
Jun-11	225	2.31	4.64	7.61	2.59	10.23	9.01	9.29
Jul-11	174	3.30	6.62	9.16	5.95	15.23	11.69	12.10
Aug-11	136	8.36	16.87	24.84	7.85	32.83	34.77	37.36
Sep-11	192	3.48	6.93	8.00	5.01	13.06	10.44	11.02

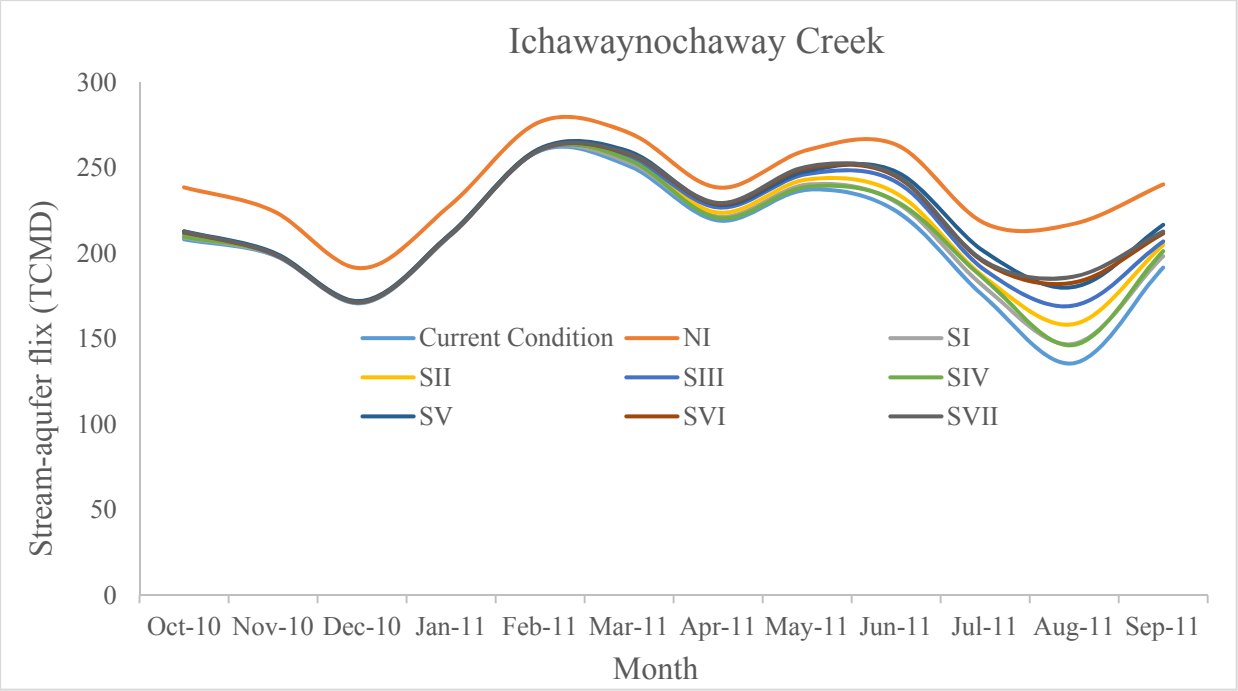

Figure 5.8. Simulated stream-aquifer flux for current and different scenarios in TCMD for Ichawaynochaway Creek.

The results for the analysis of WY 2012 also showed a similar pattern (as compared to WY 2011) of net stream-aquifer fluxes reduction due to the different water restriction scenarios (Appendix D.1).

5.4.3.3. Muckalee Creek

The irrigation pumpage in WY 2011 was much lower in Muckalee creek as compared to other creeks and lower Flint sub-basins (Table 5.7). Therefore, the net stream-aquifer fluxes from current irrigation and no-irrgation scenario were similar throughout the year except the month August and September. The various scenarios applied to recover net stream-aquifer flux (Table 5.7 and Figure 5.9) were not effective except the scenario II where the recovery of net flux was 14% (which is very low as well). This might be due to lack of available stream zones in this region. Similar results were also obtained for the WY 2012 (Appendix D.1).

Table 5.7. Irrigation withdrawal in cfd and simulated stream-aquifer flux for current and different scenarios in TCMD for Muckalee Creek.

Month	Pumpage	Current Condition	NI	SI	SII	SIII	SIV	SV	SVI	SVII
Oct-10	-27	647	663	648	648	647	647	647	647	647
Nov-10	0	606	616	606	607	606	606	606	606	606
Dec-10	0	673	681	673	673	673	673	673	673	673
Jan-11	0	684	691	684	684	684	684	684	684	684
Feb-11	0	678	684	678	678	678	678	678	678	678
Mar-11	-32	596	606	597	598	596	596	596	596	596
Apr-11	-85	592	615	595	598	592	592	592	593	593
May-11	-225	652	699	658	665	652	652	652	654	654
Jun-11	-175	642	692	649	656	642	642	642	644	644
Jul-11	-46	585	619	590	595	585	585	585	587	587
Aug-11	-347	556	627	566	576	556	556	556	559	559
Sep-11	-77	553	602	560	567	553	553	553	557	557
Total	**-1013**	**7465**	**7795**	**7505**	**7545**	**7465**	**7465**	**7465**	**7478**	**7478**

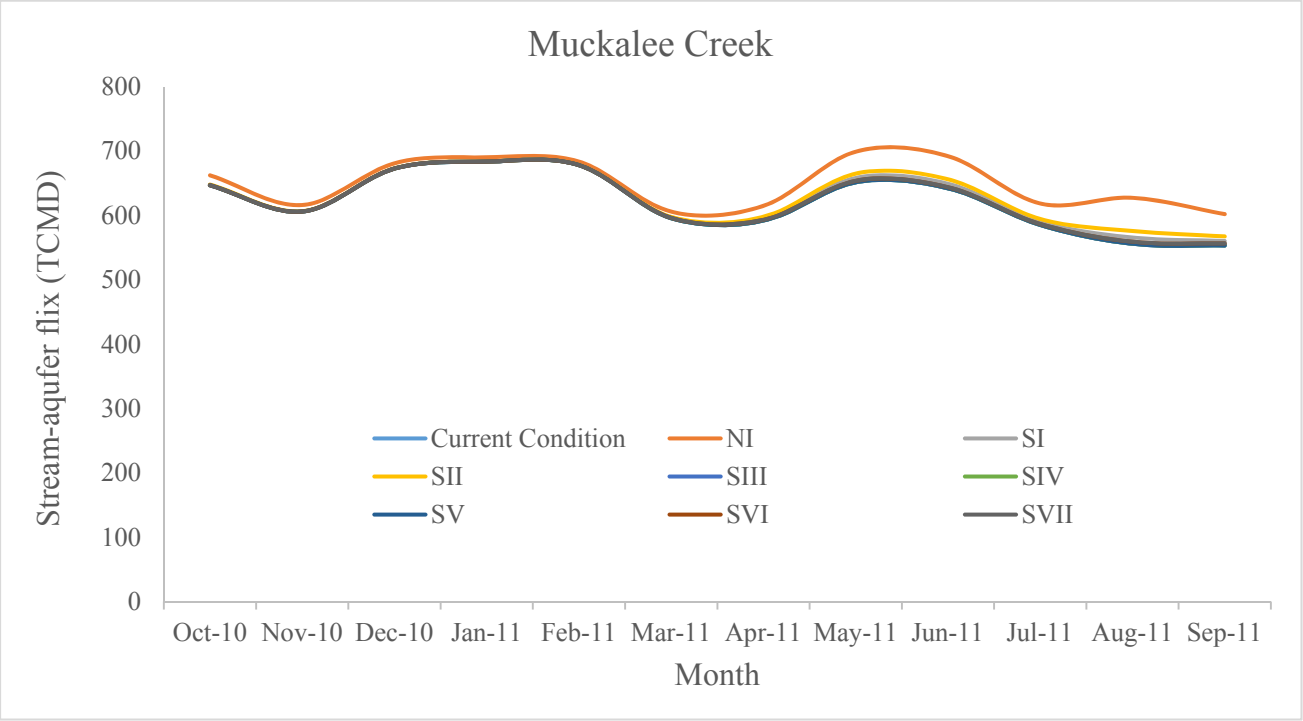

Figure 5.9. Simulated stream-aquifer flux for current and different scenarios in TCMD for Muckalee Creek.

Table 5.8. Percentage recovery of stream-aquifer flux under different scenarios as compared to current stream-aquifer flux.

Month	Current Condition	Percentage Recovery of Stream-Aquifer Flux						
		SI	SII	SIII	SIV	SV	SVI	SVII
Oct-10	647	0.10	0.19	0.00	0.00	0.00	0.03	0.03
Nov-10	606	0.05	0.09	0.00	0.00	0.00	0.02	0.02
Dec-10	673	0.03	0.06	0.00	0.00	0.00	0.01	0.01
Jan-11	684	0.02	0.04	0.00	0.00	0.00	0.01	0.01
Feb-11	678	0.02	0.03	0.00	0.00	0.00	0.01	0.01
Mar-11	596	0.16	0.32	0.00	0.00	0.00	0.09	0.09
Apr-11	592	0.49	0.99	0.00	0.00	0.00	0.20	0.20
May-11	652	1.02	2.04	0.00	0.00	0.00	0.33	0.33
Jun-11	642	1.07	2.15	0.00	0.00	0.00	0.24	0.24
Jul-11	585	0.80	1.59	0.00	0.00	0.00	0.24	0.24
Aug-11	556	1.77	3.58	0.00	0.00	0.00	0.57	0.57
Sep-11	553	1.27	2.54	0.00	0.00	0.01	0.57	0.58

5.4.3.4. Lower Flint River Basin (LFRB)

The net stream-aquifer fluxes from different scenarios for lower FRB are presented in the Table 5.9 for the WY 2011. The Table 5.9 shows that increase irrigation pumpage results in lowering of net stream-aquifer flux. The net stream-aquifer fluxes are positive values suggesting that FRB remains gaining stream throughout the year unlike Spring Creek.

The results of no-irrigation scenario show the fluctuation of net stream-aquifer flux due to variations of recharge to UFA. The results from the scenarios I and II show the increase in flow from aquifer to stream (flux) as compared to flux from current irrigation. Table 5.10 presents the percentage recovery of net stream-aquifer flux from current scenario. It was found that net stream-aquifer flux recovery was higher when irrigation levels were reduced by 30% than 15% of current irrigation pumpage i.e., approximately 21% and 10%, respectively.

Similarly, the results from the scenario III show that net stream-aquifer flux is much higher than the scenario I and II (Figure 5.10). The total percentage recovery of net stream-aquifer flux during scenario III is much higher (approximately 39%) than scenarios I and II (Table 5.10). The

results from scenario IV observed that the net flux were more or less similar to the scenario II. The total percentage recovery of net stream-aquifer flux during scenario IV was lower (approximately 10%) than scenario III since the irrigated area under scenario IV is lower than scenario III. The net stream-aquifer flux obtained from scenario V was much higher than scenario III and IV since the irrigated pumpage was stopped in both capacity and restrictive use areas.

Table 5.9. Irrigation withdrawal in cfd and simulated stream-aquifer flux for current and different scenarios in TCMD for lower Flint River basin.

Month	Pumpage	Current Condition	NI	SI	SII	SIII	SIV	SV	SVI	SVII
Oct-10	-268	3589	3806	3599	3609	3629	3598	3638	3641	3635
Nov-10	0	3291	3414	3295	3299	3305	3293	3306	3307	3306
Dec-10	0	3343	3423	3345	3347	3350	3344	3351	3351	3350
Jan-11	0	3149	3205	3151	3152	3154	3150	3154	3154	3154
Feb-11	0	2785	2826	2786	2787	2788	2786	2788	2788	2788
Mar-11	-203	3120	3184	3126	3131	3137	3125	3143	3146	3144
Apr-11	-475	3058	3207	3077	3096	3125	3081	3149	3144	3134
May-11	-1044	3435	3772	3482	3530	3637	3475	3679	3659	3642
Jun-11	-1504	3332	3878	3410	3488	3658	3434	3765	3672	3616
Jul-11	-625	3197	3579	3251	3306	3409	3246	3460	3416	3396
Aug-11	-1564	3160	3644	3229	3300	3387	3229	3457	3458	3438
Sep-11	-355	3382	3718	3432	3482	3527	3419	3561	3557	3547
Total	**-6038**	**38841**	**41656**	**39183**	**39527**	**40106**	**39179**	**40451**	**40293**	**40149**

Table 5.10. Percentage recovery of stream-aquifer flux under different scenarios as compared to current stream-aquifer flux.

Month	Current Model	Percentage Recovery of Stream-Aquifer Flux						
		SI	SII	SIII	SIV	SV	SVI	SVII
Oct-10	3589	0.28	0.57	1.13	0.25	1.38	1.45	1.28
Nov-10	3291	0.12	0.24	0.41	0.05	0.46	0.48	0.46
Dec-10	3343	0.07	0.13	0.22	0.03	0.25	0.24	0.23
Jan-11	3149	0.04	0.09	0.14	0.02	0.16	0.14	0.14
Feb-11	2785	0.03	0.06	0.09	0.01	0.11	0.10	0.09
Mar-11	3120	0.18	0.37	0.56	0.17	0.74	0.85	0.78
Apr-11	3058	0.62	1.25	2.19	0.77	2.98	2.83	2.50
May-11	3435	1.38	2.77	5.90	1.17	7.11	6.52	6.04
Jun-11	3332	2.33	4.68	9.78	3.05	12.98	10.19	8.51
Jul-11	3197	1.69	3.41	6.62	1.52	8.23	6.85	6.21
Aug-11	3160	2.20	4.43	7.21	2.20	9.40	9.46	8.81
Sep-11	3382	1.47	2.95	4.27	1.10	5.30	5.18	4.87

The sensitivity analysis and buffer analysis results in Ichawaynochaway Creek for scenario VI showed that the net flux was higher than other scenarios except the scenario V. The total percentage recovery of net stream-aquifer flux during scenario VI was approximately 44% as compared net flux obtained from current irrigation situation in WY 2011. The net stream-aquifer flux obtained from scenario VII was similar to scenario V (Table 5.10 and Figure 5.10) and gave the second best recovery of net flux among all the scenarios (Table 5.11).

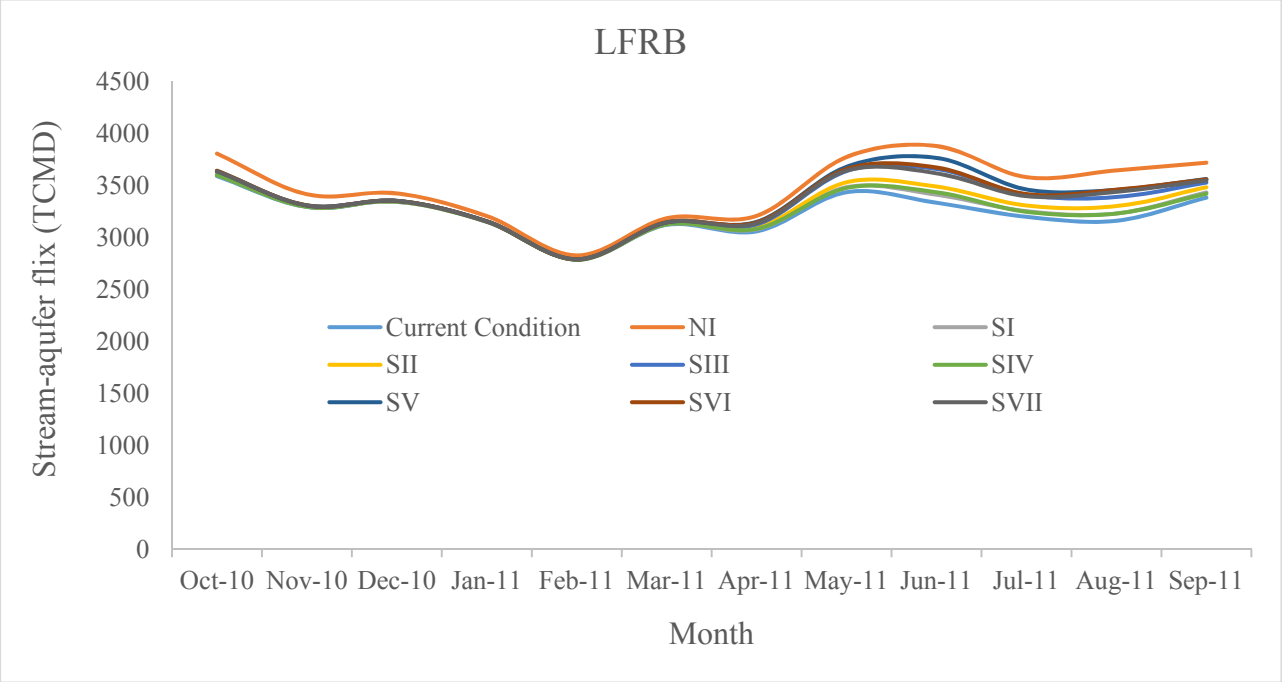

Figure 5.10. Simulated stream-aquifer flux for current and different scenarios in TCMD for Lower Flint River Basin.

The results for the analysis of WY 2012 also showed similar pattern (as compared to WY 2011) of net stream-aquifer fluxes reduction due to the different water restriction scenarios (Appendix D.1).

5.4.4. Cost Analysis

A cost analysis of the different scenarios was done to give policy makers a rough estimate of the costs to implement a particular scenario to meet the FRDPA objectives. The cost estimates for different simulated scenarios with different prices per acre are presented in the Table 5.11. The cost estimates for scenario SI and SII were not calculated since these scenarios are not based on acreage buyout rather on reduction of irrigation intensity in the study area. The cost analysis results show that with a price of approximately $150/acre the cost of buying out the irrigated acreage of scenario IV and VI would be around $17 million and $21 million, respectively, which is less than the cost of SV and SVII (Table 5.11). Further, stopping irrigation pumpage in the vulnerable sub-basins such as Spring Creek and Ichawaynochaway Creek would recover more stream-aquifer fluxes, especially for scenarios III and VI would cost less than the acreage buyout for entire study area (Table 5.11).

Table 5.11. Acreage buyout analysis for different water restriction scenarios.

Scenarios	Area (Acres)	Percentage Acreage (%)	Cost (Millions of Dollars)		
			at $150/ac	at $200/ac	at $300/ac
Total Area	536810	100	81	107	161
SIII	69678	13	10	14	21
SIV	116443	22	17	23	35
SV	186121	35	28	37	56
SVI	138487	26	21	28	42
S2*	95154	18	14	19	29
SVII	233641	44	35	47	70

S2 indicate water restriction for the moderate sensitive zones*

5.5. Conclusion

The purpose of this chapter was to understand the effects of La Niña induced drought (2010-2012) and simulated irrigation pumpage on stream-aquifer flow levels in the lower FRB. MODFE model was also used to identify critical reaches and tributaries of the Flint River that

particularly supports baseflow and are responsible for lowering of stream-aquifer flux due to drought and pumpage. The model uses inputs such as infiltration, irrigation pumpage, stream stage, and head in the USCU to simulate the groundwater components such as ground water levels and stream-aquifer flux. The simulated stream-aquifer fluxes under various water restrictions scenarios on irrigation withdrawal were obtained and the effectiveness of the proposed scenarios results were compared. Percentage recovery of stream-aquifer fluxes were studied at different water restrictions scenarios. Additionally, acreage buyout under different water restrictions scenarios were studied and compared.

The results of the study indicated that ground-water withdrawal from the UFA in the lower FRB resulted in decrease of streamflow/baseflow since the lower FRB hydraulically connected to the karstic UFA. Especially, during droughts (La Niña phases), when ground water levels are already low (Mitra et al, 2014), increased irrigation water withdrawal in the WY 2011 leads to further lowering of groundwater levels and are hence responsible for greater decrease in the stream-aquifer flux. Particularly, in the Spring Creek, increased pumpage during the months of April, June and July resulted in significantly decreased stream-aquifer flux that changed the stream characteristics from gaining to losing stream in this region. The results from sensitivity analysis identified the critical reaches where stream-aquifer hydraulic connectivity is strong and stream-aquifer flux is sensitive to pumpage. The results from various possible simulated water restrictions suggested that reducing the pumpage in the sensitive areas are more effective in stream-aquifer flux recovery than reducing irrigation intensity (15% or 30%) throughout the study area. The different scenarios analyzed can be helpful in determining the amount of irrigation shutdown that will help maintain the flow levels in the FR during droughts. Moreover, analysis of acreage buyout suggested that water restrictions on irritation withdrawal can have significant impacts on stream-

aquifer flux in the study area especially the critical watersheds such as Spring Creek and Ichawaynochaway Creek. The results have also indicated that applying scenario IV and VI can have better percentage recovery of streamflow than applying other scenarios which are costly.

The above results may provide useful information to decision-makers in evaluating policies or management strategies in accordance to maintain the flow in the lower FRB. Understanding the climate induced droughts and anthropogenic stresses on stream-aquifer flux might help Georgia develop a new water policy that can address the current water scarcity condition. The ranking of stream reaches conducted in this study can be helpful to better manage groundwater in order to protect surface water from irrigation-induced streamflow reduction during droughts in the lower FRB. Irrigation restrictions in the Spring and Ichawaynochaway Creek can be helpful in avoiding irrigation induced streamflow depletion in the study area.

Chapter 6

Conclusions

6.1. Summary and Conclusions

The combined stress of climate variability induced droughts and irrigation withdrawal on water resources has resulted in water wars among the neighboring states in the Southeast United States. One of the major reason behind the conflict is the streamflow/baseflow depletion due to droughts and increased irrigation water withdrawal from the UFA. Therefore, understanding and quantifying the effects of climate variability induced droughts on hydrologic cycle components and its interaction with anthropogenic activities such as irrigation in southwest Georgia can provide insight on the lowering of flow levels in the Flint River and help solve the present and future water issues in the region.

The hydrologic connectivity of groundwater with surface water through UFA has become an issue of interest among researchers in the area since it supports baseflow and serves as a major freshwater resource for agricultural purposes in the region (Southwest GA) during droughts. This study focused on understanding the relationships among droughts, irrigation, and streamflow levels in the study area with the final goal of identifying critical reaches and tributaries of the lower Flint River that are responsible for lowering of flow levels in the river and suggesting better water restriction scenarios. Additionally, this study also offers a powerful nonparametric Joint Rank Fit (JRFit) procedure that can be used for the analysis of cluster correlated climatic and hydrologic datasets.

The major findings of four objectives mentioned earlier in the Chapter 1 are presented below.

6.1.1. Objective 1

Quantify the impact of interannual and multidecadal climate variability cycles on baseflow levels.

The nonparametric JRFit procedure was used to test and estimate the individual impacts of the phases of PDO, AMO, NAO, and ENSO on baseflow. Additionally, the coupled responses of PDO, AMO, and NAO with ENSO were evaluated to determine the severity of ENSO-induced drought on baseflow levels in the study area. The percentage change in median baseflows were also studied for individual and coupled analyses.

The specific conclusions are listed below:

1. Individual analyses of ENSO, PDO, AMO and NAO showed that the phases of ENSO, AMO and NAO had significant impact on baseflow. However, the effect of the phases of PDO was not highly significant.
2. Coupled analysis of the effect of ENSO-PDO, ENSO-AMO and ENSO-NAO on baseflows indicated that the interactive effect of the phases of ENSO-PDO and ENSO-AMO on baseflows was highly significant.
3. Occurrence of La Niña during positive phases of AMO and PDO are responsible for greater decrease in flow levels in the Flint River, thus are associated with severe drought in this region.
4. The negative effect of La Niña on baseflows appeared to have been mitigated by the effects of the negative phase of AMO resulting in above normal baseflows.

5. Therefore, the study suggests that analysis of La Niña induced droughts on baseflow and its interaction with other multidecadal cycles can help in giving a clearer picture of the severity of droughts and its impacts on baseflow in the region.

6.1.2. Objective 2

Comparison of non-parametric statistical procedures for the testing of climatic and hydrologic datasets.

The purpose of this chapter was to evaluate the accuracy of the JRFit procedure that was used to estimate effect sizes as well as test their significance in the analysis of baseflow/streamflow data (Chapter 3 and 4). In this study, Monte Carlo simulation experiment was done where data were generated under various scenarios. Moreover, the efficiency of JRFit was compared to three other methods: the traditional methods such as restricted maximum likelihood (REML) and least absolute deviations as well as the nonparametric Wilcoxon rank-sum (WRS) method. The specific conclusions are:

1. The results confirm that JRFit provides more efficient result than all three methods for heavy tailed data.
2. JRFit is more efficient as compared to restricted maximum likelihood method with high clustered correlation.
3. JRFit procedure provide a genuine nonparametric alternative to REML for fitting linear mixed effect models which allows for simultaneous estimation and testing of effects.

6.1.3. Objective 3

Quantify the combined effect of droughts and irrigation water withdrawal on surface and baselow levels in the study area.

This study estimated the effect of ENSO induced drought and irrigation on flow levels of lower Flint River Basin (FRB) using non-parametric JRFit procedure. Particularly, streamflow, baseflow and low flow levels for the pre and post irrigation periods were compared and quantified along with ENSO. Additionally, presumptive standard water level for lower Flint River were studied and compared for specific La Niña-induced severe drought events. The major conclusions of this objective are:

1. The analysis of non-irrigation (NI) and irrigation (IR) period showed that since 1970s overall streamflow and baseflow levels have reduced substantially in the lower Flint River and its tributaries.
2. The analysis of 1-day and 7-day low flows and flow duration curve showed that frequency of low flows has increased during IR period and tributaries have changed from perennial stream to intermittent which suggests that groundwater withdrawal has intensified the extreme low flows in this region.
3. During the growing period, flow levels has reduced substantially during La Niña phases, which suggests that the combination of irrigation withdrawal and La Niña induced drought have significant impact on flow levels of the lower FRB causing stream reaches to go dry.
4. The analysis of presumptive water use also demonstrated that the flow levels are always lower than the presumptive flow band during the drought events in the IR period and flow levels have reduced substantially during the growing season.

6.1.4. Objective 4

Quantify the effect of irrigation water withdrawal and effectiveness of water restriction scenarios on stream-aquifer interactions in the lower Flint River and its tributaries.

The MODFE model was used was used to evaluate the impact of pumping groundwater from the UFA on stream aquifer interaction during the 2010-2012 drought (La Niña phase) event in the lower ACF region. The overarching goal of this study was to understand the relationships among droughts, irrigation, and stream-aquifer fluxes in the study area and to identify critical reaches and tributaries of the Flint River that are sustained by baseflows and are majorly responsible for lowering of flow levels in the river. Moreover, effectiveness of various water restriction scenarios were analyzed. Additionally, costs of acreage buyout under different water restrictions scenarios were studied and compared. The major conclusions of this objective are:

1. The results of the study indicated that groundwater withdrawal from the UFA in the lower ACF resulted in lowering of stream-aquifer flux during droughts.
2. In the Spring Creek, increased pumpage during the months of April, June and July resulted in significant decrease in stream-aquifer flux that changed the stream characteristics from gaining to losing stream in this region.
3. The results from sensitivity analysis identified the critical reaches where stream-aquifer hydraulic connectivity is strong and stream-aquifer flux is sensitive to pumpage.
4. The results from the simulated water restriction scenarios suggested that reducing the pumpage in highly sensitive and capacity use areas were more effective in streamflow recovery than reducing the irrigation intensity (15% or 30%) throughout the study area.

5. Analysis of acreage buyout suggested that water restrictions on irritation withdrawal can have significant impacts on stream-aquifer flux in the study area especially the critical watersheds such as Spring Creek and Ichawaynochaway Creek.

6.2. Implication of the Study

This study can help and inform water managers and policy makers to promote severity-based water restrictions in the study area. This study provides an evidence that policy makers need to consider the effects of multidecadal phenomenon along with ENSO while managing water resources in the region. The results of study can also be helpful in better understanding the combined impact of the climate induced droughts and anthropogenic stresses on stream-aquifer dynamics of Flint River that might help the state of Georgia to formulate an alternative drought-water policy that can address the current water scarcity condition. Additionally, the results from this study can be helpful to better manage groundwater resources, protect surface water flows, and help avoid irrigation induced streamflow depletion in some of the most vulnerable tributaries of the Flint River.

Chapter 7

Future Research

This study improved the understanding of how stream-aquifer dynamics in the ACF is affected by individual and coupled large-scale interannual and interdecadal ocean-atmosphere phenomena. This study also helped us understand the relationships among droughts, irrigation, and streamflow levels in the study area while identifying critical reaches and tributaries of the lower Flint River that are responsible for lowering of flow levels in the river. The study also evaluated water restriction scenarios on irrigation pumpage that can be implemented during droughts. This chapter provides some recommendations for possible future work. These suggested future research are presented below:

1. The information provided in Chapter 2 can be used to develop methodologies for possible short-term (3-6 months) forecasting of baseflow in the study area that will give prior information of the severity of droughts and possible baseflow depletion during impending drought event.
2. This study identified the tele-connections of interannual, decadal, and multi-decadal climatic oscillation with baseflow levels in the ACF. The study of other climatic oscillation such as Bermunda High Index (BHI) and their interaction with ENSO, PDO, AMO and NAO can also provide information on the effect of these oscillations on baseflow and other hydrologic components.

3. The climate change effect on climate variability can also be studied to understand the modulation of these oscillations due to future climate change and its impacts on groundwater resources and stream-aquifer interaction in the study area.

References

Aceituno, P., 1992. El Niño, the southern oscillation, and ENSO: Confusing names for a complex ocean-atmosphere interaction. *Bulletin of the American Meteorology Society,* 73, 483–485.

Adichie, J. N., 1967. Estimates of Regression Parameters Based on Rank Tests. *Ann. Math. Statist.*, 38, 894-904.

Aguado, D., Montoya, T., Borras, L., Seco, A., Ferrer, J., 2008. Using SOM and PCA for analysing and interpreting data from a P-removal SBR. Eng. Appl. Artif. Intell. 21, 919–930.

Albertson, Phillip N., and Torak, Lynn J., 2002, Simulated effects of ground-water pumpage on stream-aquifer flow in the vicinity of federally protected species of freshwater mussels in the lower Apalachicola–Chattahoochee–Flint River Basin (Subarea 4), southeastern Alabama, northwestern Florida, and southwestern Georgia: *U.S. Geological Survey Water-Resources Investigations Report* 02-4016, 53 p.

Barlow, M., S.Nigam, and E.H. Berbery, 2000: ENSO, Pacific decadal variability, and U.S. summertime precipitation, drought, and stream flow. *J. Climate*, 14, 2105-2128.

Barnston, A., and R. Livezey, 1986: Classification, seasonality and persistence of lowfrequency atmospheric circulation patterns. *Mon. Wea. Rev.*, 115, 1083-1126.

Barsugli, J. J., Whitaker, J. S., Loughe, A. F., Sardeshmukh, P. D., and Toth., Z., 1999. The effect of 1997/98 El Niño on individual large scale weather events. *Bullentin of American. Meterological. Soc*iety, 80, 1399-1411.

Bartlein, P. J., 1982: Streamflow anomaly patterns in the USA and southern Canada: 1951-1970. *Journal of Hydrology*, 57, 49-63.

Beebee, R.A. and Manga M., 2004. Variation in the Relationship Between Snowmelt Runoff in Oregon and ENSO and PDO. *Journal of the American Water Resources Association*, 40:1011–1024.

Berri, J. G., and Flamenco, E. A., 1999. Seasonal volume forecast of the Diamante river, Argentina, based on El Niño observations and predictions. *Water Resources Resesearch*, 35(12), 3803-3810.

Bindele, H. F., and Abebe, A., 2012. Bounded influence nonlinear signed-rank regression. *The Canadian Journal of Statistics,* 40, 172-189.

Boulton, A.J., and Hancock, P.J., 2006. Rivers as groundwater-dependent ecosystems: a review of degrees of dependency, riverine processes and management implications. *Australian Journal of Botany*, 54: 133-144.

Brizga SO, Arthington AH, Choy SC, Kennard MJ, Mackay SJ, Pusey BJ, Werren GL. 2002. Benchmarking, a 'top-down' methodology for assessing environmental flows in Australian rivers. In Proceedings of International Conference on Environmental Flows for Rivers. Cape Town: Southern Waters Consulting.

Bunn SE, Arthington AH. 2002. Basic principles and ecological consequences of altered flow regimes for aquatic biodiversity. *Environmental Management* 30: 492–507. DOI: 10.1007/s00267-002-2737-0.

Bush, P.W., and Johnston, R.H., 1988, Ground-water hydraulics, regional flow, and ground-water development of the Floridan aquifer system in Florida and in parts of Georgia, South Carolina, and Alabama. *U.S. Geological Survey*. Professional Paper 1403-C.

Cane, M. A., 2005. The evolution of El Niño, past and future. *Earth Planet Sci. Lett*., 230(3-4), 227-240.

Carlisle DM, Wolock DM, Meador MR. 2010. Alteration of streamflow magnitudes and potential ecological consequences: a multi-regional assessment. *Frontiers in Ecology and the Environment* 2010; doi:10.1890/100053.

Charles, C. D., Hunter, D. E., and Fairbanks, R. G., 1997. Interaction between the ENSO and the Asian monsoon in a coral record of tropical climate. *Science,* 277(5328), 925.

Chen C, Pei S, Jiao JJ., 2003. Land subsidence caused by groundwater exploitation in Suzhou City, China. *Hydrogeology Journal* 11: 275–287. DOI: 10.1007/s10040-002-0225-5.

Chen, W. Y., 1982. Assessment of Southern Oscillation Sea-Level Pressure Indices. *Mon. Wea. Rev.*, 110, 800–807.

Chiew, F.H.S., Piechota, T.C., Dracup, J.A., and McMahon, T.A., 1998. El Niño/Southern Oscillation and Australian rainfall, streamflow, and drought: links and potential for forecasting. *Journal of Hydrology,* 204, 138–149.

Climate Research Committee and National Research Council. (1995). Natural Climate Variability on Decade-to-Century Time Scales. Washington, DC: National Academy Press.

Cooley, R.L., 1983, Analysis of an incongruity in the standard Galerkin finite-element method. *Water Resources Research*, 19(1), 289 – 291.

Cooley, R.L., 1992, A MODular Finite-Element model (MODFE) for areal and axisymmetric ground-water flow problems, Part 2 — Derivation of finite-element equations and comparisons with analytical solutions: *U.S. Geological Survey Techniques of Water-Resources Investigations*, Book 6, Chap. A4, 108 p.

Cusick, Daniel, 2007. "Ga. has 'no choice' but to sue Army Corps—Gov. Perdue." *Greenwire*. 18 Oct. 2007 (electronic newsletter).

Dai,A., and Wigley, T. M. L., 2000. Global Patterns of ENSO-induced Precipitation. *Geophysical Research Letters*, 27, 1283-1286.

Datta, S., and Satten, G. A., 2005. Rank-Sum Tests for Clustered Data. *Journal of the American Statistical Association*, 100, 471.

Diaz, H. F. and Markgraf, V., 1992. El Niño: historical and paleoclimatic aspects of the Southern Oscillation. *Cambridge University Press*.

Earth Systems Research Laboratory (ESRL), 2012. Climate Timeseries: AMO (Atlantic Multidecadal Oscillation) Index. <http://www.esrl.noaa.gov/psd/data/ timeseries/AMO/>

Easterling DR, Meehl GA, Parmesan C, Changnon SA, Karl TR, Mearns LO. 2000. Climate extremes: observations, modeling, and impacts. *Science* 289: 2068–2074. DOI:10.1126/science.289.5487.2068.

Eckhardt, K., 2005. How to Construct Recursive Digital Filters for Baseflow Separation. *Hydrological Processes*, 19(2):507-515.

Eltahir, E. A. B., 1996. The role of vegetation in sustaining large scale atmospheric circulations in the tropics. *J . Geophys Res*., 101, 42-55.

Enfield, D.B., Mestas-Nuez, A.M., Trimble, P.J., 2001. The Atlantic multi-decadal oscillation and its relation to rainfall and river flows in the continental US. *Geophysical Research Letters*, 28 (10), 2077-2080.

Esselman PC, Opperman JJ. 2010. Overcoming information limitations for the prescription of an environmental flow regime for a Central American river. *Ecology and Society* 15: 6. URL http://www.ecologyandsociety.org/vol15/iss1/art6/.

Faye, R.E., and Mayer, G.C., 1990, Ground-water flow and stream–aquifer relations in the northern Coastal Plain of Georgia and adjacent parts of Alabama and South Carolina: U*.S. Geological Survey Water-Resources Investigations Report* 88-4143, 83 p., 7 plates.

Faye, R.E., and Mayer, G.C., 1996, Simulation of ground-water flow in southeastern coastal plain clastic aquifers in Georgia and adjacent parts of Alabama and South Carolina: *U.S. Geological Survey Professional Paper* 1410-F, 77 p., 16 plates.

Fraedrich, K., and Muller, K., 1992. Climate anomalies in Europe associated with ENSO extremes. *Int. J. Climatol*., 12(1).

Galbraith, S., Daniel, J. A., and Vissel, B., 2010. A Study of Clustered Data and Approaches to Its Analysis. *The Journal of Neuroscience*, 30(32), 10601–10608.

Gershunov, A., and Barnett, T.P., 1998a. ENSO influence on intraseasonal extreme rainfall and temperature frequencies in the contiguous United States: Observations and model results. *Journal of Climate*, 11(7), 1575-1586.

Gershunov, A., and Barnett, T.P., 1998b. Interdecadal modulation of ENSO teleconnections. *Bulletin of American Meteorological Society*, 79, 2715–2726.

Gilbert, Debbie, 2007. "Corps wants a drought summit." *The Times, Gainesville*. 15 June 2007.

Gillilan DM, Brown TC. 1997. Instream Flow Protection: Seeking A Balance in Western Water Use. *Island Press:* Washington, DC.

Glantz, M., 2001. Currents of Change: Impacts of El Niño and La Niña on Climate and Society, Second edition. *Cambridge University Press*, Cambridge, UK.

Glennon RJ. 2002. Water Follies: Groundwater Pumping and the Fate of America's Fresh Waters. *Island Press:* Washington, DC; 314.

Golladay SW, Gagon P, Kearns M, Battle JM, Hicks DW. 2004. Response of freshwater mussel assemblages (Bivalvia :Unionidae) to record drought in the Gulf Coastal Plain of southwest Georgia. *Journal of the North American Benthological Society,* 23: 494–506.

Green, P.M., D.M. Legler, C.J. Miranda V., and J.J. O'Brien, 1997: The North American climate patterns associated with the El Niño-Southern Oscillation. Unpublished manuscript, COAPS Report Series 97-1, Center for Ocean-Atmosphere Prediction Studies, Florida State University, Tallahassee. [Available online at http://www.coaps.fsu.edu/lib/booklet/.]

Gurdak, J. J., Hanson, R. T., McMahon, P. B., Bruce, B. W., McCray, J. E., Thyne, G. D., and Reedy, R. C., 2007. Climate Variability Controls on Unsaturated Water and Chemical Movement, High Plains Aquifer, USA. *Vadose Zone Journal*, 6, 533–547.

Halpert, M. S., and Ropelewski, C. F., 1992. Surface temperature patterns associated with the Southern Oscillation. *J. Clim*., 5(6), 577-593.

Hansen, D. V., and Maul, G. A., 1991. Anticyclonic current rings in the eastern tropical Pacific Ocean. *Journal of Geophysical Research*, 96(C4), 6965-6979.

Hansen, J., Jones, J., Irmak, A., and Royce, F., 2001. El Niño-southern oscillation impacts on crop production in the southeast United States. *ASA Special Publication*, 63, 55-76.

Hanson, K., and Maul, G.A., 1991. Florida precipitation and the Pacific El Niño, 1895–1989. Florida Scientist 54 (3/4), 160–168.

Harbaugh, A.W., Banta, E.R., Hill, M.C., and McDonald, M.G., 2000. MODFLOW-2000, the U.S. Geological Survey modular ground-water model -- User guide to modularization concepts and the Ground-Water Flow Process: *U.S. Geological Survey Open-File Report* 00-92, 121 p.

Hayes, L.R., Maslia, M.L., and Meeks, W.C., 1983. Hydrology and model evaluation of the principal artesian aquifer, Dougherty Plain, southwest Georgia: *Georgia Geologic Survey Bulletin* 97, 93 p.

Hettmansperger, T. P. and McKean, J. W., 2011. Robust nonparametric statistical methods, volume 119 of Monographs on Statistics and Applied Probability. CRC Press, Boca Raton, FL, second edition.

Hicks DW, Gill HE, Longsworth SA. 1987. Hydrogeology, Chemical Quality, and Availability of Ground Water in the Upper Floridan Aquifer, Albany Area. *U.S. Geological Survey; Water-Resources Investigations Report* 87–4145; 31 p.

Hidalgo, H. G., 2004. Climate precursors of multidecadal drought variability in the western United States. *Water Resources Research*, 40, W12504, doi:10.1029/2004WR003350.

Hidalgo, H. G., and Dracup, J. A., 2003. ENSO and PDO effects on hydroclimatic variations of the upper Colorado River basin. *J. Hydrometeorol.*, 4(1), 5 – 23.

Hidalgo, H. G., and J. A. Dracup, 2001. Evidence of the signature of North Pacific multidecadal processes on precipitation and streamflow variation in the upper Colorado River basin, paper presented at the 6th Biennial Conference of Research on the Colorado River Plateau, *U.S. Geol. Surv.*, Phoenix, Ariz.

Hodges, J. L. and Lehmann, E. L. (1963), Estimates of location based on rank tests, *Ann. Math. Statist.*, 34, 598-611.

Hoerling, M., Kumar, A., and Zhong, M., 1997. El Niño, La Niña, and the nonlinearity of their teleconnection. *J. Clim.,* 10, 1769–1786.

Hopkin, M., 2007. Climate takes aim. *Nature,* 446 (12), 706–707. http://www.atmos.washington.edu/~mantua/REPORTS/PDO/PDO_cs.htm]

Hurrell, J.W., 1995. Decadal Trends in the North Atlantic Oscillation Regional Temperatures and precipiatation. *Science*, 269, 676-679.

Hurrell, J.W., Y. Kushnir, M. Visbeck, and G. Ottersen, 2003: An Overview of the North Atlantic Oscillation. The North Atlantic Oscillation: Climate Significance and Environmental

Impact, J.W. Hurrell, Y. Kushnir, G. Ottersen, and M. Visbeck, Eds., Geophysical Monograph, 134, *American Geophysical Union*, 35 pp.

IFC (Instream Flow Council). 2001. Instream flows for riverine resource stewardship. URL http://www.instreamflowcouncil.org

IPCC (Intergovernmental Panel on Climate Change), 2001. Climate Change 2001: Impacts, adaptations, and vulnerability. In Contribution of working group II to the third assessment report of the Intergovernmental Panel on Climate Change. Cambridge: *Cambridge University Press*.

Jackson, J.E., 2003. A User's Guide to Principal Components. *Wiley & Sons, Inc.*, New Jersey.

Jaeckel, L. A., 1972. Estimating regression coefficients by minimizing the dispersion of the residuals. *Annals of Mathematical Statistics*, 43:1449–1458.

Johnson, N. T., Martinez, C. J., Kiker, G. A., Leitman, S., 2013. Pacific and Atlantic sea surface temperature influences on streamflow in the Apalachicola–Chattahoochee–Flint river basin. *Journal of Hydrology*, 489, 160–179.

Joint Institute for the Study of Atmosphere and Ocean (JISAO), 2012. PDO Index. <http://jisao.washington.edu/pdo/PDO.latest> (retrieved 09.18.13).

Jones, L.E., and Torak, L.J., 2004. Simulated effects of impoundment of Lake Seminole on ground-water flow in the Upper Floridan aquifer in southwestern Georgia and adjacent parts of Alabama and Florida: *U.S. Geological Survey Scientific Investigations Report* 2004-5077, 18 p.

Jones, L.E., and Torak, L.J., 2006. Simulated effects of seasonal ground-water pumpage for irrigation on hydrologic conditions in the lower Apalachicola–Chattahoochee–Flint River Basin, southwestern Georgia and parts of Alabama and Florida, 1999–2002: *U.S. Geological Survey Scientific Investigations Report* 2006-5234, 115 p., a Web-only publication at http://pubs.usgs.gov/sir/2006/5234/.

Jordan, J.L. and A.T. Wolf, 2006. Interstate Water Allocation in Alabama, Florida, and Georgia: New Issues, New Methods, New Models. *University Press of Florida*.

Jureckova, J., 1971. Nonparametric Estimate of Regression Coefficients. *Ann. Math. Statist.*, 42, 1328-1338.

Kahya, E., and Dracup, J. A., 1993. US streamflow patterns in relation to the El Niño/Southern Oscillation. *Water Resources Research*, 29(8), 2491-2503.

Kahya, E., Dracup, J. A., 1993. US streamflow patterns in relation to the El Niño/Southern Oscillation. *Water Resources Research*, 29(8), 2491-2503.

Keener, V.W., G.W. Feyereisen, U. Lall, J.W. Jones, D.D. Bosch and R. Lowrance, 2010. El-Niño/Southern Oscillation (ENSO) influences on monthly NO3 load and concentration, stream flow and precipitation in Little River Watershed, Tifton, Georgia (GA). *J. Hyd.* 381: 352-363.

Keener, V.W., Ingram, K.T., Jacobson, B., and Jones, J.W., 2007. Effects of El-Niño/ Southern Oscillation on simulated phosphorus loading. *Transactions of the ASABE*, 50(6), 2081–2089.

Kelly, Martin, 2004: Florida river flow patterns and the Atlantic Multidecadal Oscillation. Southwest Florida Water Management District. Unpublished manuscript available from SWFWMD, 10 Aug. 2004.

Kevin E. Trenberth and David P. Stepaniak, 2001: Indices of El Niño Evolution. *J. Climate*, 14, 1697–1701.

Kiladis, G.N., and Diaz, H.F., 1989. Global climate anomalies associated with extremes in the Southern Oscillation. *Journal of Climate*, 2 (9), 1069–1090.

Kinnaman, S.L., and Dixon, J.F., 2011, Potentiometric surface of the Upper Floridan aquifer in Florida and parts of Georgia, South Carolina, and Alabama, May – June 2010: *U.S. Geological Survey Scientific Investigations Map* 3182, 1 sheet.

Kloke, J., and McKean, J. W., 2014. Nonparametric Statistical Methods Using R. *CRC Press, Taylor & Francis Group, FL*.

Kloke, J.D., McKean, J.W., and Rashid, M., 2009. Rank-Based Estimation and Associated Inferences for Linear Models with Cluster Correlated Errors. *Journal of the American Statistical Association*, 104 (485), 384-390.

Koenker, R. and Bassett, G., 1978. REGRESSION QUANTILES. *Econometrica*, 46 (1), 33-50.

Koul, H.L., Sievers, G.L., and McKean, J.W. (1987) An esimator of the scale parameter for the rank analysis of linear models under general score functions, *Scandinavian Journal of Statistics*, 14, 131-141.

Kulkarni, J.R., 2000. Wavelet analysis of the association between the southern oscillation and the Indian summer monsoon. *International Journal of Climatology*, 20, 89–104.

Lehmann, E. L. and Romano, J. P., 2005. Testing statistical hypotheses. Springer Texts in Statistics. *Springer*, New York, third edition.

Light, H.M., K.R. Vincent, M.R. Darst, and F.D. Price, 2006: Water-level decline in the Apalachicola River, Florida, from 1954 to 2004, and effects on floodplain habitats: *U.S. Geological Survey Scientific Investigations Report* 2006-5173, 83 pp.

Lim, K.J., Engel, B.A., Tang, Z., Choi, J., Kim, K., Muthukrishnan, S., and Tripathy, D., 2005. Web GIS-based Hydrograph Analysis Tool, WHAT. *JAWRA*, 41(6): 1407-1416.

Lins, H. F., 1985: Streamflow variability in the United States: 1931-1978. *Journal of Climate and Applied Climatology*, 24, 463-471.

Litts, T., H. Russell, A. Thomas, and R. Welch. 2001. Mapping irrigated lands in the ACF riverbasin. Pages 79–83 *in* K. J. Hatcher (editor). *Proceedings of the 2001 Georgia Water Resources Conference*. Institute of Ecology, University of Georgia, Athens, Georgia.

MacQueen, J. (1967). Some methods for classification and analysis of multivariate observations. Proc. *5th Berkeley Symposium*, 281–297.

Mantua, N. J., and Hare, S. R., 2002. The Pacific Decadal Oscillation. *J. Oceanogr.*, 59 (1), 35–44.

Mantua, N. J., Hare, S. R., Zhang, Y., Wallace, J. M., and Francis, R. C., 1997. A Pacific interdecadal climate oscillation with impacts on salmon production. *Bull. Am. Meteorol. Soc.*, 78, 1069–1079.

Mantua, N., cited, 2007: The Pacific decadal oscillation and climate forecasting for North America. Unpublished manuscript, Joint Institute for the Study of the Atmosphere and Oceans, University of Washington, Seattle, Washington, USA. [Available online at http://www.atmos.washington.edu/~mantua/REPORTS/PDO/PDO_cs.htm]

McCabe, G. J., and Dettinger, M. D., 1999. Decadal variations in the strength of ENSO teleconnections with precipitation in the western United States. *International Journal of Climatology*, 19(13), 1399-1410.

McCabe, G. J., M. Palecki, and J.L. Betancourt, 2004: Pacific and Atlantic Ocean influences on multidecadal drought frequency in the United States. *Proc. Nat. Acad. Sci.,* 101, 4136-4141.

Mearns, L.O., Giorgi, F., Shields, C., and McDaniel, L., 2003. Climate scenarios for the southeastern US based on GCM and regional modeling simulations. *Climatic Change*, 60:7-36.

Meruelo, N., 2006. Considering a Cooperative Water Management Approach in Resolving the Apalachicola-Chattahoochee-Flint River Basin Water War. *Fordham Envtl. L. Rev*. 18:335.

Mitra, S., Srivastava, P., Singh, S., and Yates, D., 2014. Effect of ENSO-Induced Climate Variability on Groundwater Levels in the Lower Apalachicola-Chattahoochee-Flint River Basin. *Transactions of the ASABE*, 57(5), 1393-1403.

Molnar, P., and Cane, M. A., 2007. Early Pliocene (pre-Ice Age) El Niño-like global climate: Which El Niño. *Geosphere.*, 3(5), 337.

Montroy, D., Richman, M., Lamb, P., 1998. Observed nonlinearities of monthly teleconnections between tropical Pacific sea surface anomalies and central and eastern North American precipitation. *J. Clim.,* 11, 1812–1835.

Mosner MS. 2002. Stream-Aquifer Relations and the Potentiomentric Surface of the Upper Floridan Aquifer in the Lower Apalachicola-Chattahootchee-Flint River Basin in Parts of Florida, Georgia, and Alabama, *1990–1998* . U.S. Geological Survey; *Water-Resources Investigations Report* 02–4244; Atlanta, GA; 45 p.

Nicholls, N., Lavery, B., Friedericksen, C., Drodowsky, W., and Torok, S., 1996. Recent apparent changes in relationships between the ENSO and Australian rainfall and temperature. *Geophys. Res. Letters,* 23, 3357-60.

Opsahl SP, Chapal SE, Hicks DW, Wheeler CK. 2007. Evaluation of ground-water and surface-water exchanges using streamflow difference analyses. *Journal of the American Water Resources Association* 43:1132–1141.

Philander, S. G. H., and Rasmusson, E. M., 1985. The Southern Oscillation and El Niño. *Advances in Geophysics*, 28(A), 197-215.

Philander, S. G., 1990. El Niño, La Niña and the Southern Oscillation. *Elsevier*, New York.

Piechota, T. C. and Dracup. J. A., 1996. Drought and regional hydrologic variation in the United States: Associations with the El Niño-Southern Oscillation, *Water Resources Research*, 32 (5), 1359-1373.

Piechota, T. C. and Dracup, J. A., 1999. Long-Range Streamflow Forecasting Using El Ni ñ o-Southern Oscillation Indicators. *Journal of Hydrologic Engineering*, 4(2), 144-151.

Pierce, R., R. Barber, and H. R.Stiles, 1984, Georgia Irrigation, 1970-1980: A decade of growth, *U.S. Geological Survey Water-Resources Investigations Report* 83-4177, 29 p.

Pinheiro, J. C., and Douglas M. B., 2000. Mixed-effects models in S and S-PLUS. Springer.

Pollard, L.D., R.G. Grantham, and H.E. Blanchard, Jr., 1978, A preliminary appraisal of the impact of agriculture on ground-water availability in southwest Georgia: *U.S. Geological Survey Water-Resources Investigations Report* 79-7, 21 p.

Postel S. 1999. Pillar of Sand: Can the Irrigation Miracle Last? W.W. Norton: New York and London; 313.

Postel, S. L., G. C. Daily, and P.R. Ehrlich. 1996. Human appropriation of renewable fresh water. *Science*. 271(5250): 785.788.

Preisendorfer, R. W., 1988: Principal component analysis in meteorology and oceanography. Elsevier Science Publishing Company, New York, 425 pp.

Pringle CM, Triska FJ. 2000. Emergent biological patterns and surface-subsurface interactions at landscape scales. In *Stream and Groundwaters*, Jones JB, Mulholland PJ (eds). Academic Press: San Diego; 167–193.

Quinn, W. H. 1994. Monitoring and predicting El Niño invasions. *J. App. Meteor*. 9: 20–28.

Quinn, W. H., D. O. Zopf, K. S. Short, and R. T. Kuo Yang. 1978. Historical trends and statistics of the Southern Oscillation, El Niño, and Indonesian droughts. *Fish. Bull*. 76: 663–678.

Rajagopalan, B., and Lall, U., 1998. Interannual variability in western US precipitation. *Journal of Hydrology*, 210, 51–67.

Rasmusson, E. M., and Carpenter, T. H., 1982. Variations in Tropical Sea Surface Temperature and Surface Wind Fields Associated with the Southern Oscillation/El Niño. *Mon. Wea. Rev.*, 110, 354–384.

Rasmusson, E. M., and Wallace, J. M., 1983. Meteorological aspects of the El Niño/southern oscillation. *Science,* 222(4629), 1195-1202.

Redmond K. T., and Koch, R. W., 1991. Surface climate and streamflow variability in western United States and their relationship to large-scale circulation indices. *Wat. Resources Res*., 27(9), 2381–2399.

Richter BD, Baumgartner JV, Wigington R, Braun DP. 1997. How much water does a river need? *Freshwater Biology*, 37: 231–249.

Richter BD, Mathews R, Harrison DL, Wigington R. 2003. Ecologically sustainable water management: managing river flows for ecological integrity. *Ecological Applications,* 13: 206–224.

Richter BD, Warner AT, Meyer JL, Lutz K. 2006. A collaborative and adaptive process for developing environmental flow recommendations. *River Research and Applications*, 22: 297–318.

Richter BD. 2009. Re-thinking environmental flows: from allocations and reserves to sustainability boundaries. *Rivers Research and Applications*, 25: 1–12.

Richter, B. D., Davis, M. M., Apse, C., and Konrad, C., 2011. Short Communication a Presumptive Standard for Environmental Flow Protection. *River Research and Applications*, 28, 1312-1321.

Rogers, J. C., and Coleman, J. S. M., 2003. Interactions between the Atlantic Multidecadal Oscillation, El Niño/La Niña, and the PNA in winter Mississippi Valley stream flow. Geophys. *Res. Lett.*, 30 (10), 1518, doi:10.1029/2003GL017216.

Ropelewski, C. F., and Halpert, M. S., 1987. Global and regional scale precipitation patterns associated with the El Niño Southern Oscillation. *Mon. Weather Rev.*, 115 (8), 1601-1626.

Ropelewski, C.F. and Jones, P.D., 1987. An extension of the Tahiti-Darwin Southern Oscillation Index. *Monthly Weather Review*, **115**, 2161-2165.

Ropelewski, C.F., and Halpert, M.S., 1986. North American precipitation and temperature patterns associated with the El Niño/Southern Oscillation. *Monthly Weather Review*, 114, 2352–2362.

Rose S. 2009. Rainfall runoff trends in the southeastern USA: 1938–2005. *Hydrological Processes* 23: 1105–1118. DOI: 10.1002/hyp.7177.

Roy, S.S., 2006. The impacts of ENSO, PDO, and local SSTs on winter precipitation in India. *Physical Geography*, 27(5), 464-474.

Rugel, K., Jackson, C. R., Romeis, J. J., Golladay, S. W., Hicks, D.W., and Dowd, J. F., 2011. *Hydrol. Process., 26: 523-534.* DOI: 10.1002/hyp.8149

Ruhl, J. B., 2005. Water wars eastern style: Divvying up the Apalachicola-Chattahoochee-Flint river basin. *Journal of Contemporary Water Research and Education*, 131, 47–54.

Schlesinger, M. E., and Ramankutty, N., 1994. An oscillation in the global climate system of period 65-70 years. *Nature*, 367, Issue 6465, pp. 723-726, DOI: 10.1038/367723a0.

Schmidt, N., and Luther, M. E., 2002. ENSO impacts on salinity in Tampa Bay, Florida. *Estuaries and Coasts*, 25(5), 976-984.

Schmidt, N., Lipp, E.K., Rose, J.B., and Luther, M., 2001. ENSO influences on seasonal rainfall and river discharge in Florida. *Journal of Climate*, 14 (4), 615–628.

Seager R, Tzanova A, Nakamura J. 2009. Drought in the southeastern United States: causes, variability over the last millennium, and the potential for future hydroclimate change. *Journal of Climate* 22: 5021–5045. DOI: 10.1175/2009JCLI2683.1.

Shah T, Molden D, Sakthivadivel R, Seckler D. 2000. *The Global Groundwater Situation: Overview of Opportunities and Challenges*. International Water Management Institute: Colombo, Sri Lanka; 21 p.

Sharda, V., Srivastava, P., Ingram, K., Chelliah, M., Kalin, Latif, 2012. Quantification of El Niño Southern Oscillation (ENSO) Impact on Precipitation and Stream flows for Improved Management of Water Resources in Alabama. *Journal of Soil and Water Conservation*, 67(3), 158-172.

Shi X-Q, Xue Y-Q, Ye S-j, Wu J-C, Zhang Y, Yu J. 2007. Characterization of land subsidence induced by groundwater withdrawals in Su-Xi-Chang area, China. *Environmental Geology* 52: 27–40. DOI: 10.1007/s00254-006-0446-3 123.

Sievers, G. L. (1983). A weighted dispersion function for estimation in linear models. Communications in Statistics, *Theory and Methods*, 12(10), 1161–1179.

Simpson, H. J., and Colodner, D. C., 1999. Arizona precipitation response to the Southern Oscillation: A potential water management tool. *Wat. Resources Res*., 35(12): 3761-3769.

Smith S.R., P. M.Green, A. P. Leonardi and J. J. O'Brien. 1998: Role of multiple-level tropospheric circulations in forcing ENSO winter precipitation Anomalies. *Mon. Weather Rev.*: 126, No. 12, 3102–3116.

Sophocleous M. 2002. Interactions between groundwater and surface water: the state of the science. *Hydrogeology Journal* 10: 52–67. DOI: 10.1007/s10040-001-0170-8.

Stanford JA, Ward JV. 1993. An ecosystem perspective of alluvial rivers: connectivity and the hyporheic corridor. *Journal of North American Benthological Society* 12: 48–60.

Steinemann, Anne, 2003: Drought indicators and triggers: A stochastic approach to evaluation. *J. Am. Water Resour. Assoc.,* 39(5), 1217-1233.

Thuiller, W., 2007. Climate change and the ecologist. *Nature*, 448 (2), 550–552.

Tootle, G.A., Piechota, T.C., Singh, A., 2005. Coupled oceanic–atmospheric variability and US streamflow. *Water Resour. Res.*, 41, 1–11.

Torak, L.J., 1993a, A MODular Finite-Element model (MODFE) for areal and axisymmetric ground-water flow problems, Part 1— Model description and user's manual: U.S. Geological Survey Techniques of Water-Resources Investigations, Book 6, Chap. A3, 136 p.

Torak, L.J., 1993b, A MODular Finite-Element model (MODFE) for areal and axisymmetric ground-water flow problems, Part 3 — Design philosophy and programming details: U.S.

Geological Survey Techniques of Water- Resources Investigations, Book 6, Chap. A5, 243 p.

Torak, L.J., and McDowell, R.J., 1996, Ground-water resources of the lower Apalachicola – Chattahoochee– Flint River Basin in parts of Alabama, Florida, and Georgia–Subarea 4 of the Apalachicola– Chattahoochee – Flint and Alabama –Coosa–Tallapoosa River Basins. *U.S. Geological Survey Open-File Report*, 95-321.

Torak, L.J., and Painter, J.A., 2006, Geohydrology of the lower Apalachicola–Chattahoochee–Flint River Basin, southwestern Georgia, northwestern Florida, and southeastern Alabama: *U.S. Geological Survey Scientific Investigations Report 2006-5070*, 80 p.

Torak, L.J., Davis, G.S., Strain, G.A., and Herndon, J.G., 1996, Geohydrology and evaluation of stream aquifer relations in the Apalachicola–Chattahoochee–Flint River Basin, southeastern Alabama, northwestern Florida, and southwestern Georgia. *U.S. Geological Survey Water-Supply Paper,* 2460.

Trenberth, K. E., and Stepaniak, D. P., 2001. Indices of El Niño Evolution. *J. Climate*, 14, 1697–1701.

Trenberth, K.E., 1997. The Definition of El Ni\ No. *Bulletin of the American Meteorological Society,* 78:2771–2777.

Trenberth, K.E., and Hoar, T. J., 1996. The 1990-1995 El Niño Southern Oscillation event: Longest on record. *Geophysical Research Letters*, 23, 57-60.

Troup, A. J., 1965. The 'southern oscillation'. *Q.J.R. Meteorol. Soc.*, 91, 490–506.

U.S. Fish and Wildlife Service, 1998. Endangered and threatened wildlife and plants; Determination of endangered status for five freshwater mussels and threatened status for two freshwater mussels from the Eastern Gulf Slope drainages of Alabama, Florida, and Georgia, Federal Register: March 16, 1998, 63(50), 84 p.

USACE (U.S. Army Corps of Engineers),1998: Draft Environmental Impact Statement on Water Allocation for the Apalachicola-Chattahoochee-Flint (ACF) River Basin. Alabama, Florida, and Georgia, Main Report, Mobile District, Mobile, Alabama.

Walsh, J. E., and A. Mostek, 1980: A quantitative analysis of meteorological anomaly patterns over the United States: 1900-1977. *Monthly Weather Review*, 108, 615-630.

White, H., 1982. Maximum Likelihood Estimation of Misspecified Models. *Econometrica*, 50, 1-25.

White, M.S., Xenopoulos, M.A., Hogsden, K., Metcalfe, R.A., Dillon, P.J., 2008. Natural lake level fluctuation and associated concordance with water quality and aquatic communities within small lakes of the Laurentian Great Lakes region. *Hydrobiologia,* 613, 21–31.

Winter TC, Harvey JW, Franke OL, Alley WM. 1998. Ground Water and Surface Water: A Single Resource. *U.S. Geological Survey Circular,* 1139; Denver, CO; 4 p.

Woessner WW. 2000. Stream and fluvial plain ground water interactions: rescaling hydrogeologic thought. *Ground Water* 38: 423–429.

Wolter, K., and Timlin, M. S., 1993. Monitoring ENSO in COADS with a seasonally adjusted principal component index, in *Proc. 17th Climate Diagnostics Workshop.,* 52–57.

Zektser S, Lo´aiciga HA, Wolf JT. 2005. Environmental impacts of groundwater overdraft: selected case studies in the southwestern United States. *Environmental Geology* 47: 396–404. DOI: 10.1007/s00254-004-1164-3.

Zienkiewicz, O.C., 1977, The finite element method: New York, *McGraw-Hil*l, 787 p.

Appendix A

Streamflow Gauging Stations from USGS

A. 1. USGS long term streamflow gauging stations

Table A.1. List of long-term streamflow gauging stations with their coordinates in degree decimals used for JRFit analysis used in Chapter 2.

Station ID	Latitude	Longitude
02344500	30.90	-84.90
02347500	30.96	-84.60
02349500	31.07	-84.52
02349605	31.09	-84.44
02352500	31.11	-84.68
02353000	31.17	-84.83

A. 2. USGS long term streamflow gauging stations in Chapter 4

Table A. 2. USGS long term streamflow gauging stations used in Chapter 4.

Station ID	Latitude	Longitude
02344500	33.244	-84.429
02347500	32.721	-84.233
02349500	32.298	-84.044
02349605	32.293	-84.044

Appendix B

Irrigated Acreage in the lower Flint River Basin

B. 1. Irrigated acreage in the lower Flint River Basin

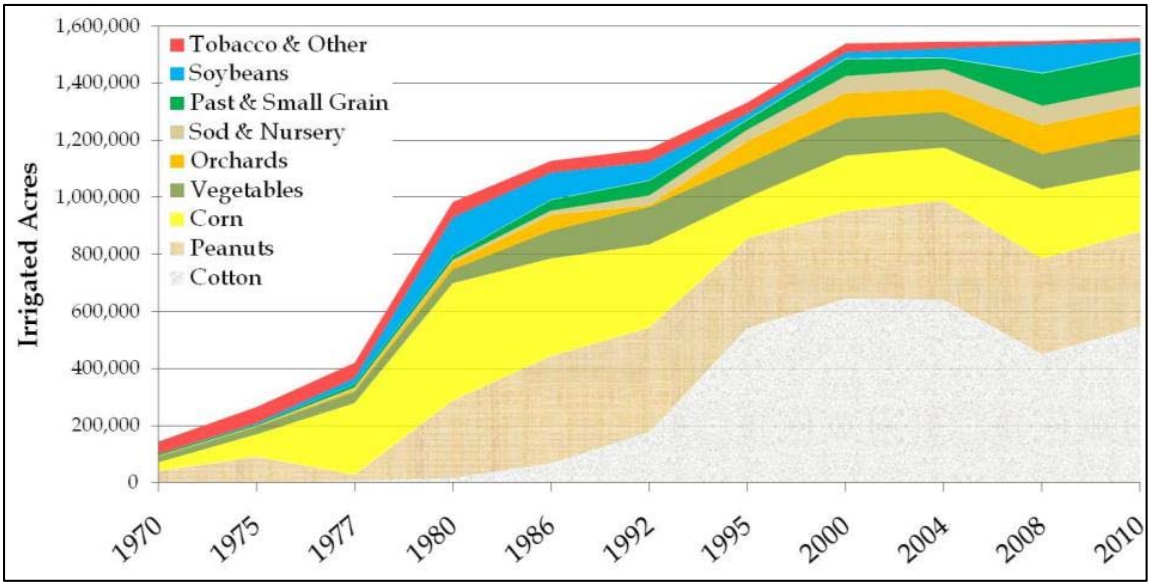

Figure B. 1. Increase in irrigated acreage in the lower Flint River Basin since 1970s.

Appendix C

Precipitation Analysis

C.1. Precipitation Analysis for Irrigated and Non-Irrigated period for Albany station in chapter 4.

Table C.1. Precipitation Analysis for Irrigated and Non-Irrigated period for Albany station.

Precipitation	Non-Irrigation Period	Irrigation Period	p-value
Overall	93.9	95.8	0.704
El Niño	102.8	106.7	0.630
La Niña	83.4	78.2	0.553

Appendix D

MODFE Simulated Stream-Aquifer Flux for WY 2012

D. 1. MODFE simulated irrigation and stream-aquifer flux for WY 2012 in Chapter 4

Table D.1. Irrigation withdrawal in cfd and simulated stream-aquifer flux for current and different scenarios in TCMD for Spring Creek.

Month	Pumpage	Current Condition	NI	SI	SII	SIII	SIV	SV	SVI	SVII
Oct-11	-20	144	170	149	154	155	149	160	151	162
Nov-11	0	168	182	172	176	176	170	177	173	178
Dec-11	0	171	179	174	175	175	173	176	174	176
Jan-12	0	220	225	221	222	222	221	222	221	222
Feb-12	0	253	258	254	255	254	254	255	254	254
Mar-12	-91	57	83	61	65	68	63	75	65	74
Apr-12	-120	61	97	66	72	78	69	86	73	86
May-12	-209	43	111	52	62	83	53	94	69	85
Jun-12	-286	34	122	46	58	86	49	102	72	95
Jul-12	-596	21	152	37	54	89	41	115	71	110
Aug-12	-128	108	167	118	127	135	123	148	126	152
Sep-12	-121	108	159	117	124	135	118	143	127	146
Total	**-1571**	**1388**	**1905**	**1466**	**1543**	**1656**	**1484**	**1752**	**1575**	**1741**

Table D.2. Percentage recovery of stream-aquifer flux under different scenarios as compared to current stream-aquifer flux for Spring Creek.

Month	Current Condition	Percentage Recovery of Stream-Aquifer Flux						
		SI	SII	SIII	SIV	SV	SVI	SVII
Oct-11	144	3.38	6.82	8.01	3.49	11.03	4.67	12.90
Nov-11	168	2.11	4.38	4.53	1.22	5.24	2.73	5.67
Dec-11	171	1.41	2.34	2.11	0.95	2.51	1.52	2.45
Jan-12	220	0.44	0.83	0.65	0.31	0.89	0.38	0.80
Feb-12	253	0.26	0.52	0.36	0.22	0.55	0.19	0.43
Mar-12	57	7.22	14.33	20.46	11.83	32.25	14.55	30.47
Apr-12	61	8.86	17.70	27.42	13.62	41.01	19.95	40.92
May-12	43	20.78	42.64	92.04	23.23	116.75	59.08	97.23
Jun-12	34	36.12	72.77	153.45	45.12	202.13	113.41	182.63
Jul-12	21	78.36	160.51	328.07	98.09	450.35	239.36	429.00
Aug-12	108	9.04	17.47	25.29	14.01	36.81	16.49	40.73
Sep-12	108	8.50	15.50	25.35	9.17	33.03	18.29	35.83

Table D.3. Irrigation withdrawal in cfd and simulated stream-aquifer flux for current and different scenarios in TCMD for Ichawaynochaway Creek.

Month	Pumpage	Current Condition	NI	SI	SII	SIII	SIV	SV	SVI	SVII
Oct-11	-64	189	241	196	204	206	200	218	210	212
Nov-11	0	178	212	184	189	187	187	196	190	190
Dec-11	0	176	206	181	185	183	183	191	185	186
Jan-12	0	195	219	198	202	201	201	207	202	202
Feb-12	0	249	275	254	259	254	258	263	256	257
Mar-12	-52	196	214	199	202	203	200	206	204	204
Apr-12	-63	204	222	207	210	211	207	213	212	213
May-12	-91	208	229	211	214	215	211	218	217	218
Jun-12	-118	200	224	204	207	208	204	212	212	212
Jul-12	-255	211	253	217	224	231	217	236	236	237
Aug-12	-60	202	227	206	209	209	206	213	212	213
Sep-12	-60	193	217	197	201	200	198	205	203	204
Total	**-764**	**2401**	**2739**	**2453**	**2505**	**2508**	**2471**	**2577**	**2538**	**2547**

Table D.4. Percentage recovery of stream-aquifer flux under different scenarios as compared to current stream-aquifer flux for Ichawaynochaway Creek.

Month	Current Condition	Percentage Recovery of Stream-Aquifer Flux						
		SI	SII	SIII	SIV	SV	SVI	SVII
Oct-11	189	3.76	7.78	9.12	5.95	15.37	11.23	12.30
Nov-11	178	3.28	6.14	5.23	5.15	10.24	6.70	7.11
Dec-11	176	2.78	5.47	4.40	4.11	8.47	5.38	5.76
Jan-12	195	1.88	3.86	3.16	3.05	6.29	3.56	3.85
Feb-12	249	1.84	3.91	2.15	3.74	5.82	2.84	3.09
Mar-12	196	1.53	2.94	3.18	1.65	4.79	3.80	4.11
Apr-12	204	1.36	2.69	3.15	1.42	4.55	3.84	4.13
May-12	208	1.50	3.00	3.56	1.38	4.93	4.59	4.85
Jun-12	200	1.71	3.40	3.96	1.66	5.61	5.51	5.84
Jul-12	211	2.92	5.84	9.29	2.53	11.82	11.56	12.04
Aug-12	202	1.75	3.59	3.26	2.12	5.38	4.80	5.14
Sep-12	193	1.99	4.02	3.43	2.54	5.96	5.27	5.60

Table D.5. Irrigation withdrawal in cfd and simulated stream-aquifer flux for current and different scenarios in TCMD for Muckalee Creek.

Month	Pumpage	Current Condition	NI	SI	SII	SIII	SIV	SV	SVI	SVII
Oct-11	-20	548	585	553	559	548	548	548	551	551
Nov-11	0	517	543	521	525	517	517	517	519	519
Dec-11	0	593	615	596	599	593	593	593	595	595
Jan-12	0	613	631	615	618	613	613	613	614	614
Feb-12	0	637	651	639	641	637	637	637	638	638
Mar-12	-21	558	573	560	562	558	558	558	559	559
Apr-12	-23	569	584	571	573	569	569	569	570	570
May-12	-65	603	626	606	610	603	603	603	604	604
Jun-12	-43	587	610	591	594	587	587	587	589	589
Jul-12	-124	567	602	572	577	567	567	567	569	569
Aug-12	-47	573	603	577	582	573	573	573	575	575
Sep-12	-25	532	557	536	539	532	532	532	534	534
Total	**-369**	**6897**	**7178**	**6938**	**6978**	**6897**	**6897**	**6898**	**6916**	**6916**

Table D.6. Percentage recovery of stream-aquifer flux under different scenarios as compared to current stream-aquifer flux for Muckalee Creek.

Month	Current Condition	Percentage Recovery of Stream-Aquifer Flux						
		SI	SII	SIII	SIV	SV	SVI	SVII
Oct-11	548	0.98	1.95	0.01	0.00	0.01	0.53	0.53
Nov-11	517	0.73	1.45	0.01	0.00	0.01	0.39	0.39
Dec-11	593	0.55	1.09	0.01	0.00	0.01	0.30	0.30
Jan-12	613	0.42	0.83	0.01	0.00	0.01	0.22	0.22
Feb-12	637	0.32	0.63	0.01	0.00	0.01	0.17	0.17
Mar-12	558	0.38	0.76	0.01	0.00	0.01	0.19	0.19
Apr-12	569	0.37	0.75	0.01	0.00	0.01	0.20	0.20
May-12	603	0.53	1.07	0.01	0.00	0.01	0.20	0.20
Jun-12	587	0.56	1.12	0.01	0.00	0.01	0.24	0.24
Jul-12	567	0.89	1.78	0.01	0.00	0.01	0.33	0.33
Aug-12	573	0.77	1.53	0.01	0.00	0.01	0.33	0.33
Sep-12	532	0.67	1.36	0.01	0.00	0.01	0.33	0.33

Table D.7. Irrigation withdrawal in cfd and simulated stream-aquifer flux for current and different scenarios in TCMD for lower Flint River basin.

Month	Pumpage	Current Condition	NI	SI	SII	SIII	SIV	SV	SVI	SVII
Oct-11	-346	3361	3626	3402	3442	3461	3391	3489	3493	3485
Nov-11	0	3327	3500	3354	3381	3390	3343	3404	3402	3397
Dec-11	0	3168	3296	3188	3208	3211	3179	3221	3219	3216
Jan-12	0	2899	2993	2914	2928	2929	2907	2936	2934	2931
Feb-12	0	2967	3039	2978	2989	2988	2973	2994	2992	2990
Mar-12	-197	3005	3101	3019	3034	3037	3018	3050	3048	3042
Apr-12	-266	3341	3456	3358	3375	3383	3358	3399	3395	3387
May-12	-560	3442	3621	3468	3494	3517	3466	3542	3525	3513
Jun-12	-569	3328	3546	3360	3392	3419	3360	3451	3434	3416
Jul-12	-1022	3386	3698	3431	3476	3529	3425	3571	3553	3535
Aug-12	-279	3324	3551	3358	3391	3411	3345	3433	3430	3421
Sep-12	-212	3400	3592	3430	3459	3476	3419	3494	3487	3479
Total	-3451	38947	41019	39260	39571	39751	39185	39982	39910	39814

Table D.8. Percentage recovery of stream-aquifer flux under different scenarios as compared to current stream-aquifer flux for lower Flint River basin.

Month	Current Condition	Percentage Recovery of Stream-Aquifer Flux						
		SI	SII	SIII	SIV	SV	SVI	SVII
Oct-11	3361	1.22	2.42	2.96	0.90	3.81	3.94	3.69
Nov-11	3327	0.81	1.61	1.88	0.47	2.30	2.24	2.11
Dec-11	3168	0.63	1.25	1.35	0.36	1.66	1.60	1.50
Jan-12	2899	0.51	1.02	1.03	0.28	1.27	1.21	1.13
Feb-12	2967	0.38	0.76	0.73	0.20	0.91	0.85	0.79
Mar-12	3005	0.49	0.98	1.09	0.45	1.52	1.44	1.26
Apr-12	3341	0.52	1.03	1.25	0.50	1.74	1.60	1.37
May-12	3442	0.77	1.53	2.18	0.72	2.90	2.41	2.08
Jun-12	3328	0.96	1.93	2.72	0.96	3.69	3.16	2.65
Jul-12	3386	1.33	2.68	4.25	1.17	5.46	4.93	4.41
Aug-12	3324	1.01	2.03	2.63	0.64	3.27	3.19	2.92
Sep-12	3400	0.87	1.73	2.23	0.54	2.75	2.55	2.32